Fundamental Engineering Studies of Magnetic Particle Inspection and Impact on Standards and Industrial Practice

February 2018

Final Report

This document is available to the U.S. public through the National Technical Information Services (NTIS), Springfield, Virginia 22161.

This document is also available from the Federal Aviation Administration William J. Hughes Technical Center at actlibrary.tc.faa.gov.

U.S. Department of Transportation
Federal Aviation Administration

NOTICE

Technical Report Documentation Page

1. Report No. DOT/FAA/TC-17/20	2. Government Accession No.	3. Recipient's Catalog No.
4. Title and Subtitle FUNDAMENTAL ENGINEERING STUDIES OF MAGNETIC PARTICLE INSPECTION AND IMPACT ON STANDARDS AND INDUSTRIAL PRACTICE		5. Report Date February 2018
		6. Performing Organization Code
7. Author(s) David Eisenmann, Darrel Enyart, Daigo Kosaka, Lisa Brasche, and Chester Lo		8. Performing Organization Report No.
9. Performing Organization Name and Address Iowa State University Center for NDE 1915 Scholl Road Ames, IA 50011		10. Work Unit No. (TRAIS)
		11. Contract or Grant No. Grant No. 10-G-002
12. Sponsoring Agency Name and Address FAA National Headquarters 950 L'Enfant Plaza N SW 950 L'Enfant Plaza Washington, DC 20024		13. Type of Report and Period Covered Final Report
		14. Sponsoring Agency Code AIR-100

15. Supplementary Notes

The FAA William J. Hughes Technical Center Aviation Research Division Technical Monitors were David Westlund and Ahmet Oztekin.

16. Abstract

Magnetic particle inspection (MPI) has been widely used for decades and sees considerable use in the aerospace industry, with 90% of the steel parts being inspected with MPI at some point in their life cycle. Typical aircraft inspection locations are landing gear, engine components, attachment hardware, and doors. Despite its numerous applications, MPI remains poorly understood, and there are many aspects that would benefit from in-depth study. MPI is poorly understood because it combines the complicated nature of electromagnetics, metallurgical material effects, fluid-particle motion dynamics, and physiological human factors into a single inspection. Research studies will be prioritized through the guidance of a panel of industry experts to promote understanding of the intricate issues with this method that affect sensitivity or that would assist with the revision of industry specifications and standards. This approach has worked successfully in past fluorescent penetrant inspection research efforts.

The MPI technique has been used for many years for aviation applications, but unfortunately very few aids exist that assist in proper test setup. There are many rule-of-thumb equations available to calculate current settings for a given sample geometry, but very often this results in gross over-magnetization and reduced sensitivity. Magnetic particle test specifications also prescribe current values that are affected by the control waveforms used for regulating the current intensity. This introduces harmonics in the waveforms, making it difficult to establish a relationship between peak and root mean square values of a current waveform, which is important in the practical use of MPI. Each of the waveforms has its own characteristics and interactions between leakage fields at discontinuities, and the particles can vary significantly. It is therefore possible to miss the detection of defects by choosing inappropriate current waveforms. In recent Air Transport Association Non-Destructive Testing Forums, the airlines have identified the need for additional research to support fundamental understanding of the MPI technique and the factors that affect sensitivity. Of particular concern is the direction "complete 100% magnetic particle inspection" without specific guidance on setup parameters, which is common in original equipment manufacturer procedures. Another issue with overwhelming support is the impact of coatings and platings on MPI sensitivity.

17. Key Words Magnetic particle, Flux leakage, Permeability, Head shot, Coil shot	18. Distribution Statement This document is available to the U.S. public through the National Technical Information Service (NTIS), Springfield, Virginia 22161. This document is also available from the Federal Aviation Administration William J. Hughes Technical Center at actlibrary.tc.faa.gov.		
19. Security Classif. (of this report) Unclassified	20. Security Classif. (of this page) Unclassified	21. No. of Pages 145	22. Price

Form DOT F 1700.7 (8-72)   Reproduction of completed page authorized

TABLE OF CONTENTS

APPENDICES

LIST OF FIGURES

LIST OF TABLES

LIST OF ACRONYMS

AC	Alternating current
CNDE	Center for Nondestructive Evaluation
DC	Direct Current
EDM	Electric discharge machining
FMPI	Fluorescent magnetic particle inspection FPI Fluorescent penetrant inspection
FS	Full scale
FWDC	Full wave direct current
HVOF	High-velocity oxygen fuel
HWDC	Half wave direct current
ISU	Iowa State University
LCF	Low-cycle fatigue
MP	Magnetic particle
MPI	Magnetic particle inspection
MTS	Materials Testing System
NDE	Nondestructive evaluation
NDI	Nondestructive inspection
Oe	Oersted
OEM	Original equipment manufacturer PI Principal investigator
QQI	Qualitative Quality Indicator
RMS	Root mean square
VBT	Vibrothermography

EXECUTIVE SUMMARY

Magnetic particle inspection (MPI) has been widely used for decades and sees considerable use in the aerospace industry, with 90% of steel parts being inspected with MPI at some point in their life cycle. Typical aircraft inspections are landing gear, engine components, attachment hardware, and doors. Despite numerous applications, the method remains poorly understood, with many aspects that would benefit from in-depth study. This is because MPI combines the complicated nature of electromagnetics, metallurgical material effects, fluid-particle motion dynamics, and physiological human factors into a single inspection.

Research studies were prioritized through the guidance of a panel of industry experts to promote understanding of the intricate issues with this method that affect sensitivity or that would assist with the revision of industry specifications and standards. To address these issues, the program had the following objectives:

- To identify the most relevant factors in MPI for which existing engineering data is insufficient, assess the parameter ranges that provide acceptable performance for typical aircraft and engine components, and document the results of these studies for use in revision of industry specifications.
- To complete an assessment of existing process control/monitoring tools and provide needed improvements.
- To develop/validate MPI guidance materials for use by the airlines and original equipment manufacturers that incorporate lessons learned in this program, and incorporate other recently developed data and information.

In the first 2 years of the program, relevant samples have been fabricated, experimental protocols developed, and a work plan for engineering studies developed. The work in year 3 included a study of the effects of magnetizing switching frequency; effects of part orientation, surface roughness, surface coatings, part cleanliness, geometry, field strength on detectability, impact of bath characteristics, and defect morphology on MPI response; and the development of five training modules.

Departure of Key Personnel

At the beginning of the second quarter for FY 2013, the principal investigator (PI) for this project departed the university, and the team member who headed up the electromagnetics portion of the research departed a month after to pursue opportunities in the private sector. From this point on, the research team has operated without a PI and an electromagnetics team member. A postdoctoral researcher was hired to replace the departed team member, and one of the remaining team members assumed the position of the PI.

1. INTRODUCTION

1.1 BACKGROUND

Magnetic particle inspection (MPI) is used for surface and near-surface crack detection on ferromagnetic materials. For commercial aviation applications, most inspections are done using a wet, horizontal bench with a direct contact shot for circular magnetization and coil-shot capabilities to ensure inspection in the longitudinal direction. A magnetic field is generated though the specimen, and the oil-based fluid containing magnetic particles is poured over the areas of interest. Cracks and other discontinuities will result in a localized change in flux density that attracts the magnetic particles, which are then detected using a blacklight in the case of fluorescent MPI or contrast in dry-powder MPI. Sensitivity also depends on crack orientation with respect to the flux direction, which is why most inspections use either two orthogonal shots or multidirectional coils.

In addition to the bench unit described above, the use of yokes, coil wraps, and permanent magnets to induce the magnetic field is also possible (note that inspection using prods is also practiced in some industries; however, this practice is not allowed in commercial aviation because of concerns with arcing, which could lead to localized damage and incipient defects that eventually lead to failure). Choices also exist with regard to the current supply. Units that offer alternating current (AC), half-wave direct current (HWDC), and/or full-wave direct current (FWDC) exist with increasing subsurface detection possible with the direct current (DC) options.

Successful MPI requires that the flux density in and around the sample be within a given range. Low flux density may not lead to particle attraction, resulting in lack of indications from defects, and too high of a density will result in high background noise and reduced sensitivity. Parts with complex geometries may result in areas with little or no magnetic flux being present in extremities or recesses. Typical MPI tests are developed through the reiterative use of quantitative quality indicators (QQIs) affixed to critical areas and progressively increasing current until the artificial defects are visible. Industry specifications, such as ASTM E-1444–Standard Practice for Magnetic Particle Testing, provide guidance on performance of MPI.

1.2 OBJECTIVES

The objectives of MPI testing are as follows:

- To identify the most relevant factors in magnetic particle inspection for which existing engineering data is insufficient, assess the parameter ranges that provide acceptable performance for typical aircraft and engine components, and document the results of these studies for use in revision of industry specifications.
- To complete an assessment of existing process control/monitoring tools and provide needed improvements.
- To develop/validate MPI guidance materials for use by the airlines and original equipment manufacturers (OEMs) that incorporate "lessons learned" in this program and incorporate other recently developed data and information.

1.3 TECHNICAL APPROACH

MPI is a widely used inspection method with numerous commercial options available to practice the method. Though commercial equipment is readily available, and numerous inspection techniques have been issued for use in maintenance, repair, and overhaul situations, industry partners have expressed considerable interest in accessibility to public-domain engineering data for MPI. Iowa State University (ISU) has recently completed a multiyear program in fluorescent penetrant inspection (FPI) under FAA support as part of contract number DTFA03-98-D-00008. The generic approach used in that program was duplicated in this effort and was as follows:

- Define factors for which engineering data is deficient.

    – Examples include the impact of part geometries, coatings, and plating

- Design an engineering study that provides quantitative assessment of performance.

    – Brightness measurements
    – Digital recording of UVA indication
    – Probability of detection
    – Magnetization methods
    – Magnetic field measurement

- Complete study using either lab or shop facilities as appropriate (several industry partners have offered access to their facilities including Delta, American, and United; ISU also has an opportunity to work with the Iowa Air National Guard Nondestructive Inspection (NDI) shop, located at the Des Moines Airport).
- Distribute results through use of the Web.
- Support changes to industry specifications as warranted.
- Use results to update/create guidance materials.

1.4 COMMON ISSUES

In an effort to focus the program on those issues of most relevance, an informal survey of industry partners was completed. The common issues are categorized as follows:

- Geometry effects–Electromagnetic theory is often based on simple shapes with minimal or no geometric changes. However, real parts have complex geometries, such as fir trees in disks, threaded bolts, and large landing gear assemblies that can have multiple flanges, races, tapers, shafts, etc. Simple formulas exist for determining proper current values such as those published in ASTM 1444. However, errors can occur and better direction has been requested by the industry partners on the limitations of the formulas. Just as questions exist with the adequate magnetization of complicated geometries, similar issues exist with demagnetization.
- Comparison of magnetization methods–The selection of a wet, horizontal inspection bench for MPI is often the preferred method. However, in some cases, the use of yokes or permanent magnets may be preferred or is the only available option because of accessibility or inability to bring the part to the bench. In addition, there are options for

selection of the current type between AC, DC, FWDC, or HWDC. Quantitative data comparing sensitivity of the different approaches is needed.

- Magnetization parameters and their measurement–Questions have been raised regarding adequate flux density and the ability to make accurate measurements. Clear guidance for using Gauss Meters and Hall effect probes for determining adequate field strength for both circular and longitudinal fields was identified by several partners, including input provided by Air Force NDI personnel.

- Comparison of fluorescent magnetic particle inspection (FMPI) to contrast MPI and dry-particle MPI–Most aviation inspection is accomplished using FMPI. However, there have been reports of improved sensitivity using black magnetic ink on complex geometry (disk fir tree) parts. A quantitative assessment of the various media would be beneficial in OEM inspection specifications.

- Best practices for QQIs–The use of notched shims for inspection sensitivity for various materials has been questioned. Guidance on the adequacy of flux density for a given volume, and comparison of single, longer duration shot to multiple, shorter duration shots are among the items identified as relevant. Best practice guidance on the use of Ketos rings and other calibration approaches was also suggested as a needed item.

- Manufacturing and shop practices on sensitivity–Many ferrous parts are coated using either metallic or inorganic coatings to provide necessary corrosion, wear, or thermal protection. Removal of coatings is costly and can be detrimental to performance/safety upon return to service. Therefore, there is a desire to perform inspections with coatings intact. However, there are concerns about the effectiveness of the inspection if this practice is allowed. Clear guidance on the limitation of inspection through coatings is needed and was the most predominant request among the industrial partners. A second "shop practices" question arose regarding the effect of using "shop air" to remove puddled magnetic particle (MP) fluids and the effect of this practice on sensitivity.

A working group was established with industry partners through discussion held individually with participants and at annual Air Transportation Association nondestructive testing forums. In addition to the individual discussions, several trips were made to industry participants to collaborate on specific aspects of the inspection process and to provide an opportunity to meet with inspectors and gain an operator's perspective on the inspection process.

To compile the results of the program and develop something that could be presented to industry, a series of five training modules was developed in a standard PowerPoint® format. Each of these training modules focuses on a different aspect of the inspection process, focused primarily on the use of a bench-type operation. The first three modules are more quantitative in nature, concentrating on the numerical aspects such as flux leakage occurring around a defect, current resulting from energizing the bench, or the calculations used to determine the initial current settings. The final two modules are more qualitative in nature, discussing some of the aspects that are not as readily quantifiable, such as bath concentration or the effects of bath heating.

2. EQUIPMENT AND SOFTWARE/PROCEDURE DEVELOPMENT

2.1 MPI BENCH ACQUISITION

It was realized early in the project that the single MPI bench located at the Center for Nondestructive Evaluation (CNDE) would not be sufficient to sustain the experimental work needed to be conducted for this research project. Not only was the single bench a lower end model with few features, it was also shared with CNDE's Iowa Company Assistance Program and with an undergraduate laboratory class on nondestructive evaluation (NDE). Therefore, access to two new MPI benches were made available to the program.

The second MPI bench was provided by the FAA through excess government equipment inventories—the bench was a Magnaflux AD-945, which was very similar to the existing bench. On arrival at ISU, the bench was stored in a warehouse in Ames Lab until arrangements to move the bench to its final position were made. The bench needed significant cleaning and a service visit from a qualified technician recommended by Magnaflux for repairs and calibration prior to its use. When in place, the bench was adjacent to an existing AD-945 bench, which allowed for comparison of many different settings and carrier fluids without changes to the benches. This second AD-945 was used with a water-based carrier fluid, which allowed for comparison to the standard fluid and presented some daily operational maintenance issues not experienced with the standard fluid carrier used in MPI benches. The use of this bench was set aside in the later stages of the program due primarily to input from industry that water-based carrier fluid was not common in the aviation industry, and comparison studies for water-based carrier were concluded.

An additional state-of-the-art bench was donated to ISU from Magnaflux for use in the program. The third bench has capacities to adjust magnetic field directions and changes to the energizing cycles that are not normally available to the standard user, which greatly expanded the MPI capabilities and enhanced the research. Prior to delivery to ISU, the unit was used for demonstrations to potential customers in the Magnaflux Chicago facility. It was shipped to the Magnaflux manufacturing facility in DeWitt, IA for refurbishing and service prior to delivery to ISU. During the refurbishing process, a problem with the programmable logic controller interface was detected and repaired on the donated bench. Once the system was repaired, it was shipped directly to CNDE.

A visit to Magnaflux in DeWitt, IA was conducted early in the program to tour the facility prior to the bench delivery, learn about some of the research work the company does, and discuss parameters that might be investigated in the research program. Discussions were held regarding the ways in which Magnaflux qualifies the performance of their MPI materials. These ideas and others borrowed from industry specifications and standards organization literature were used to develop a method to capture variability present in the MPI bath for purposes of maintaining repeatability. While at Magnaflux, a presentation of how benches are certified was provided, and a bench similar to the one provided to ISU was demonstrated. Once received, the MD3 bench did not need to be calibrated because it was received from the factory in a newly refurbished condition and considered calibrated.

Details of the three systems are provided in table 1 along with photographs of two of the systems.

Table 1. MPI bench parameters

	Current and Waveform	Number of Vectors	Coil Size	Demag	Photographs
ISU AD-945	5000 amp FWDC and 4000 amp AC	Single vector	20 inch	1000 amp AC decaying	
FAA AD-945	5000 amp FWDC and 4000 amp AC	Single vector	12 inch	1000 amp AC decaying	
MD3-2060L	6000 amp FWDC or HWDC and 5000 amp AC (except coil)	Multidirectional power supply– three phases: contacts, induced flow coils, and auxiliary coil	20 inch	AC and DC step down in 30 ms steps from shot settings	

An example procedure for operating the MD3 bench from Magnaflux is found in appendix B.

2.2 MOTION CART SYSTEM

A site visit from the company Automation Inc., a custom integrator of Parker motion control systems, was conducted to discuss the need for a coordinate system capable of moving a UV light and camera, or the PR-880 spotmeter used to measure brightness indications on the samples at a different time. This coordinate system provides the capability to return to the same locations on samples to provide repeatable measurements of the indications as parameters are changed. Once the decisions on the needs of such a system were finalized, a quote was provided, and a system was built and delivered. After the system was delivered, a motion cart was assembled (see figure 1) to reduce human error during the experimental studies. The cart consists of a three-axis motion arm, PR-880 photometer, camera, computer, and three UV light sources. These devices are fixed in position to help limit error during measurement, similar to the process used in the prior FPI research program.
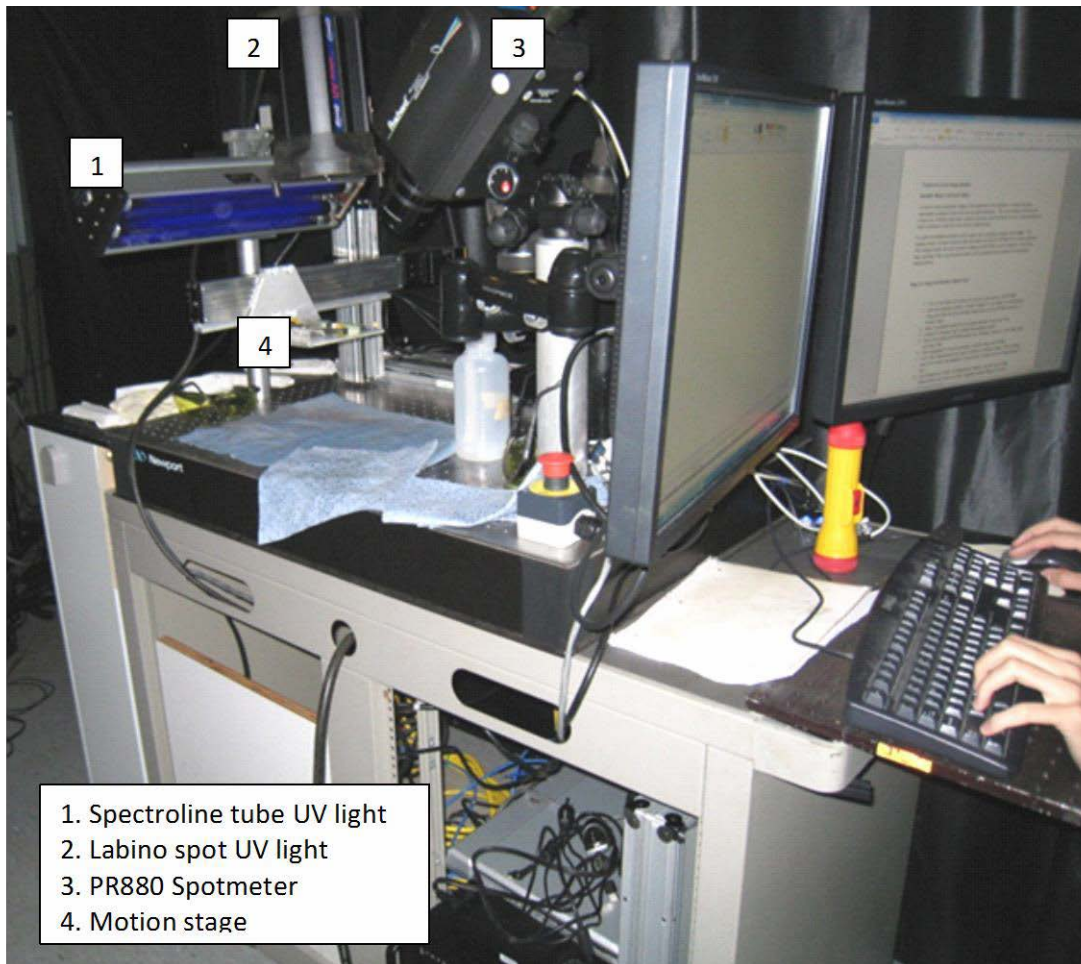
Figure 1. Portable cart used for setup of the brightness data acquisition system to control the different devices on the motion cart

A LabVIEW™ program was written and tested with the user interface shown in figure 2.
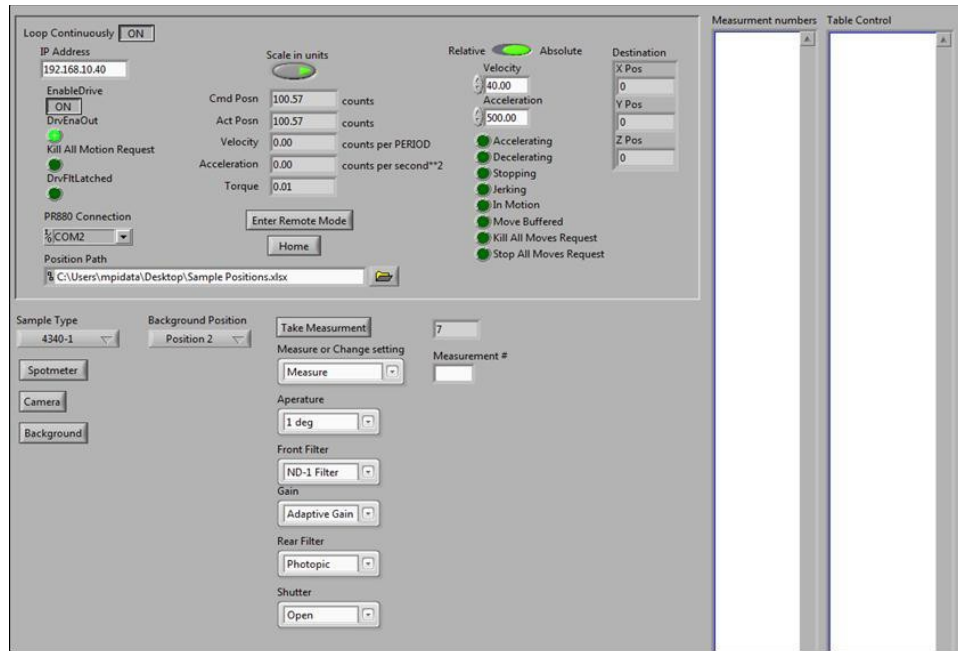
Figure 2. LabVIEW motion-controller interface

This program allows the user to control both the motion arm and the photometer from a single interface; to adjust features such as aperture, front filter, gain, and rear filter; and to move the motion tray to predetermined locations for brightness measurements. After measurements are taken, this program will display the measured values in a table format. The LabVIEW program created was also used to collect data. An example of the procedure to operate the motion control cart can be found in appendix C.

Using JMP® software, PR-880 photometer data was analyzed by comparing brightness measurements taken over the indication to background readings at the part surface but away from the indication. JMP is a commercial statistical package available at ISU for use in design of experiments and associated data analysis. The effects on indication contrast of multiple factors, including aperture size of the photometer, crack length, and amperage were studied. Using a random sampling design of experiments, the plot in figure 3 suggests that the 0.5° photometer aperture results in the greatest contrast from indication to the surroundings. Crack length and amperage have a much smaller effect (see figure 4), but larger crack sizes and lower amperages tend to increase the difference between the indication and the background. Initial studies of the effects of UV light sources on indication contrast were carried out by using two different types of UV sources. Measurements were made using either UV source, or using both simultaneously to change the intensity of the light. The results are shown in figure 5. The data was collected using five measurements at the indication and at four different background locations.
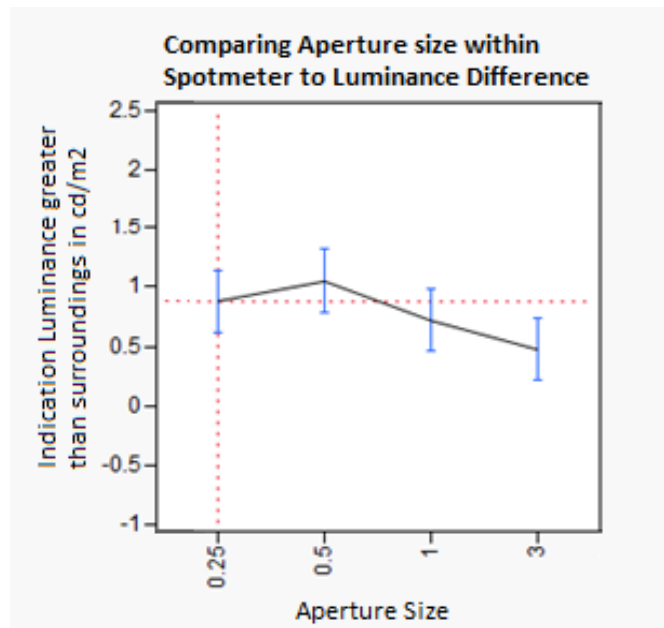
Figure 3. Results indicate that the 0.5° photometer setting is most sensitive to indication luminance when compared to the background
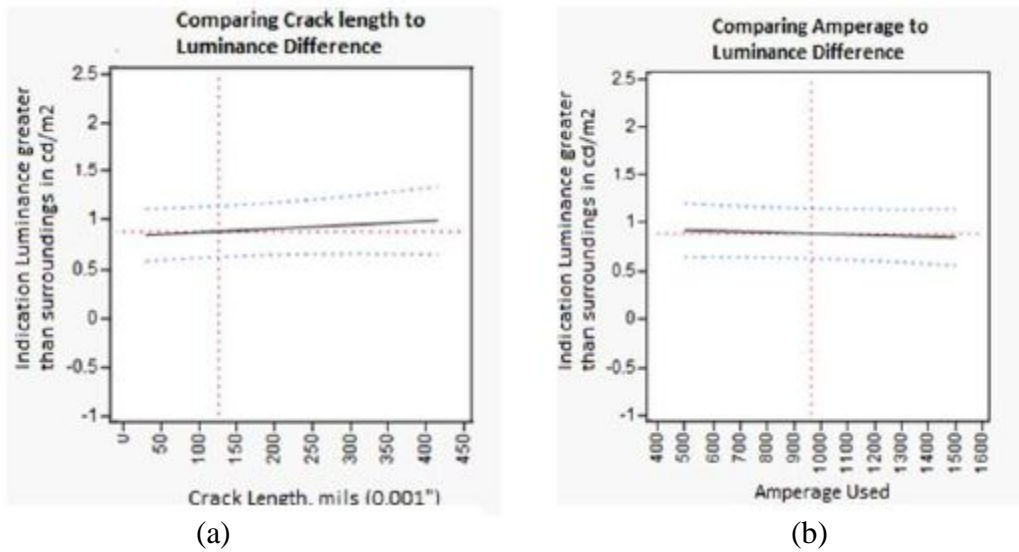
Figure 4. JMP analysis results showing (a) the effect of crack length and (b) amperage on luminance measurement
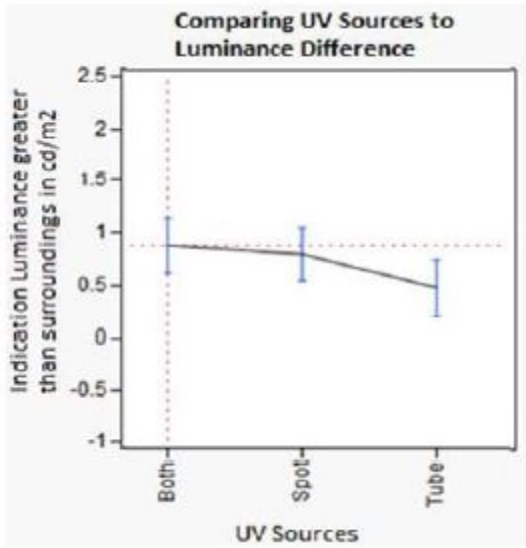
(a)
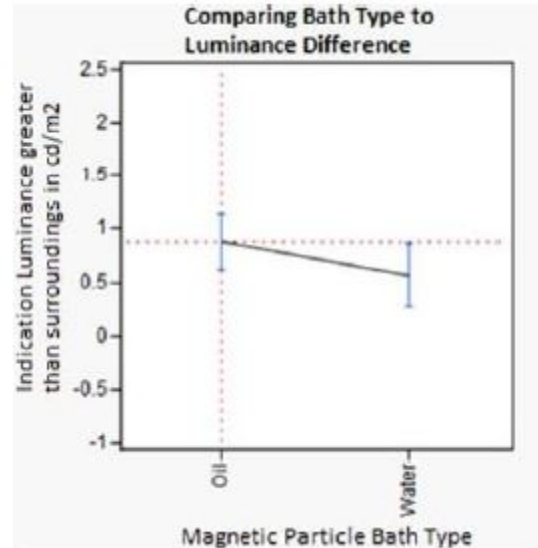
(b)

Figure 5. JMP analysis results comparing (a) UV source and MP bath type on luminance

2.3 CURRENT MEASUREMENT SYSTEM

A current measurement system developed by EM Sensors was also used for this program. The system consists of a signal processing and acquisition unit (see figure 6(a)), which is interfaced to a laptop computer via USB for portability. The system uses four linear Hall sensor arrays, each of which consists of three Hall sensors separated by known distances to detect the circumferential fields at various distances from a current-carrying cable (see figure 6(b)). The control software (see figure 6(c)) written in LabVIEW acquires the Hall sensor outputs, calculates the current from the detected circumferential field signals, and displays it over a period of time specified by the user.
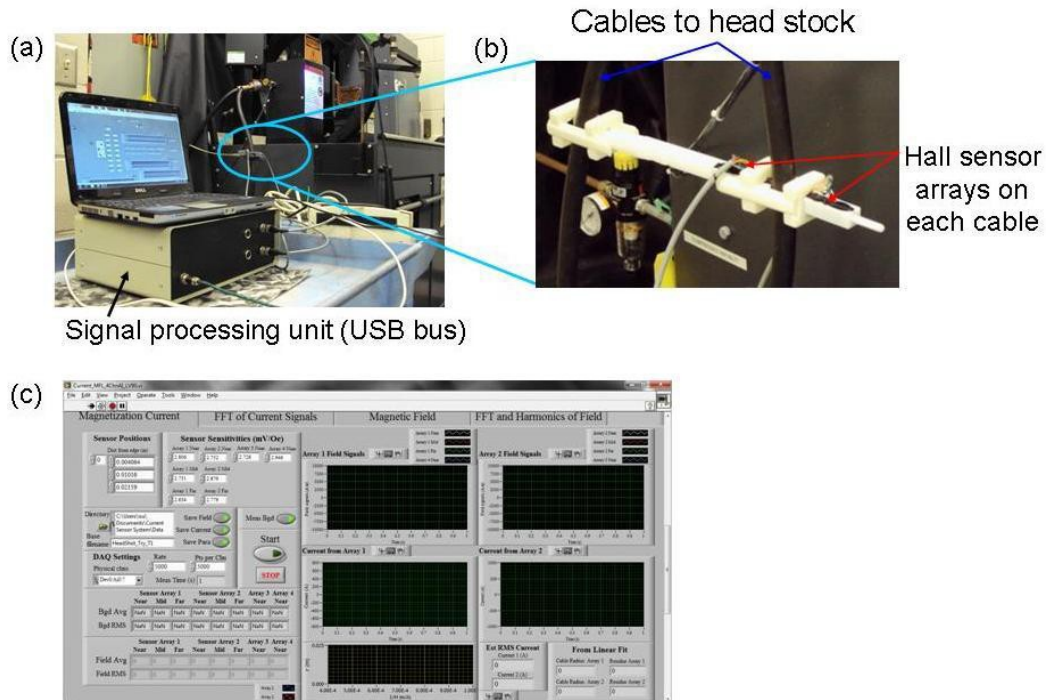
Figure 6. The (a) current measurement system; (b) two hall sensor arrays mounted on a cable of a MPI bench; and (c) the control software of the current measurement system acquires the Hall sensor outputs from which the magnetization current signal is obtained

2.4 DEVELOPMENT OF TRAINING MODULES

The program plan called for the development of education training modules that could be used in workforce development programs at FAA, companies, or other educational institutions. Development of five training modules was carried out according to the work plan defined during the early stages of the program. Each module presents different aspects of the research or issues commonly addressed in the discussion of MPI. Each of the five training modules can be found in appendices D through H.

2.4.1 Training Module #1–Variability of Equipment and Magnetizing Current

The purpose of this training module:

- MPI equipment provides users with several options of waveforms and magnetizing methods.
- Users should make the optimum choice of a waveform and magnetizing method best suited for the inspection requirement.
- For guidance, this module shows characteristics of waveforms and magnetizing methods.

The summary points from this module were:

- Several options exist for users of MPI with a bench setup, including AC, HWDC, FWDC, and flux flow.
- Certain options work better for some inspections, such as AC for surface inspection.
- Most bench readouts are within +/-10% of the bench setting.
- There are benefits and challenges to each type of option selected for MPI.
- Inductance from the inspected part can affect the amount of current required for a proper inspection.

2.4.2 Training Module #2–Material Properties and Magnetic Flux Leakage

The purpose of this training module:

- Magnetic material properties are important in MPI when users decide the magnetizing method and current value. This module explains how material properties relate to the magnetic characteristics.
- Magnetic particles attach to a specimen by magnetic flux leakage. This module demonstrates magnetic flux leakage of a specimen.

The summary points from this module were:

- There are very few parts in aviation that are made of steel, and very few alloys of steel are used in aviation.
- Parts need to be magnetized enough to create a magnetic field, but not to the point of saturation.
- Though parts do not have varying degrees of permeability within the part itself, initial studies have not shown any adverse effects to this phenomenon.
- Formulas are initially used to determine the level of current needed for magnetization, but they should always be checked with a QQI and Gauss meter in areas of interest.
- Size of the part and fill factor should be considered when using a coil for inspection.
- For any type of magnetization—either circular or longitudinal—current plays a direct role in the magnetic field created.
- For any magnetization level created, when checked with a Gauss meter, one needs to remember that the field in the Z-direction drops off rapidly with increasing distance from the surface.

2.4.3 Training Module #3–Magnetic Field Strength and Detectability

The purpose of this training module:

- Examine the strength of the excitation field or the flux leakage from a crack and how it compares to the detectability of a crack with MPI.

The summary points from this module were:

- Crack morphology (i.e., width, length, and depth—depth being the most important) can greatly affect detectability.
- Small flux leakage differences are difficult to detect; therefore, care should be taken when making measurements.
- Magnetic permeability is of greater importance when doing a coil shot.
- Residual magnetic flux direction is important when DC current is used.
- Location of the flux sensor on a part is important for coil shots.
- Permeability and position can affect sensor readings.

2.4.4 Training Module #4–Effects of Sample Status

The purpose of this training module:

- Shows what effects sample status has on magnetic particle patterns, which is important because MPI users make decisions about magnetizing methods.

The summary points from this module were:

- The roughness of a sample can have an effect on the ability to find defects due to particle accumulation on the surface.
- Coatings on the surface may hinder defect detection by creating too great a distance in the Z direction, between the generated field and the part's base material.
- Contamination may reduce the flow of particles on the surface of the part, thereby reducing effectiveness of the process.
- Geometry may be one of the biggest detractors in MPI—complex geometries may be mistaken for defects or may cover the defect by the natural accumulation of particles at sharp angles.

2.4.5 Training Module #5–Aspects That Can Affect MPI

The purpose of this training module:

- Illustrates some of the effects that bath characteristics, such as concentration and contamination, can have on the MPI process and results.

The summary points from this module were:

- There are various types of iron powder, but few are used in MPI. The most often used is Fe_2O_3.
- Pure iron powder is not used because of its low flux density.
- Particles are sized according to the use—smaller particles for smaller cracks.
- In aviation, most particles are fluorescent-polymer coated.
- Though there are recommended values for particle concentration, these values have been found to be conservative with respect to bath detriment.

- Thorough scrubbing of the holding tank prior to any settling test is one of the most important aspects of bench startup.
- There are many factors that can lead to contamination, not only to the bath itself but also to the surface of the inspected part.
- Heat damage to the bath can result from long-term operation. This can lead to a premature need for bath replacement.
- Particle clumping and wearing off of the polymer coating from the particles are just a few negative effects of heat damage.

2.5 SAMPLE MATERIALS

Based on input from the industrial members, two ferrous alloys were selected and purchased for the program. Raw stock of 4130 and 4340 steel was received and stored while sample fabrication procedures were developed. Materials were received as both round stock in 2″, 4″, and 6″ diameter, as well as 1″, 2″, 4″, and 6″ square stock. These sizes allowed for the development of fatigue samples with cracks at various orientations.

3. IN SITU MEASUREMENTS

3.1 LEAKAGE FIELDS FROM AN ELECTRICAL DISCHARGE MACHINING NOTCH

The study of in situ measurements of leakage magnetic fields from electrical discharge machining (EDM) notches in the round bar stock was aimed to help identify, with the use of artificial defects with known dimensions, the optimum magnetizing conditions for MPI indications. In this study, the radial component of the leakage field at a longitudinal EDM notch in a 1″ 4340 round stock was measured when it was magnetized by head shots (see figure 7). Two Hall sensors were used. One of them was placed directly on the EDM notch to detect the leakage field, while the other was placed away from the notch to detect any background field. The sample was first AC demagnetized. Measurements were repeated at various additional sensor liftoffs up to 12.5 mil (0.32 mm) to study how the leakage field signal decays with distance. The plots in figure 8(a)–8(e) show the time domain leakage field signals detected at various sensor liftoffs during 1-second head shots using a DC current of 480 amp. The field signals were found to have a waveform typical of a half-wave rectified DC signal. This can be explained by considering the fact that both the circumferential magnetizing field and the leakage field at the notch have the similar waveforms as the magnetizing current, which in this case has a half-wave rectified DC waveform. The root mean square (RMS) value of the detected leakage field decreases with increasing liftoff (see figure 8(f)). The result can be used to estimate, by means of extrapolation, the radial component of the leakage field and field gradient at the bar surface, which are the most relevant parameters determining the attractive forces exerting on MPs during MPI tests.
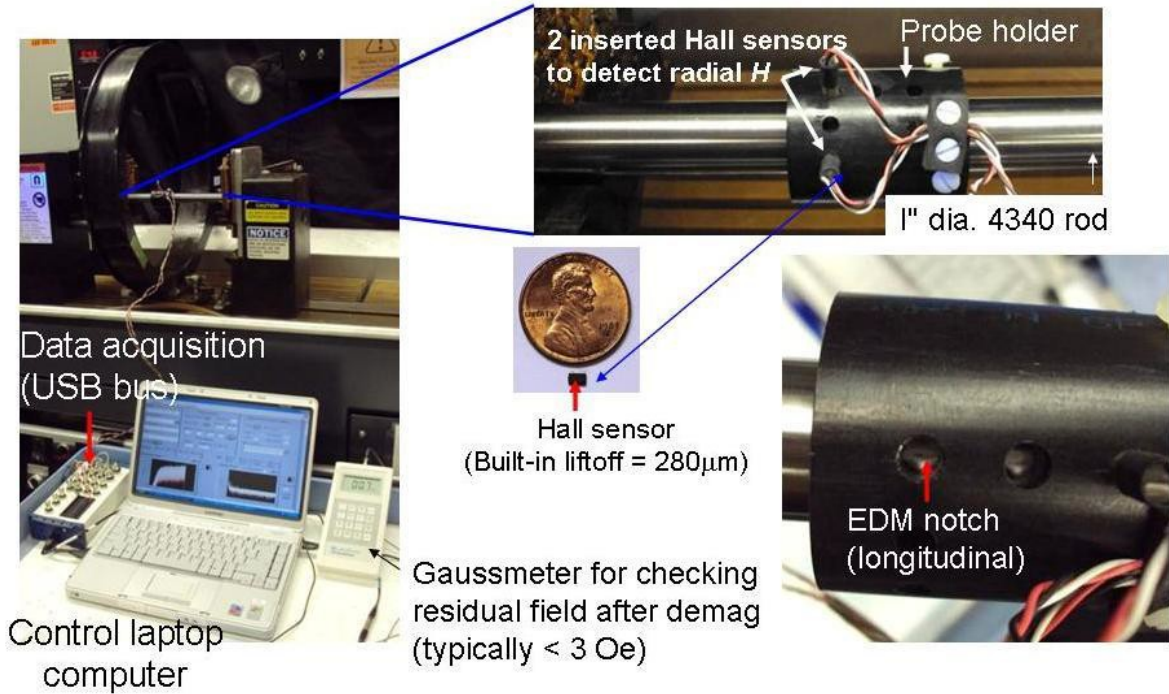
Note: Two Hall effect sensors were used to detect the radial component of field at the notch and away from the notch. The sensor outputs were recorded in a laptop PC for storage and analysis using USB-DAQ and custom software written in LabVIEW. Notice that the Hall sensors have a built-in liftoff of 0.28 mm (11 mil).

Figure 7. Experimental setup for in situ measurements of leakage flux on a longitudinal EDM notch in a 4340 round stock subjected to head shot on an MPI bench (Magnaflux AD-945)
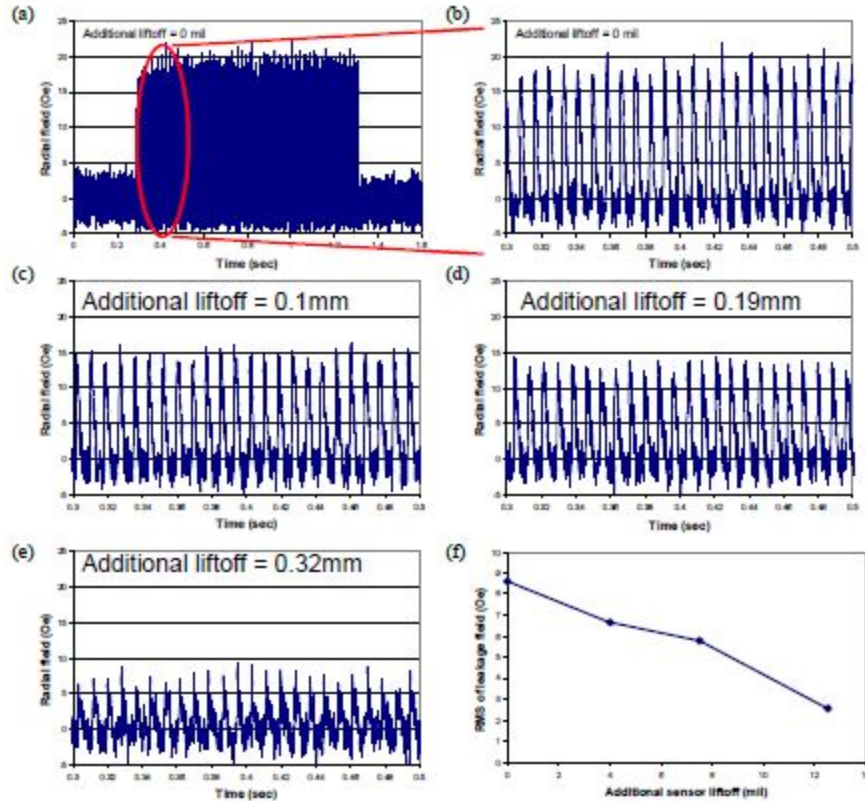
Figure 8. The (a) radial component of the leakage field measured, at no additional sensor liftoff, from the EDM notch during a 1-second head shot using a DC current of 480 amp. (The plot in (b) shows in detail the leakage field waveform that resembles a half-wave rectified DC signal. It is noted that even at no additional liftoff, the detected signal correspond to the leakage field at a distance of 0.28 mm from the bar surface due to the built-in liftoff of the hall element [see figure 1]. Plots in (c)–(e) show the leakage field signals measured at additional sensor liftoffs of (c) 0.1 mm [4mil], (d) 0.19 mm [7.5 mil], and (e) 0.32 mm [12.5 mil]. The plot in (f) shows the RMS value of leakage field as a function of the additional sensor liftoff.)

One of the objectives of this project is to provide quantitative data that will help elucidate the relationships between magnetizing current waveform and leakage fluxes from realistic defects, so that guidelines for optimizing magnetization conditions can be developed. To this end, a holder has been made for conducting in situ leakage flux measurements on the newly fabricated fatigue crack samples under coil shots on an MPI bench (see figure 9). The software of the current sensor system has been integrated into the program that was developed for leakage flux measurements so that it is possible to measure simultaneously both the magnetization current and leakage flux from defect samples when they are being magnetized on a bench.

15
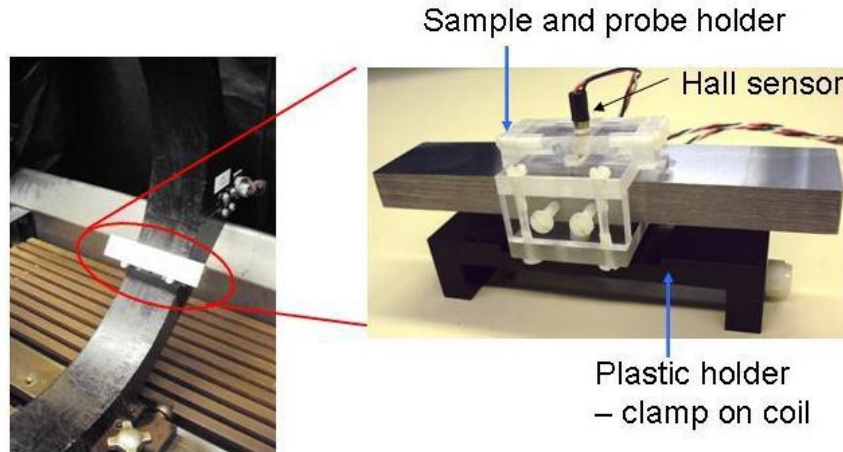
Note: A Hall sensor is used to detect the leakage field component perpendicular to the sample surface.

Figure 9. A holder for use in in situ leakage flux measurements on the newly fabricated fatigue crack samples subjected to coil shots on an MPI bench

3.2 MEASUREMENTS OF MAGNETIZATION CURRENT WAVEFORM FOR COIL AND HEAD SHOTS

The magnetization current waveforms of both coil and head shots on the MD3 bench have been characterized using a portable current sensor system. The surface fields on a steel bar subjected to head shots at various amperages have also been measured. The objectives of the study were two-fold: 1) to examine relationships between the bench current readouts and the characteristics of the current waveform, including the RMS value and peak current; and 2) to identify correlations between the magnetization current and the resulting surface magnetic field of a given part, which will be used for comparing quantitatively the sensitivities of several field indicators including Castrol Strip, QQI, and pie gauge.

Figure 10 shows the experimental setup for measuring current waveform of coils. The current sensor system consists of four linear arrays of Hall effect sensors mounted on the current-carrying cable to the magnetizing coil of the MD3 bench. The Hall sensors in each array measure the circumferential magnetic field at different distances from the cable, from which the magnetization current can be estimated. For comparison, the current was also measured by detecting the potential drop across a shunt resistor, which was connected in series with the cable to the coil. The temperature of the shunt resistor was monitored using a K-type thermocouple to make sure that measurements were made with the shunt resistor being at nominally the same ambient temperature. Waveform measurements were carried out for 1-second coil shots at various amperages ranging from 1%–50% of the full scale (FS). The outputs of the current sensor system and the potential drop across the shunt resistors were recorded in the laptop computer using a LabVIEW program for detailed analysis.
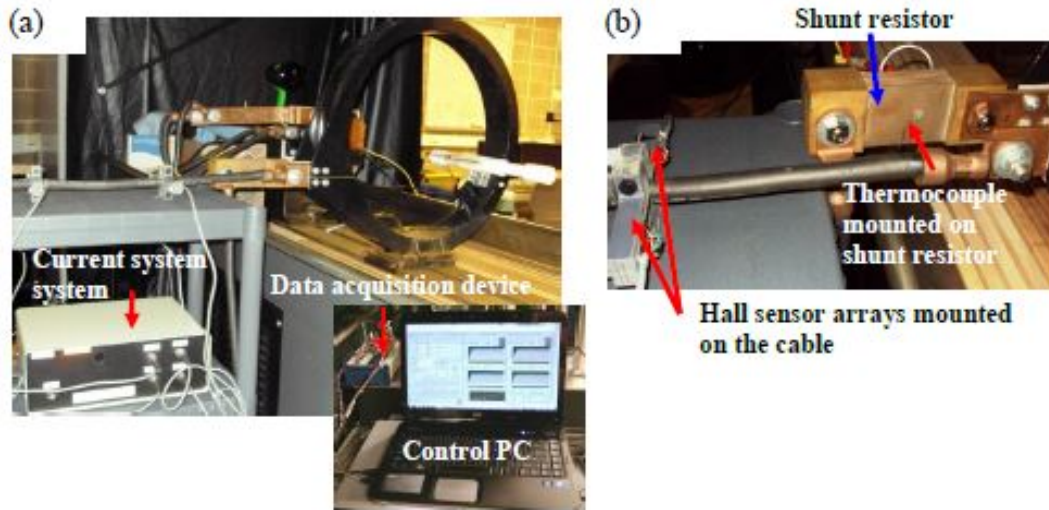
Note: A shunt resistor was also used to measure the current for comparison with the current sensor outputs. The potential drop across the shunt resistor was acquired using a data acquisition device (DAQ, USB-6251, National Instrument, Inc.) into a laptop (see inset) which was also used to control the current sensor system

Figure 10. The (a) experimental setup used to measure magnetization current waveform under coil shots on the MD3 bench; the (b) linear arrays of Hall effect sensors were attached to the cable

As an example, the current waveforms of AC coil shots at 5% and 50 % FS are shown in figure 11 for comparison. During the shot, the amplitude of the magnetization current increases rapidly within the first 0.2 second and then reaches a maximum level that increases with the amperage settings. The current waveforms were analyzed using a MATLAB® program to extract three parameters that describes the characteristics of the waveforms (i.e., the rise time, the RMS value, and the peak current level of the plateau region). The peak value of the current waveform first increases exponentially with time, with a time constant estimated by least-square fitting to be about 0.047 second (see figure 12). Of special note is that not only the peak current but also the duty cycle of the magnetization current increase with the amperage (see figures 7(c) and 7(d)).
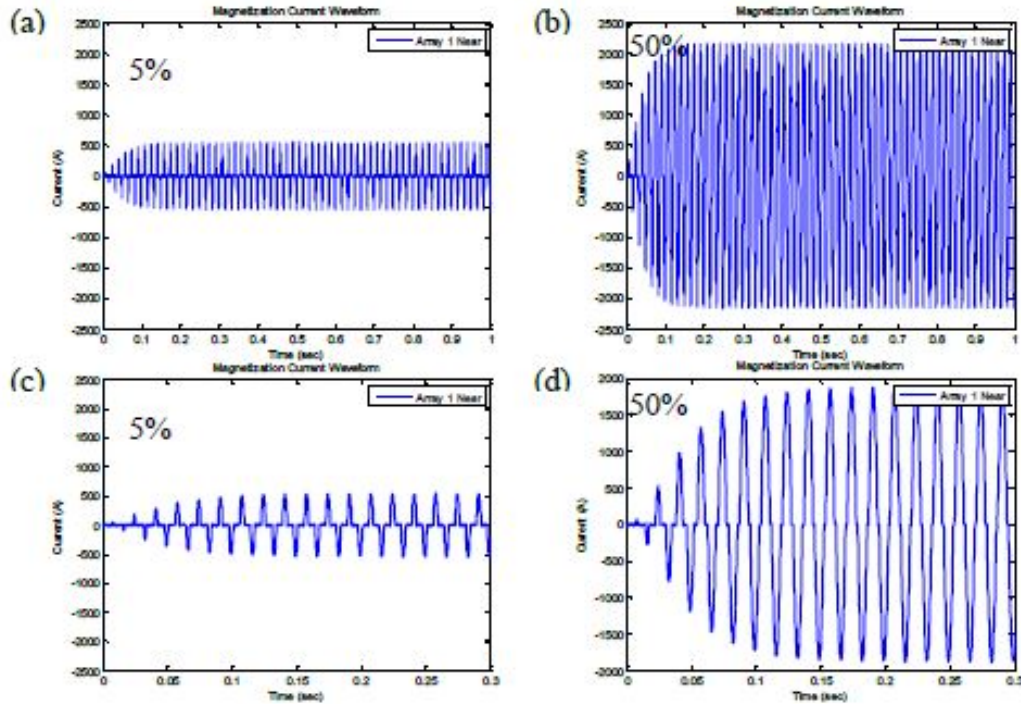
Note: Both the amplitude and duty cycle of the magnetization current increase with the amperage.

Figure 11. Current waveforms for 1-second AC coil shots at (a) 5% and (b) 50% FS (figures (c) and (d) show the corresponding waveforms for the first 0.3 second)

$$I^{Amp} \propto I_r^{Amp}\left[1 - \exp\left(-t/T_0\right)\right]$$

Current amplitude I^{Amp} increases exponentially to the peak level within the first ~0.2 sec
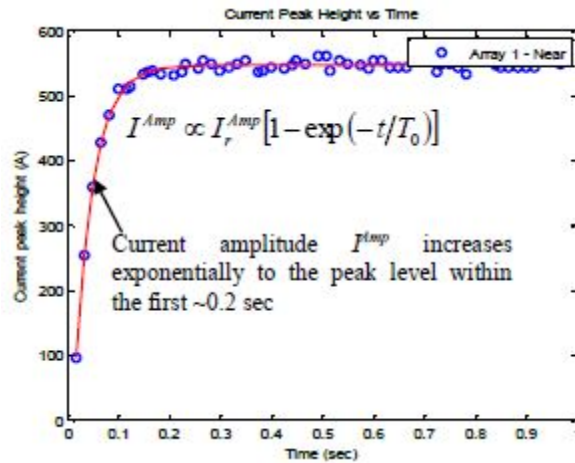
Note: The red dotted line represents the best fit of the exponential function (shown in the plot) to the data. The fitting parameter, t_0, denotes the rise time of the peak value of the current waveform.

Figure 12. Plot of the measured peak values (symbols) of the current cycles versus time

The current waveforms for HWDC and FWDC coil shots are shown in figure 13. Similar to the waveforms of AC coil shots, both the amplitude and duty cycle of the current increase with the amperage. The FWDC current has a duty cycle approximately twice as large, but a smaller peak current level than the corresponding HWDC current measured at the same amperage.
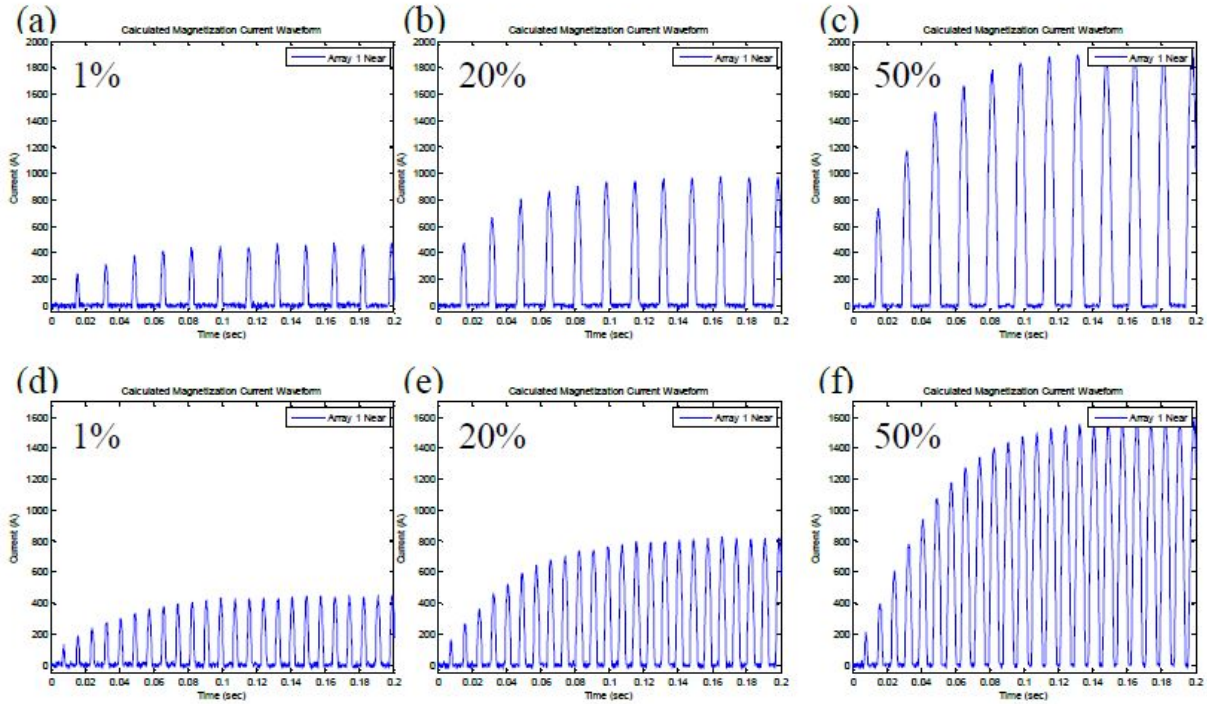
Figure 13. Current waveforms of the first 0.2 second of HWDC coil shots at (a) 1%, (b) 20%, and (c) 50% FS (figures (d) to (f) are current waveforms for FWDC coils shots at 1%, 20%, and 50%, respectively)

Figure 14 shows the plots of the RMS value and peak current level versus the bench current readout for AC, HWDC, and FWDC coil shots. It is evident that both the RMS value and the peak level of the current waveforms are linearly proportional to the bench readout within the amperage range (1%–50% FS) covered in this study. These linear relationships can be used as empirical calibrations for estimating the peak current from the bench readouts for all three types of coil shots.
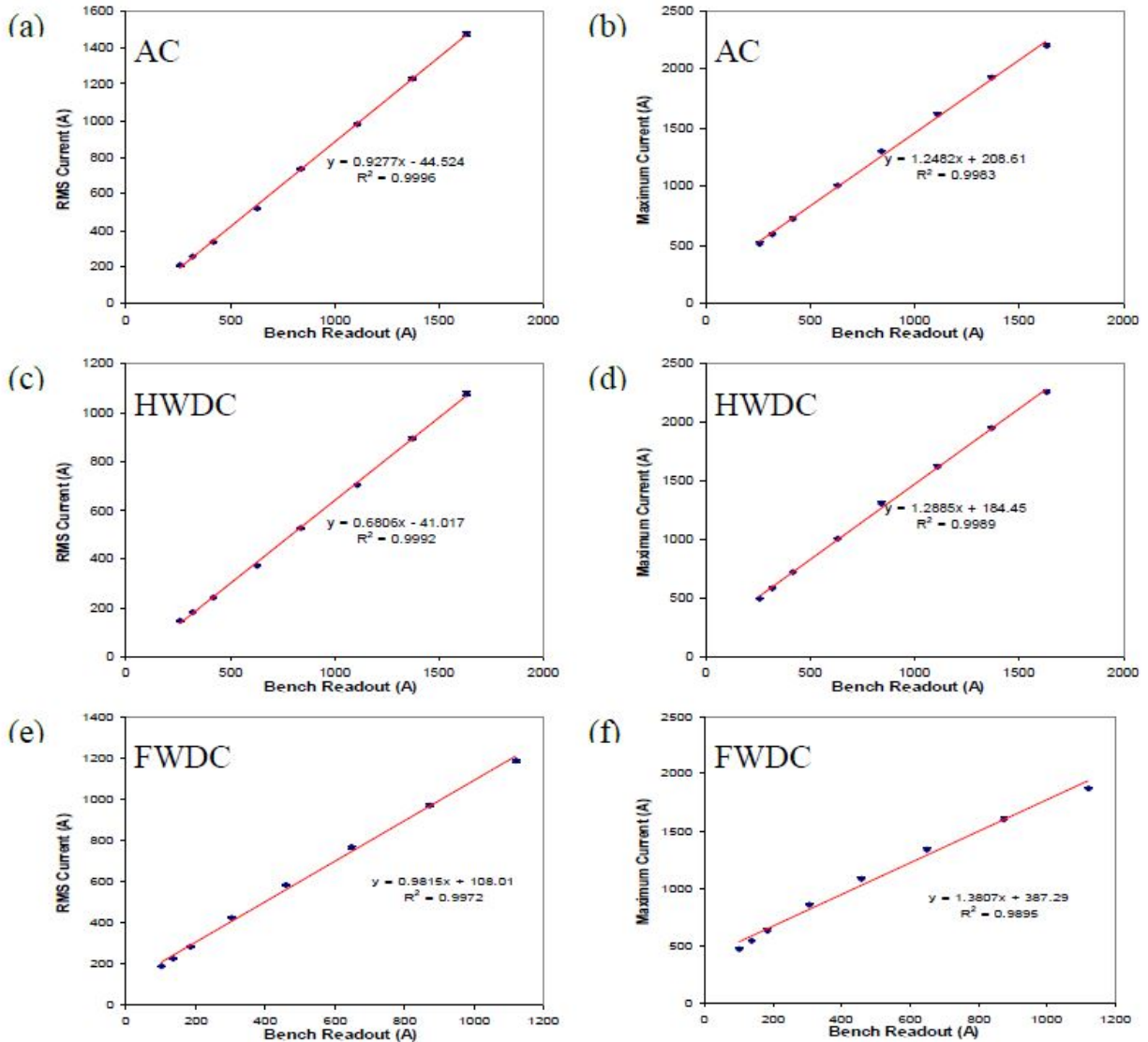
Note: In all cases the current waveform parameters vary linearly with the bench current readout.

Figure 14. Plot of (a) RMS value and (b) peak current level of the current waveforms measured for AC coil shots (figures (c) and (d) are the corresponding plots for HWDC coil shots, and (e) and (f) for FWDC shots)

The accuracy of the current sensor outputs was evaluated by performing a comparison study with the current waveforms that were measured using the shunt resistor. The RMS value and peak current level measured using the current sensor system and the shunt resistor were directly compared (see figure 15) and were found to agree with each other to within 2% in all cases. In general, the RMS values show better agreement than the peak current level, probably because any offset in the acquired potential drop signals across the shunt resistor would more strongly affect the peak values of both HWDC and FWDC waveforms than the RMS values. The present results indicate that the current sensor system can be reliably used to measure current waveforms in the time domain using detachable Hall sensor arrays, without the need to connect a shunt resistor to the cable.

20
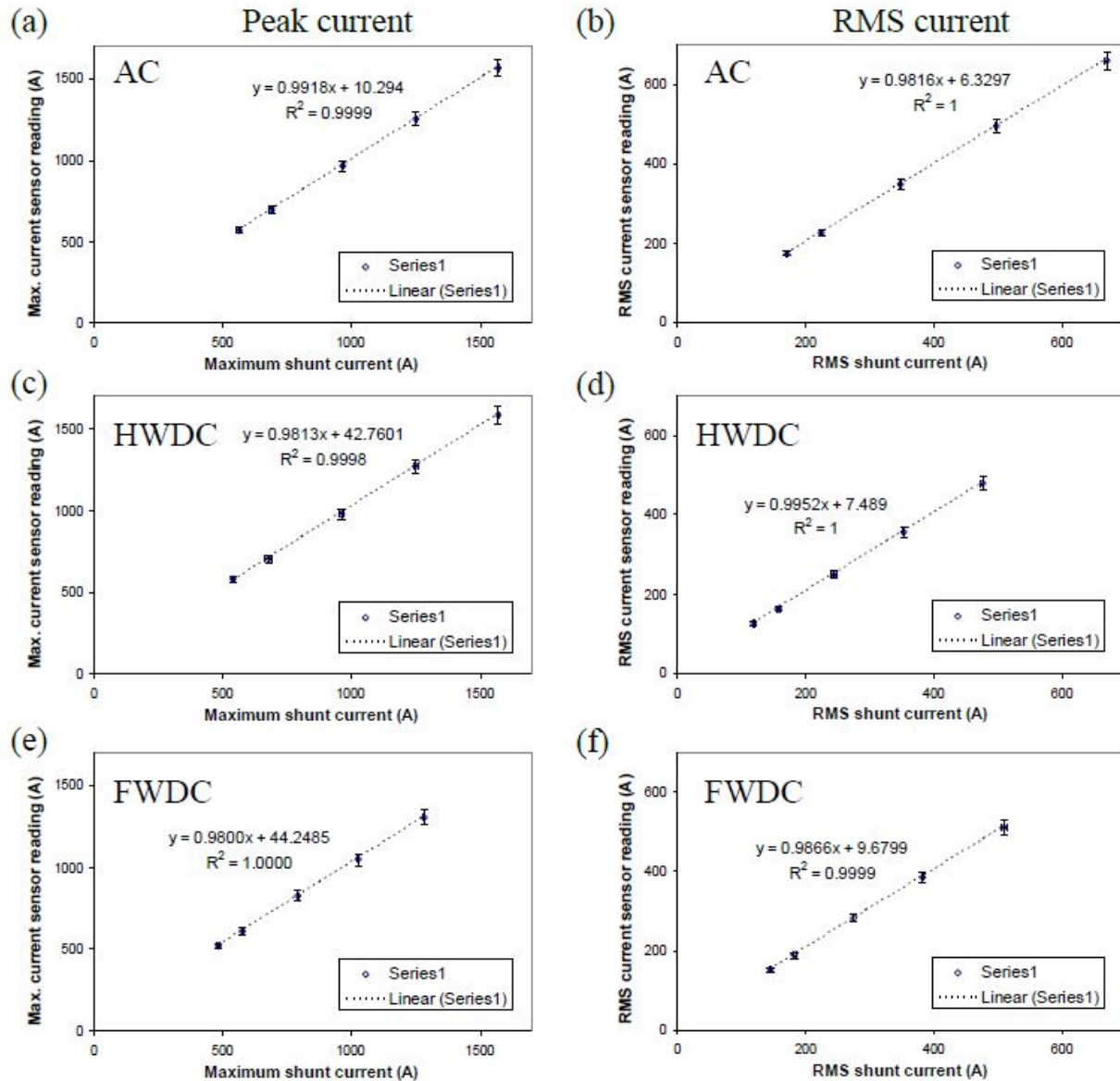
Figure 15. Plots of (a) the peak levels and (b) RMS values of the current waveforms measured with the current sensor system versus the corresponding waveform parameters measured using a shunt resistor for AC coil shots (figures (c) and (d) are the corresponding plots for HWDC coil shots, and (e) and (f) for FWDC shots)

The authors have also characterized simultaneously the time-domain current waveforms and the surface magnetic field on a steel bar subjected to HWDC head shots as part of a study aimed at comparing quantitatively the sensitivities of common field indicators including Castrol Strip, QQI, and pie gauge. The experimental setup is shown in figure 16. An 18″ long steel bar with a 2″ × 2″ cross section was subjected to 0.5 second HWDC head shots at various amperages from 1%–18% FS. The MD3 bench has three cables connected to the headstock. In this case, the current flowing through two of the cables was simultaneously measured by attaching two Hall sensor arrays onto each of the two cables (see figure 16(a)). The average current through these two cables was then

calculated and multiplied by a factor of 3 to estimate the total current flowing into the headstock. A Hall sensor integrated circuit (model: 2SA-10, Sentron) was mounted onto the steel bar to measure the magnetic field in the transverse direction (see figures 16(b) and 16(c)). Both the magnetization current and magnetic field at the bar surface were measured simultaneously. The measurements were repeated three times at each amperage to obtain the average values and standard derivations of the detected signals.
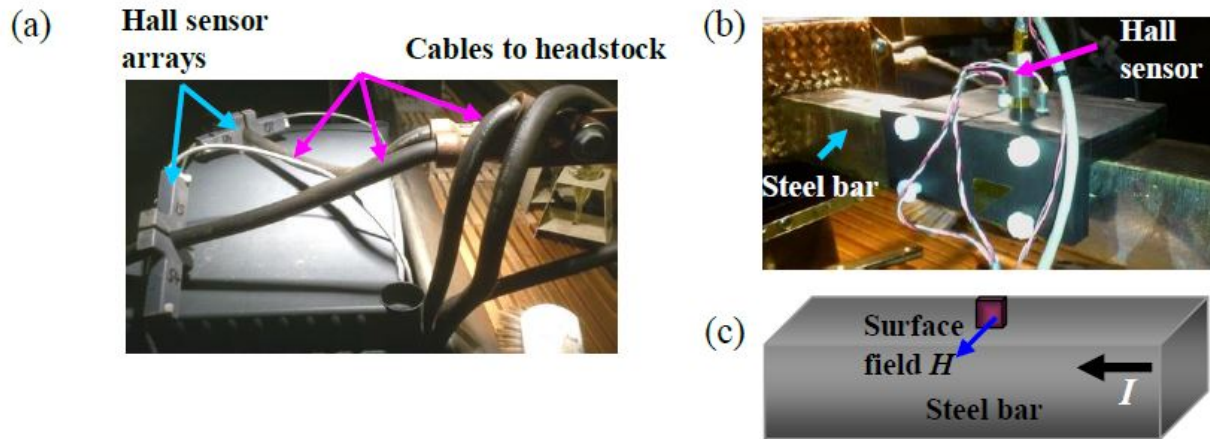
Figure 16. The (a) experimental setup showing the Hall sensor arrays attached to two of the three cables to the headstock of the MD3 bench (A (b) photograph showing a Hall sensor mounted onto the steel bar to measure the transverse magnetic field at the sample surface, as shown in the schematic diagram in (c). The Hall sensor has a built-in liftoff of 0.8 mm.)

As an example, the current waveform measured from one cable for an 18% FS head shot is shown in figure 17(a). In this case, the RMS and peak currents were measured to be 113 amp and 369 amp, respectively. The total current to the headstock was estimated from the average current through two cables to have a peak value of 1203 amp and an RMS value of 345 amp, which is comparable to the bench readout of 357 amp. Both the RMS value and the peak current level correlate linearly with the bench readout (see figure 17). The transverse magnetic field measured at the sample surface was also found to vary linearly with the peak level of the measured current waveform and the bench readout. The linear dependence of both the magnetizing current and surface magnetic field on the bench reading (see figure 18) offers empirical calibrations that were used to quantify the sensitivities of Castrol Strip, QQI, and pie gauge in a comparison study discussed later in this report.
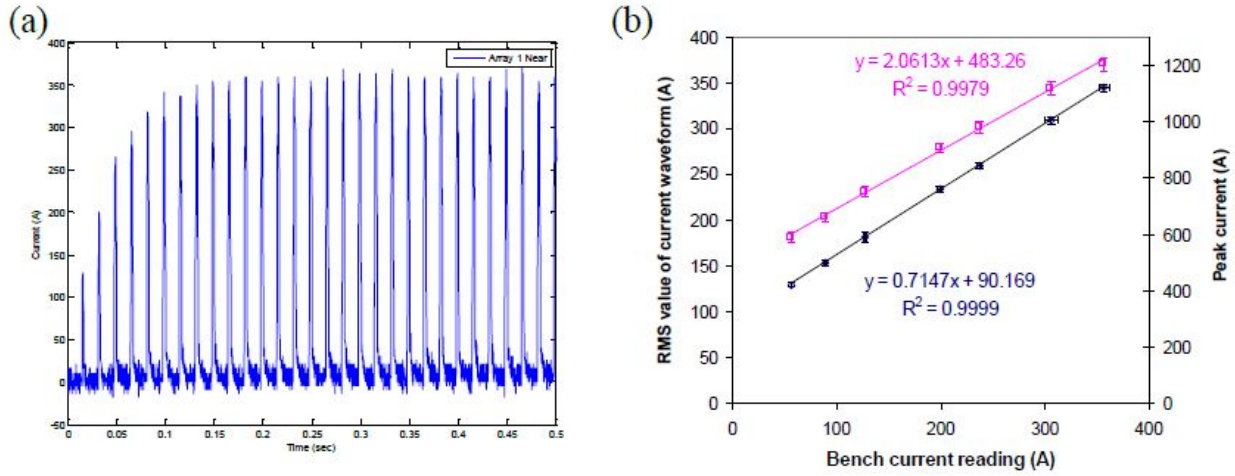
Figure 17. The (a) current waveform measured for HWDC head shots at 18% FS (The (b) plots of the RMS value (dark blue symbols) and peak current level [pink symbols] of the measured current waveforms as a function of the bench current readout. The dotted lines represent least-square linear fits to the data)
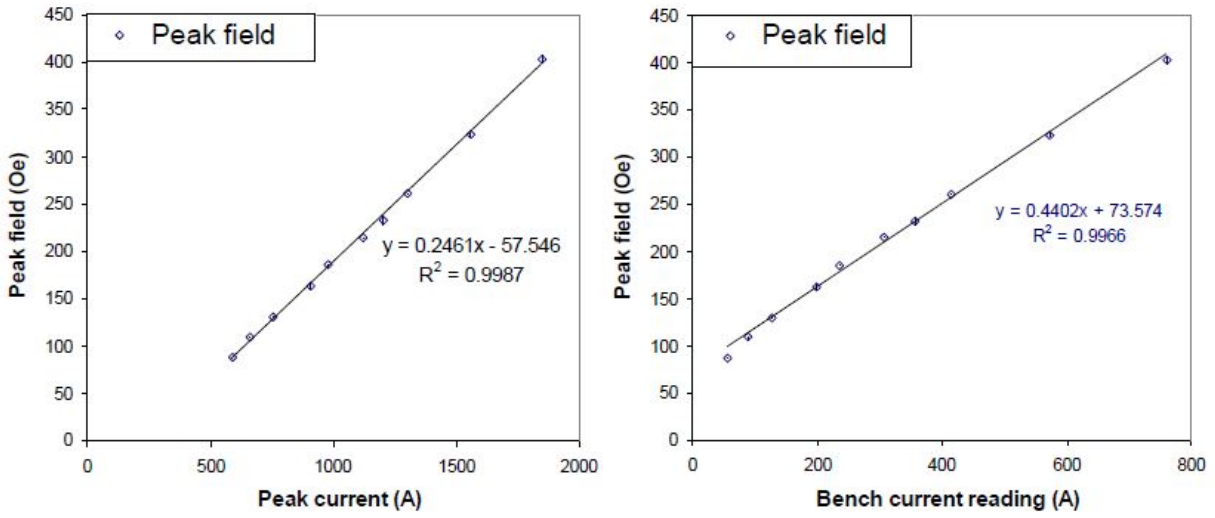
Figure 18. Plot of peak magnetic field versus (a) the peak current and (b) bench readout for HWDC head shots from 1%–18% FS

3.3 MEASUREMENTS OF MAGNETIZATION CURRENT WAVEFORM FOR AC HEAD SHOTS

The authors have characterized the magnetization current waveforms and surface magnetic field on a steel bar subjected to AC head shots as part of a study aimed at comparing the sensitivities of several field indicators including Castrol Strip, QQI, and pie gauge. The overall objective of the study was to evaluate quantitatively the usefulness of these field indicators for use in determining the adequate current level for MPI inspections.

The experimental setup for measuring head-shot current waveform and the resulting surface fields on a 2″ x 2″ x 12″ square steel bar is shown in figure 19. The steel bar was subjected to AC head shots for 1 second and various amperages ranging from 1%–45% of the full scale. The magnetizing currents were measured using a proprietary current sensor system and a shunt resistor for comparison. The current sensor system uses four detachable, linear arrays of Hall effect sensors, which were mounted on two of the three cables attached to the headstock (see figure 19(b)), to measure the circumferential fields around the cables, from which the currents through the cables were determined. The average value of the two currents was multiplied by a factor of 3 to obtain the total head-shot current. The current through one of the headstock cables was also directly measured by detecting the potential drop across a shunt resistor (see figure 19(b)) and was used to estimate the total shot current for comparison with the results from the current sensor system.
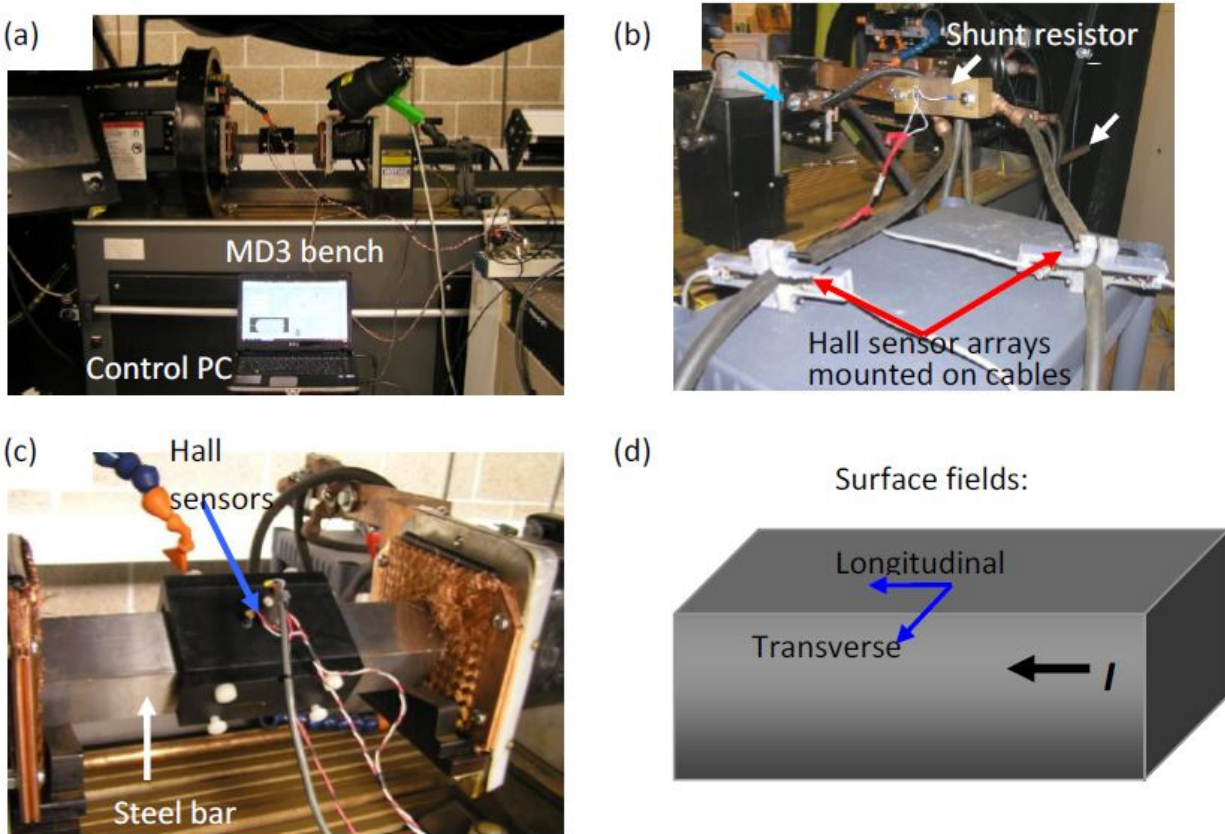
Figure 19. The (a) experimental setup used to measure magnetization current waveform and surface magnetic field under AC head shots on the MD3 bench (The (b) four linear arrays of Hall effect sensors were attached to two cables connected to the headstock. A shunt resistor was connected to one of the cables and used to measure the current directly. A (c) bi-axial Hall sensor mounted onto a 2″ □2″ □12″ steel bar to measure the surface field components. The steel bar was tilted 45□ in exactly the same orientation as it is used for the sensitivity study of QQI, Castrol Strip, and pie gauge. A (d) schematic showing the surface fields measured using the Hall sensor integrated circuit.)

The surface magnetic fields along both the transverse and longitudinal directions were measured at the center of the steel bar (see figures 19(c) and 19(d)) using a bi-axial Hall effect sensor. The

longitudinal field was measured as a means to check the alignment of Hall sensor along the samples axes, because the field induced by the head shot along the sample axis should, in principle, be zero. The longitudinal field was found to be <3 Oe in all measurements irrespective of the current levels, thereby confirming that the Hall sensor was properly along the sample axes. Both the current waveforms and surface field were measured simultaneously and acquired into a laptop computer for analysis. The measurements were repeated three times at each amperage setting. Before each head shot, the sample was first demagnetized, and its ends were wetted completely along with the copper meshes to help reduce the contact resistance.

As an example, the current waveform measured from one cable is shown in figure 20 for an AC head shot at 18% of the FS. The RMS and peak values of the currents were measured at 109 amp and 298 amp, respectively. The total current to the headstock was therefore estimated to have a peak value of 917 amp and an RMS value of 336 amp, which is approximately 65% of the average bench current readout of 497 amp.
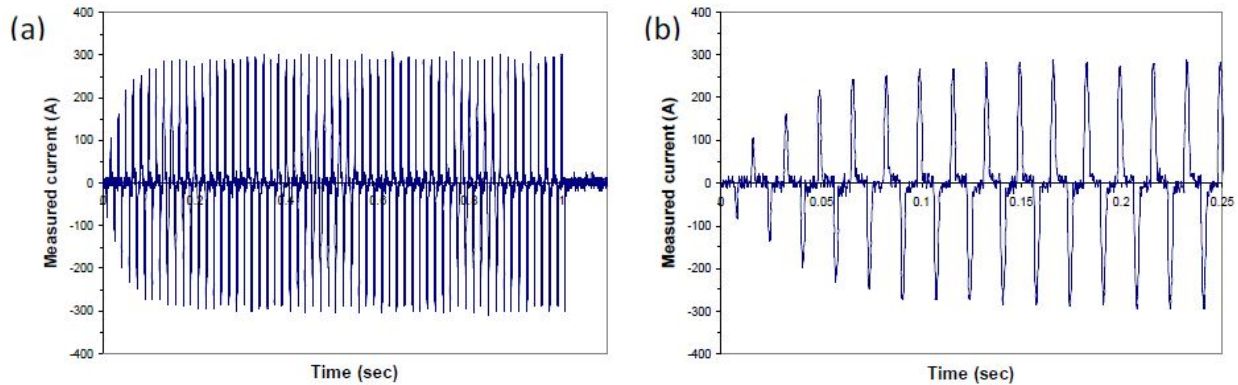
Figure 20. The (a) current waveform measured from one of the headstock cables for a 1-second AC head shot at 18% FS and an (b) expanded plot showing the details of the waveform, including the duty cycle

Both the peak height and the duty cycle of the current waveform increase with the amperage (see figure 21). The peak height and the RMS value of the current waveform were found to vary linearly with the bench reading (see figure 22), thereby offering a simple, empirical calibration for estimating the peak current from the bench reading.
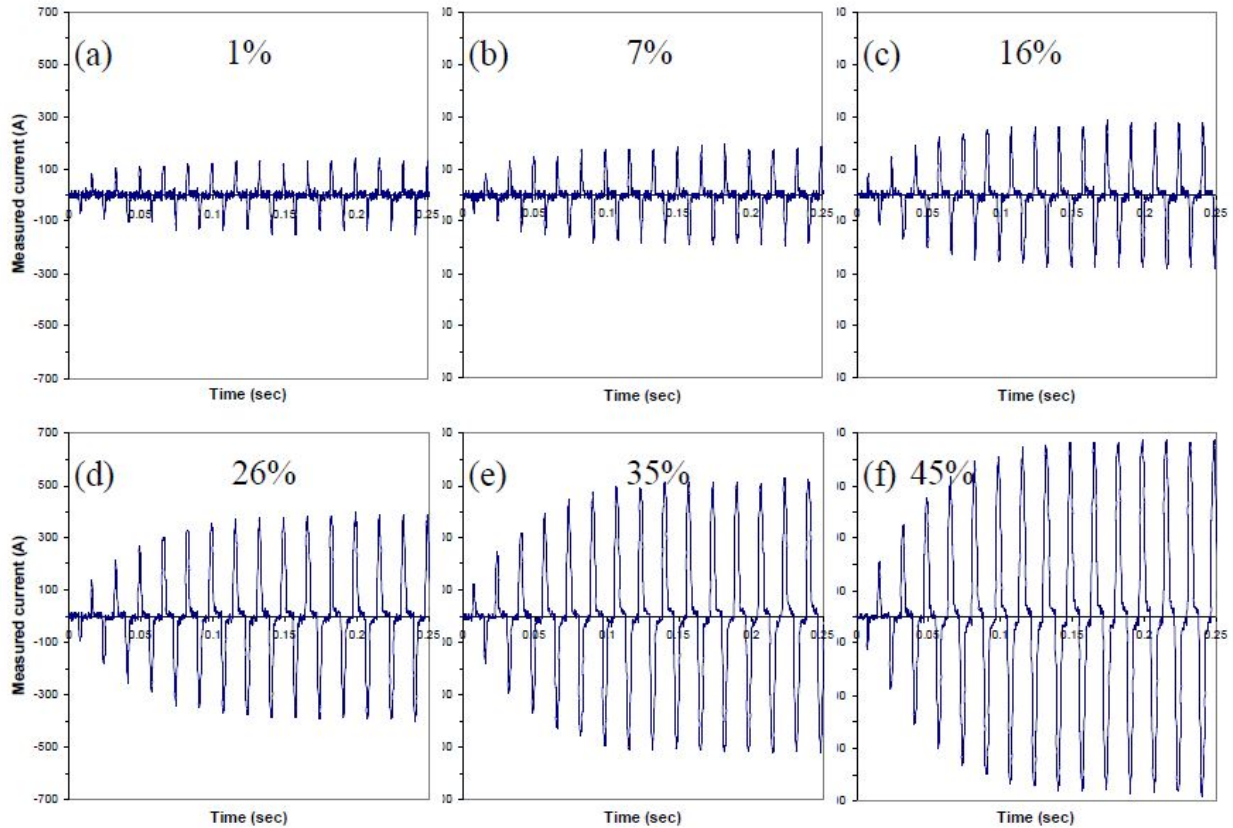
Figure 21. Current waveform of the first 0.25 second measured for amperage settings of (a) 1%, (b) 7%, (c) 16%, (d) 26%, (e) 35%, and (f) 45% of the FS
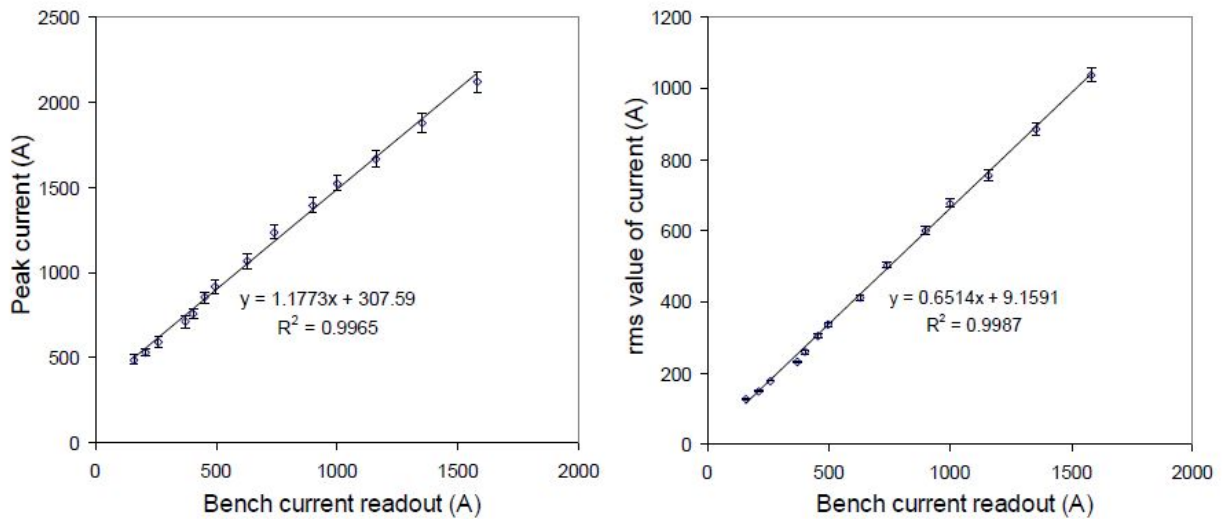
Note: Both the peak height and RMS value vary linearly with the bench readout

Figure 22. Plot of (a) peak height and (b) RMS value of the current waveforms versus the bench current readout for AC head shots

26

Figure 23 shows the waveform of the transverse magnetic field measured at the sample surface for an amperage setting of 18% of the FS. It is evident that the waveform of the surface field closely resembles that of the magnetizing current (see figures 20(b) and 23(b)). Note that the peak value of the surface field varies linearly with the peak height of the current waveform (see figure 24(a)) and the bench readout. The linear dependence of the magnetizing current and surface field on the bench reading offers useful calibrations for quantifying the sensitivities of Castrol Strip, QQI, and pie gauge when applied to the same sample.
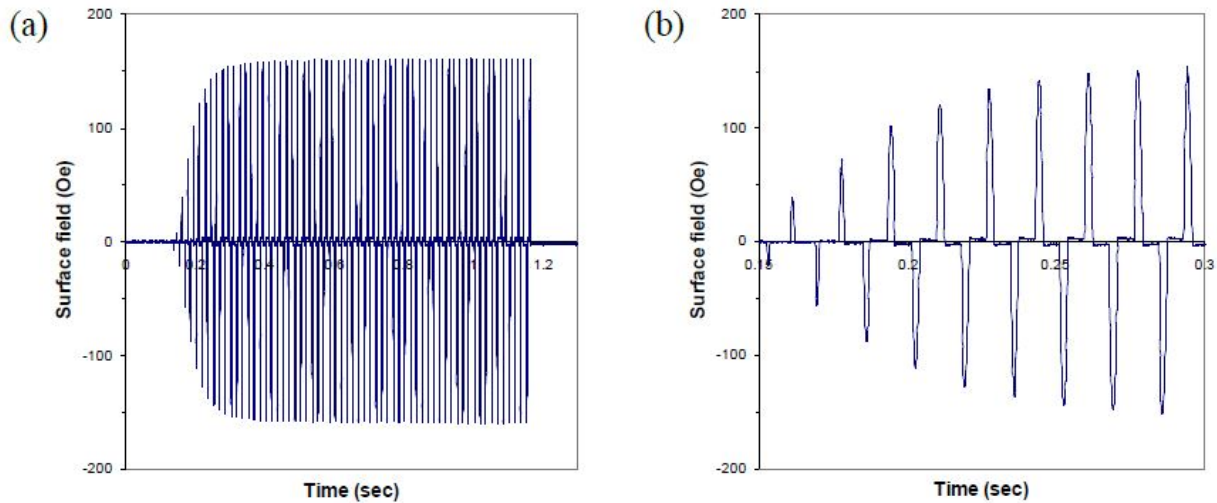
Figure 23. The (a) waveform of the transverse magnetic field measured at the center of the steel bar for AC head shots at 18% FS (An (b) expanded plot showing the details of the waveform that closely resembles the current waveform shown in figure 21)
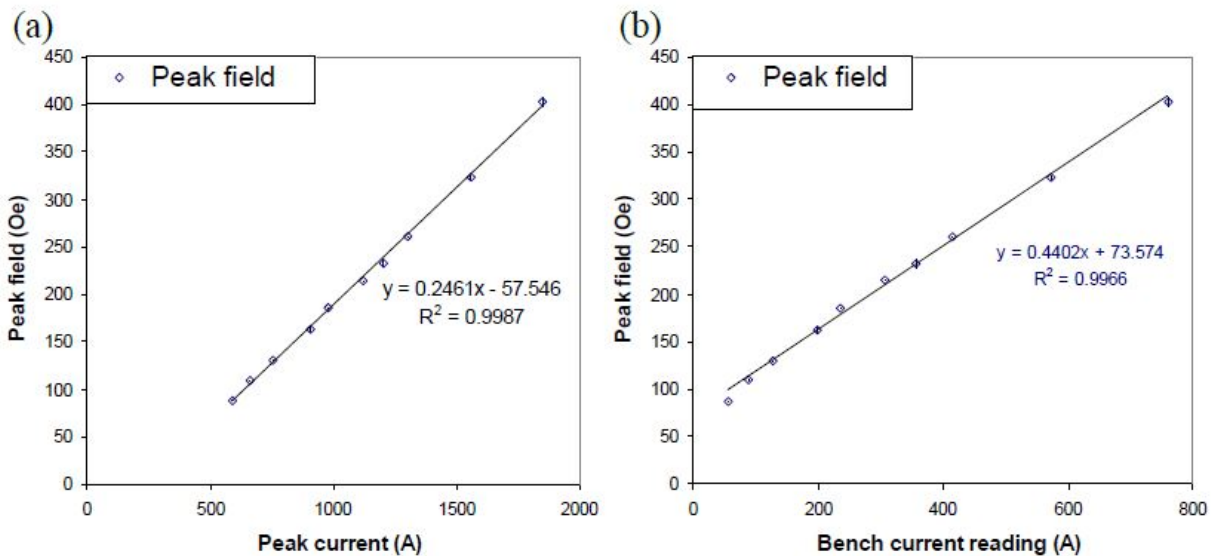
Figure 24. Plot of the peak value of the surface field versus (a) the peak current and (b) bench readout for AC head shots from amperages ranging from 1%–45% FS

4. EFFECTS OF PART PARAMETERS AND IN SITU FLUX LEAKAGE

4.1 DEVELOPMENT OF IMAGING TECHNIQUE

To quantify the ability of the particle bath to be captured by a leakage field, an image capturing technique was developed for the MTU-Type 2 block (see appendix I). After the particle bath was applied to the block, a thin line of particles was formed at the leakage field along the center of

the block. The line was bright at the edges and dim in the middle. A digital image was taken of the entire block, and the image processing software ImageJ was used to place a line profile over the entire length of the particle line. ImageJ then measured the brightness of the line. The array of brightness values was then exported to MATLAB, and a polynomial was fitted to the data. The minimum of the data was found, and a threshold value was added to the minimum. The location where the brightness equaled this threshold value was found for both sides of the block. The number of pixels between these locations was computed, and pixels can be directly related to length with the fixed imaging setup used. If the particle bath quality is compromised, the particles will not be as strongly captured by the leakage field, and the distance between the threshold value locations on each side of the block will be longer. The following parameters were examined to find the optimum settings and to determine how changing the parameters affects the results:

- Application of particles
- UV light intensity
- Angle of incidence of UV light
- Sample cleaning procedure
- Repeatability of ImageJ line profile placement
- ImageJ line width
- Order of fitted polynomial
- Threshold value

4.2 MPI INDICATION QUANTITATIVE ANALYSIS

In MPI, it is usually required for the inspector to conduct standard inspections and process control steps to attempt to verify the performance of their MPI system. There are many industry standard process control specimens used to aid in verifying the performance of the electromagnetic system as well as the magnetic particles and carrier fluid (bath). Some of the devices used include: the ISO ring (also known as Reference Block Type 1 (MTU-3)), ISO block (also known as MTU-2), and the AS5282 ring (or similar Ketos ring) (see figure 25).
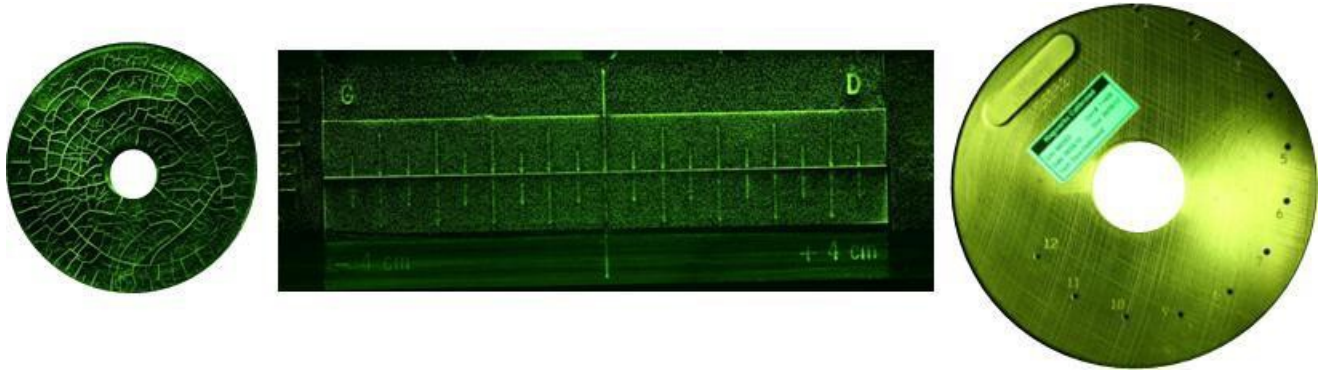
Figure 25. Shown left to right are the MTU-3, MTU-2, and an AS5282 ring

In addition to tests performed with these specimens, the inspector takes a sample of the carrier and conducts a suspension settling test. This settling test allows the inspector to verify the concentration of particles in the carrier and identify some of the possible contamination and particle degradation issues. One of the key concerns with these inspections is the variability of the test and operator subjectivity inherent in many of these process controls tests. As a result of the subjectivity, what may be an acceptable performance for one inspector may not be acceptable to another. Efforts have been concentrated on taking the subjectivity out of the process through the use of quantitative measurements.

The AS5282 ring, and similarly the Ketos ring, is a ring that is made up of a series of predrilled holes at increasing depths below the surface used to simulate subsurface defects. The distance of the holes to the surface increases as one moves to holes of increasing number. Its original purpose was to demonstrate the ability to use MPI to find subsurface flaws, but it has long since been used to perform regular performance evaluation of MPI bench systems. The intensity of the indication depends on the depth of the flaw and the amount of current passed through a central bar conductor, as shown in figure 26.
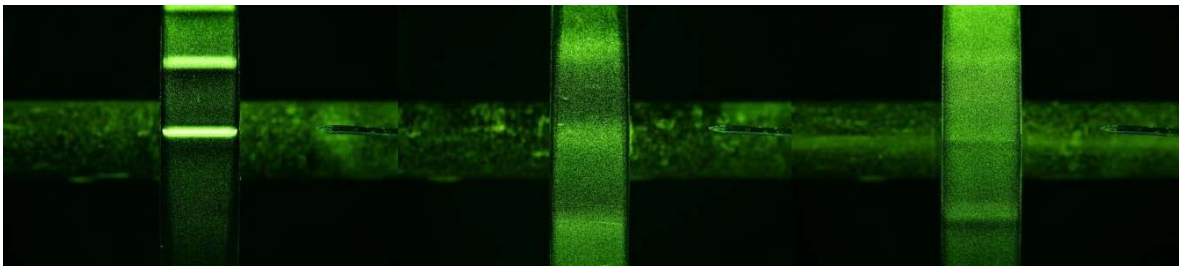
Figure 26. Images of the magnetized Ketos ring at different indication depths

When the magnetic particle fluid is applied, it contacts the surface with enough fluid flow to wash away any indications being formed by the magnetic leakage fields caused by the drilled holes. For this reason, the indications are developed by a final magnetizing shot or shots that are triggered immediately after the direct fluid flow is diverted. Orientation of the ring with respect to the fluid flow can have a significant impact on which lines develop indications with lines near the area where the fluid is applied often proving more difficult for indications to develop. A study was undertaken to determine suitability of AS5282 ring to detect an out-of-tolerance concentration of

magnetic particles, among other factors. As part of this work, an image analysis procedure was developed to reduce operator variability that is normally inherent in the ring procedure due to different operators having different thresholds for what they determine to be a formed line indication (see appendix I). Image analysis was performed using a numerical image process written in MATLAB. There are currently two MATLAB image processing and analysis procedures in use: one for the AS5282 Ring Image analysis and one for the fatigue crack image analysis. They both serve the function of eliminating subjective bias from the MPI indication and assist in collecting quantifiable data from the images.

4.3 PERMEABILITY MEASUREMENTS

The purpose of this study is to measure spatial variation in magnetic permeability in steel components, which is considered one of the component effects that could affect MPI inspection. Though magnetic permeability of a given component is usually assumed to be uniform, in reality it often varies from place to place due to several factors including, for example, variations in chemical or phase composition and non-uniform distributions of residual stress or cold work.   If spatial variation in permeability exists in a part, the MPI indication does not necessarily develop in regions with lower permeability even if an optimal magnetization condition is used for the average permeability. It is therefore the objective of this work to detect and measure the typical permeability change within a part and eventually to study how such changes affect inspection results.

In this work, the local permeability values of two square steel bars were measured using the Magnescope, which is a portable system developed at ISU for measuring magnetic hysteresis of component steel using a surface sensor probe. The experimental setup is shown in figure 27.

Note: To the right of the surface sensor probe was aligned so that the magnetizing field, H, was applied along the long axis of the steel bars. Measurements were made at spacings of 1″along the 16″ bar.

Figure 27. The experimental setup used to measure spatial variations in magnetic permeability on 4130 and 4340 alloy steel bars

Two steel bars made of 4130 and 4340 steel were studied. They have the same nominal dimensions of 2″ x2″ x18″. The surface sensor probe consists of three main components: 1) a C- core electromagnet that applies a low-frequency, periodic magnetic field to the part; 2) a Hall effect sensor to detect the tangential component of magnetic field at the part surface, and 3) a pick-up coil to detect the magnetic induction signal. The magnetic hysteresis loop was obtained by plotting the magnetic induction signal as a function of the surface field, from which the magnetic permeability can be extracted. The detected magnetic signals give an average magnetic response of the region interrogated by the applied field, which is approximately 0.5″ long for the present sensor probe. Measurements were carried out over 16″ long region of the steel bars in 1″ steps to detect permeability change within the bars.

The magnetic hysteresis loops measured from the 4130 and 4340 steel bars are shown in figure 28. Strictly speaking, permeability is not a constant. It varies over the hysteresis cycle, attaining a maximum near the coercivity and then gradually decreasing as the part approaches saturation.

In this work, the permeability at the coercivity, which represents the largest permeability values over the Hysteresis cycle, was extracted and plotted in figure 29 for the two steel bars.

The 4340 bar overall shows larger permeability values than the 4130 sample. Significant spatial changes in permeability were observed in both cases. The permeability changes by 16% and 18% for the 4130 and 4340 bars, respectively.
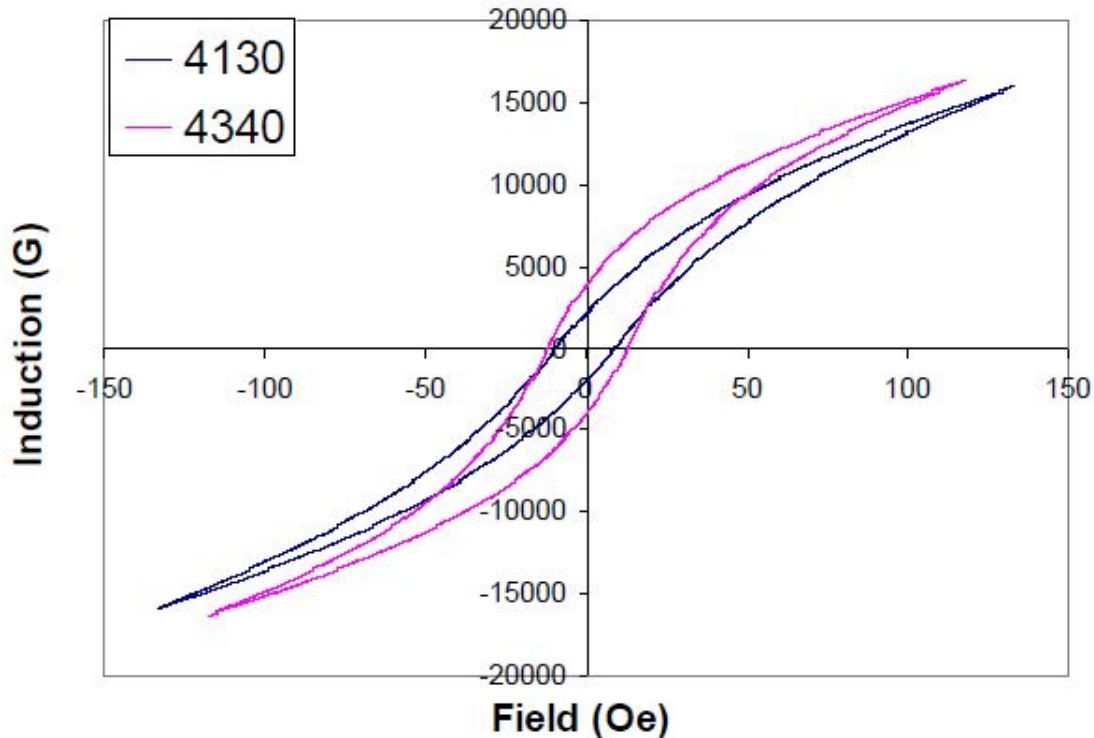
Figure 28. Magnetic hysteresis loop for 4130 and 4340 steel samples

31
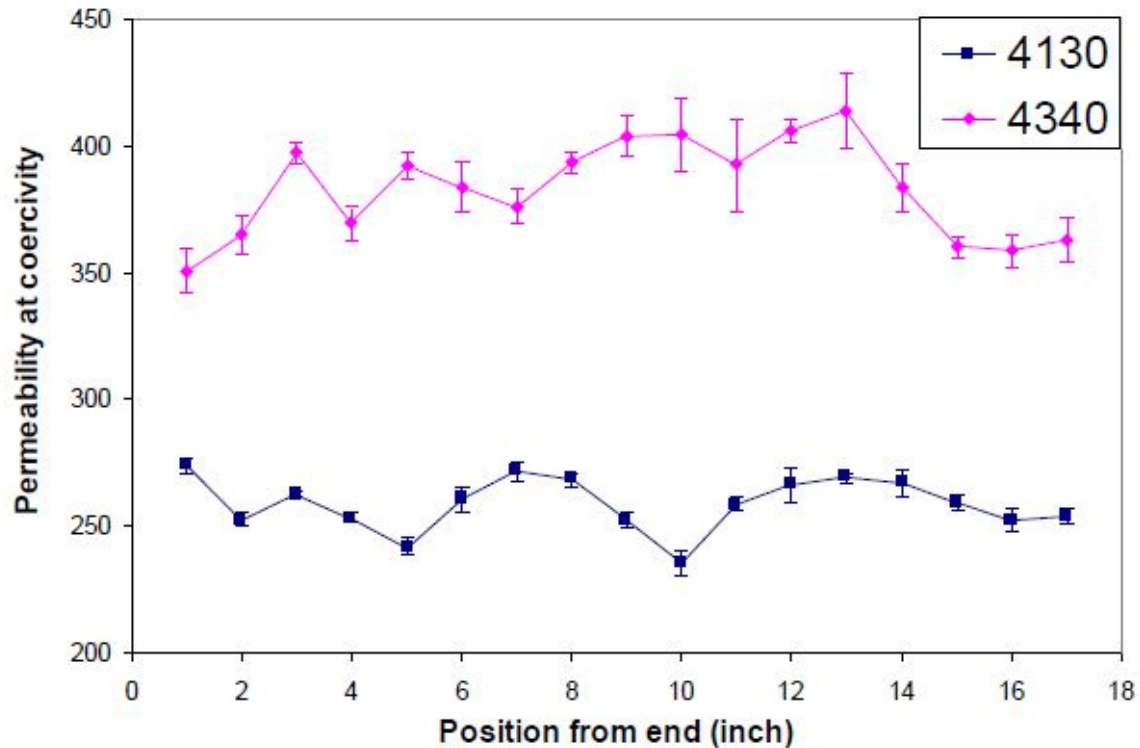
Figure 29. Plot of permeability versus position for the 4130 and 4340 steel bars

4.4 SHOT DURATION STUDY

This study was performed to determine the effectiveness of different shot durations, intending to determine the duration that maximizes contrast ratio and minimizes noisiness. Data were collected using a QQI magnetic flux indicator and interpreted using image analysis procedures (see appendix I).

4.4.1 Technical Summary

The purpose of this study was to determine the apparent effect of shot duration on contrast ratio and background fluorescence. The test was conducted using QQI testing indicators on a 2″ x2″ x12″ steel bar.

4.4.2 QQI Testing Indicator

The QQI indicator consists of three concentric rings that can be detected through the use of MPI. The brightness of the indications will fluctuate with different variables on the magnetic testing bench. The QQI was glued to the steel bar to prevent any magnetic particles or fluid from getting between the bar and the QQI, which could alter the outcome of the indication.

4.4.3 Data Collection

The bench was set to 13% DC (~250–260 Amps) using the halfwave function. For tests requiring only a single shot (e.g., 0.5, 1.0, 1.5, and 2.0 sec), the auto bath function was used to maximize the uniformity of carrier application. The auto bath was set to extend for 1 second and retract for 1 second. For tests requiring multiple shots (e.g., 0.5 sec x 2, 0.5 sec x 3, 0.5 sec x 4, 1 sec x 2), the handheld nozzle was used in place of the auto bath. The nozzle was held at a similar height as the auto bath nozzle and extended for 1 second and retracted for 1 second. After applying the carrier solution, the test sample was magnetized as quickly as the bench would allow. The sample was allowed to dwell for 1 minute before being removed from the bench. The images were taken using the GigE Vision® camera and the LabVIEW script on the MPI Motion Cart. The UV illumination was kept constant by monitoring the temperature on the control panel of the light source. After the image was captured, the sample was returned to the bench and demagnetized and rinsed thoroughly before being tested again. Each shot duration was repeated 10 times. The image analysis can be seen in appendix I.

The data shown table 2 represent an average of all the data runs collected. For each shot duration time, the data was collected 10 times to calculate an average of the contrast ratio for that shot time.

Table 2. Average contrast ratio per shot duration

Shot Duration	Operator 1	Operator 2
0.5sec	2.92365	2.99687
0.5sec*2	3.33629	3.53712
1 sec	4.01005	4.25437
1 sec*2	3.68709	4.14424
2 sec	4.34205	4.73046

Figure 30 compares various shot times to one another. In most instances, the longer the exposure of the part to the magnetic field, the greater the contrast ratio. In figure 30, the trend follows suit for the first three-shot series. The contrast ratio appears to be increasing from one 0.5-second shot, the 0.5-second shot done twice, and the full 1-second shot. For the 1 full-second shot done twice, it appears that the contrast ratio went down for both operators. The last shot appears to have increased in contrast ratio again, but at a decreasing rate than the first three shots.
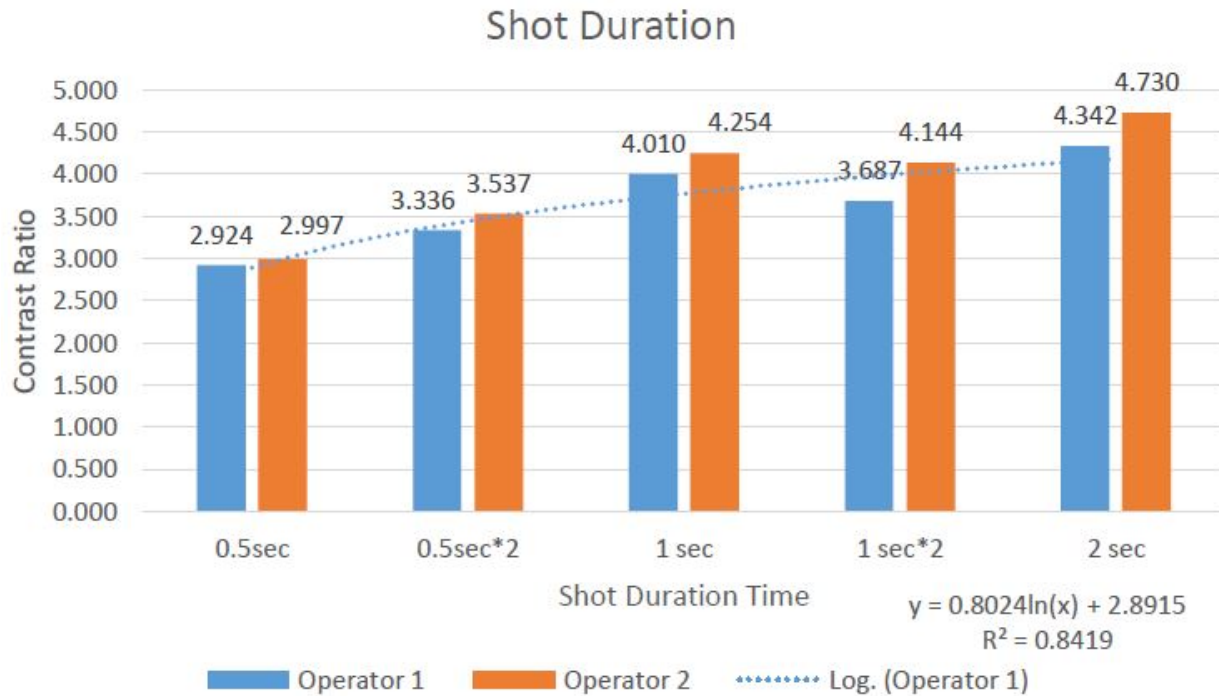
Figure 30. Shot duration contrast ratios

Some explanation for the variance in the shots could be due to the application of the bath during the second shots. As stated in the experimental description, an auto wash was used when possible and not when a hand procedure was used—trying to simulate the auto bath feature.

The difference in recorded values between operators is primarily due to the technique between operators. Though it may appear to be considerable in difference of values, it is primarily negligible, because the values shown are an average of 10 readings with overlap throughout.

5. CRACK DEVELOPMENT/DETECTABILITY AND FIELD STRENGTH MEASUREMENTS

5.1 SAMPLE FABRICATION

Sample preparation procedures have been developed to produce low-cycle fatigue (LCF) cracks for the use in quantitative FPI, MPI, and vibrothermography (VBT) studies. For this research, 24 LCF crack samples (see table 3) were produced with the crack lengths listed below in the data table. These samples were used to baseline the characteristics of the three benches being used in the study.

Table 3. LCF sample and crack length

Alloy 4340	Crack Lengths After Machining (mil)	Alloy 4130	Crack Lengths After Machining (mil)
4301	30.3	4102	30
4308	39.4	4105	30
4310	66.9	4107	50
4309	78.7	4108	50
4306	102.4	4110	70
4312	267.7	4111	70
4302	313	4103	90
4303	415.4	4104	90
4311	480.3	4106	110
4304	519.7	4112	110
4307	586.6	4101	130
4305	740.2	4109	130

Further LCF samples were produced with cracks in various orientations to assist in the studies (the procedure for producing LCF cracks is found in appendix J). For prior work, LCF cracks were grown in three-point bending, producing a crack that is perpendicular to the long axis of sample (i.e., a transverse crack). However, given that crack orientation has an effect on signal response for MPI, there was a need for cracks that were aligned along the axis of the sample (i.e., longitudinal cracks). This required development of new sample fabrication procedures. For this work, samples were fabricated using the two alloys, 4130 and 4340 steel. Starter notches are generated using electro-discharge machining. Using the Materials Testing System (MTS) machine, the transverse cracks were grown under various low-cycle conditions. Fatiguing the longitudinal EDM notches was more complicated because the starting size of the samples was 4″ x 4″, and the amount of force needed to conveniently grow the cracks was beyond the limitations of the MTS, so the longitudinal cracks had to be high-cycle, low-force fatigued. The final fatigue conditions were approximately 250,000 cycles at 22.4 kips and a frequency of 5 Hz. This is compared with approximately 100,000 cycles at 15.5 Kips and a frequency of 5 Hz for samples with transverse cracks. Six new samples with the longitudinal cracks were produced in this fashion.

5.2 SPECIMEN PREPARATION AND CRACK ASPECT DETERMINATION

5.2.1 Specimen Configuration

The sample configuration selected for this study was a 1″ x6″ x 0.5″ specimen with a single low-cycle surface fatigue crack located near the center. This sample configuration provided cracks that were representative of those found in service and was relatively easy to manufacture. Having a single crack in each specimen also allowed the greatest flexibility in specimen usage.

5.2.2 Specimen Material

The samples were fabricated from either a 4340 low-carbon steel or a 4130 low-carbon steel. These materials were chosen because of their common use for aviation, as recommended by several different OEMs and air carriers.

5.2.3 Preparation of Specimen Blanks

Samples were fabricated from either a 6″ x 6″ square piece of steel or from a 4″ x 4″ piece of steel. The raw steel was first sliced into pieces slightly greater than 0.5″ thick, then each slice was cut into 1″-wide pieces. The surfaces of each sample were sanded with 50-grit aluminum- oxide sandpaper on a belt sander or milled to remove the relatively rough mill finish or the sawn edges. The corners were also rounded to discourage crack initiation at the edges. It was planned to fabricate all of the specimens from 0.5″-thick material to ensure crack length to depth aspect ratios in the range of 2:1 to 3:1.

5.2.4 Stress Riser Introduction

A stress riser to encourage crack initiation was introduced near the center of the sanded surface on each specimen. The stress riser (notch) used was produced from an EDM notch. The EDM notch is the more traditional method of starting cracks, but it has some drawbacks. These drawbacks include the high relative cost of placement of very small EDM notches. It is also very difficult to grow cracks that are shorter than the EDM starter notch. Figure 31 is a photograph of a fatigue crack that was initiated at an EDM notch.
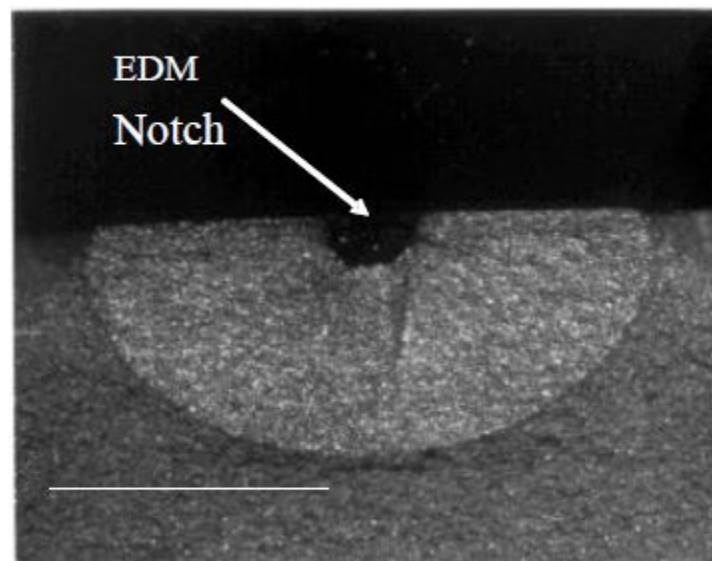

Figure 31. Photograph of a fatigue crack fracture face that was started from a 0.3mm (0.012″-) long by 0.12 mm-(0.007″-) deep EDM notch

36

5.2.5 Fatigue Crack Initiation and Growth

LCF cracks were generated at room temperature using an MTS 22 kip load frame fitted with a three-point bend fixture. A computer controlled servo-hydraulic system was used to generate sine-wave cyclic loading. An R ratio of 0.1 was used with the maximum load set to produce a bending stress of approximately 80% of the material yield strength. Figure 32 shows the setup used to fatigue the specimen in three-point bending.
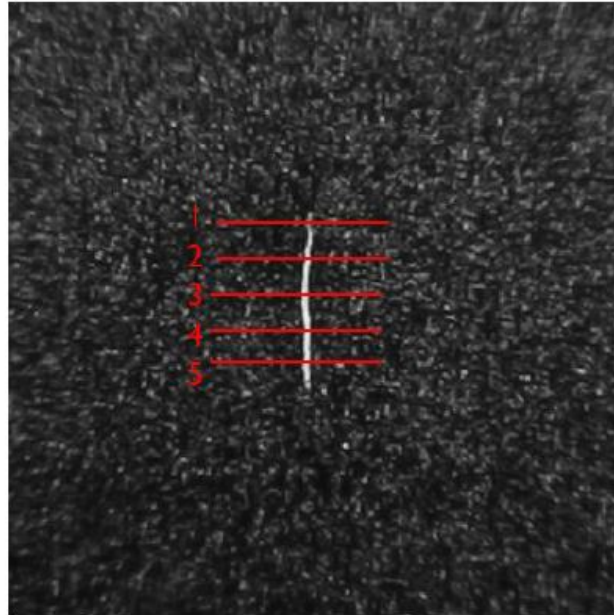

Figure 32. Sample loaded in three-point bending

The crack starter defect was monitored with a light microscope at 500x magnification periodically to ensure crack initiation had begun but had not overgrown the target length of 32– 35 mil. Samples were fatigued until a small crack was noted at the stress riser, typically between 80,000 and 150,000 cycles.

Efforts on the quantification of MPI indications required the development of a MATLAB program to quantify the brightness of known, controlled artifacts, including both representative standards and the LCF samples described previously. The approach was as follows:

- Convert all images to grayscale (as exemplified here). The image is a matrix of pixel brightness values between 0 and 255 (0=black, 255=white) (i.e., brightness = $f(x,y)$ where x and y define the pixel's location).
- Analyze the indication row by row, then average the results to get final results. For example, analyze pixel row 1, then pixel row 2, which will result in CR_1, CR_2, where CR is defined as mean $(CR_1,…,CR_n)$.
- Run MATLAB script, and choose image.
- Place vertical line from one endpoint of indication to the other. This defines the range of rows in the pixel matrix to analyze and also provides a length estimate.

- Place horizontal line so that the entire width of the indication lies within the endpoints, which defines a window that will be used to locate the maximum indication brightness. A typical example is shown in figure 33.
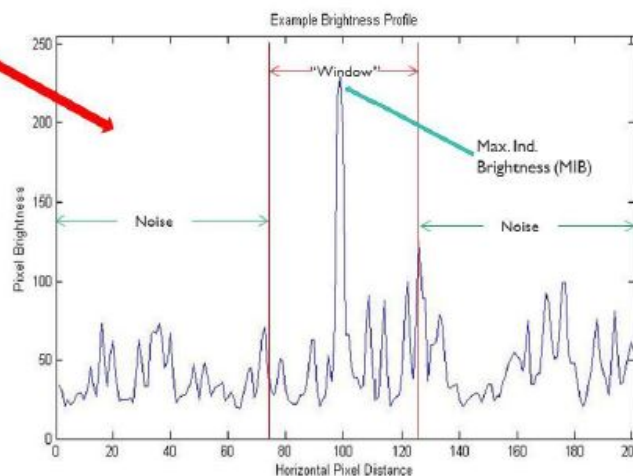
Figure 33. Brightness determination

After development of the MATLAB script, a number of runs were made to test the utility of the software and determine the sensitivity of this method to variability in the MPI process. An example

of two runs on the same sample is shown in figure 34, with the signal-to-noise ratio reported below the image.

SNR = 10.5   SNR = 6.25
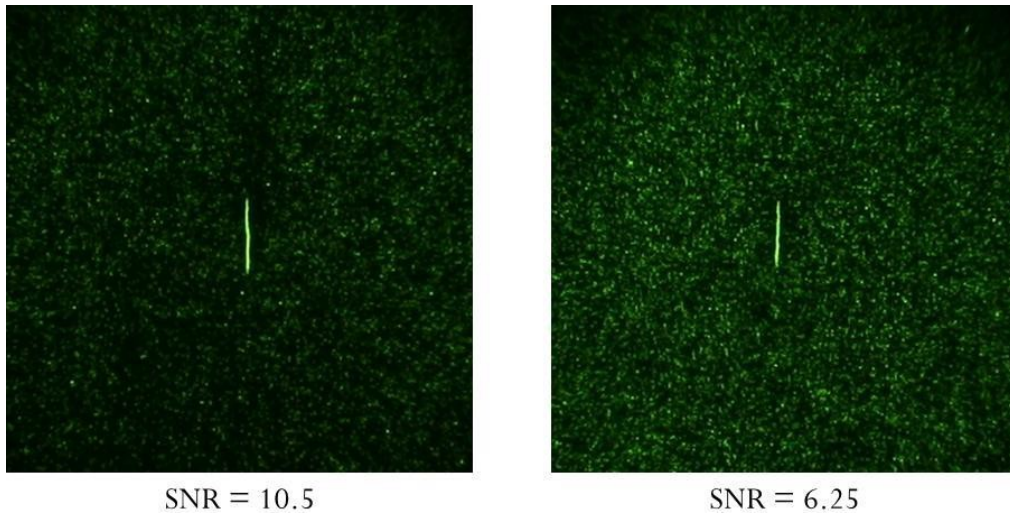
Figure 34. Signal-to-noise ratio images

5.3 COMPARATIVE STUDY OF OIL VERSUS WATER BATH

A comparative study of oil and water bath approaches was completed for both the oil- and water-based baths. For this study, the two alloys of steel selected for the research have cracks ranging from 30–130 mil. Each sample was placed into the coil on either one of the AD-945 benches, and the current was set to AC. One of the benches was filled with the oil-based carrier, and the other bench contained the water-based carrier. Images of the indications were taken, and the images were processed with the image analysis software developed for the program. The results for the comparison study for the two alloys are shown in figures 35 and 36.

Figure 35. Alloy 4130 bath comparison

Figure 36. Alloy 4340 bath comparison

Initial results indicate that the water MPI carrier seemed to do a better job with the contrast ratio for most of the LCF samples. However, though attempts were made to keep the comparisons the same, the water-based samples were processed on a different bench with a smaller 12″-diameter, five-turn coil, and the oil-based runs were on a larger 18″-diameter, five-turn coil with newer electronics.

5.4 QUALITY INDICATOR STUDY
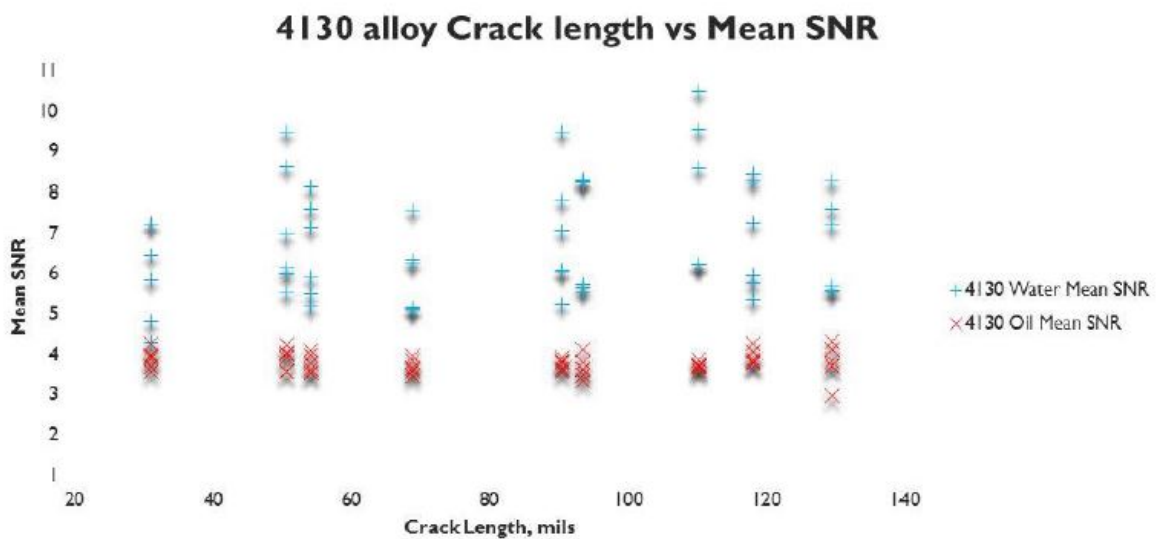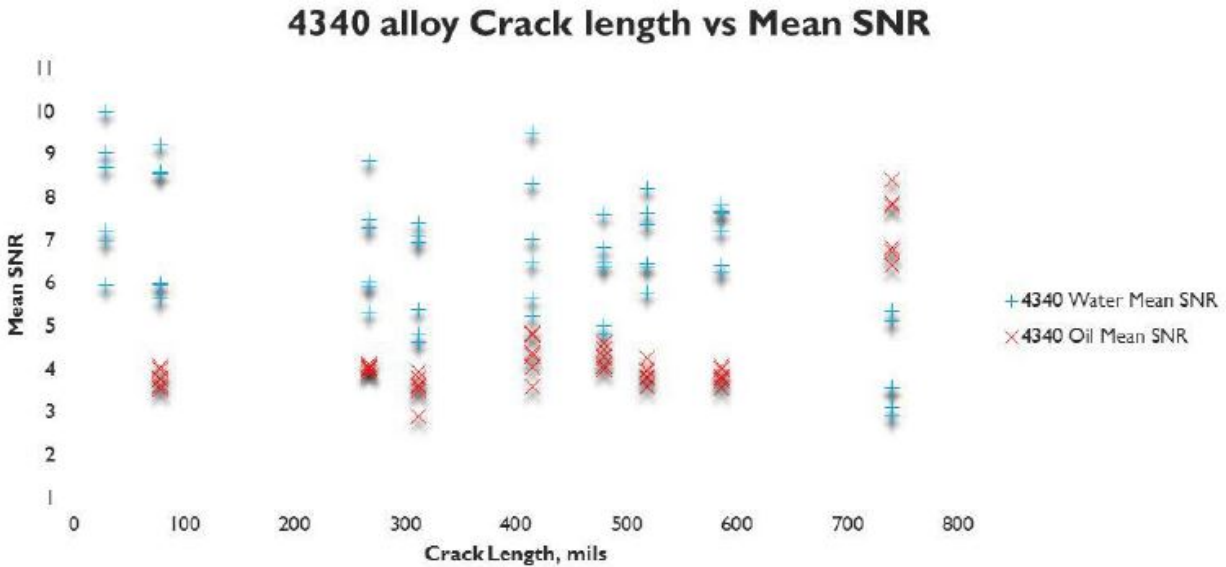
Effort was spent to try and determine the response, sensitivity, and effective current ranges for three different magnetic flux indicators (i.e., Castrol Strip, QQI, and pie gauge). Plans for the study called for the use of a single 2″ x 2″ steel bar on which all three gauges would be mounted, and magnetizing the bar with AC current in a current flow (head shot) at different levels and in three wet-horizontal benches. The magnetic-field strength was measured using a Hall sensor at the surface of the part. Image repeatability measurements were made and analyzed using the adapted MATLAB script procedure found in appendix I.

5.4.1 QQI Testing Indicator

The QQI indicator used consists of three concentric circles etched into the backside of the shim, which will develop indications of sections of the circle when magnetic field strength on the surface of the part is sufficient for MPI. The procedure for using the QQI is found in appendix K. The brightness of the indications will fluctuate with different variables on the magnetic testing bench. The QQI was glued to the steel bar to minimize any air gap and to prevent any magnetic particles or fluid from getting between the bar and the QQI.

5.4.2 Castrol Strip

The Castrol Strip consists of three internal parallel line defects that can be detected through the use of MPI. The brightness of the indications will fluctuate with different variables of the magnetic test. The Castrol Strip was glued to the steel bar with the defects parallel to the length of the bar in order to prevent any magnetic particles or fluid from getting between the bar and the Castrol Strip, which could alter the outcome of the indication.

5.4.3 Pie Gauge

The pie gauge consists of eight wedges of ferromagnetic material brazed together with nonmagnetic material and coated with a layer of magnetic material for linear indications to form. These linear indications can be detected through the use of MPI. The brightness of the indications will fluctuate with different variables on the magnetic testing bench. The pie gauge was taped tightly to the bar to prevent magnetic particles and fluid from getting between the pie gauge and the bar. The large size of the pie gauge made gluing it down problematic.

5.4.4 Bench Procedures

The tests were conducted on all three of the MPI available at CNDE. The procedures used for the test is shown below, noting that the MD3 has extra capabilities mentioned earlier in this report and emphasized here again.

5.4.4.1 MD3 Bench

The MD3 oil bench has the capabilities to execute an auto bath:

1. A wooden block was placed between the head stocks to raise the testing face of the sample to 30° from level.
2. The auto bath was set to extend for 1 second and then retract for 1 second.
3. The bench was set to 1%, and the sample was magnetized by engaging the auto bath, which automatically magnetizes the sample after being flooded with MPI carrier.
4. The sample was allowed to dwell between the head stocks for 1 minute before being transferred to the imaging cart.
5. The GigE Vision camera was used to capture an image of the sample, and the corresponding current from the bench readout was recorded.
6. The sample was then returned to the bench, demagnetized, rinsed, and the process repeated.
7. The entire process is repeated with each of the following current levels (i.e., 1%, 4%, 7%, 11%, 13%, 16%, and 18%) and performed three times each.

5.4.4.2 MPI Lab (Oil 945 and Water 945 benches)

The second oil bench and the water bench follow a slightly different procedure, because they do not have the capabilities to execute an auto bath.

1.   Because the second oil bench and the water bench do not list current in percentages on the user input, the sample bar was magnetized 20 times between the maximum and minimum recorded current from the first bench.
2.   A wooden block was placed between the head stocks to raise the testing face of the sample to 30° from level.
3.   The hand nozzle was used to replicate the auto bath, extended for 1 second and retracted for 1 second, and then the sample was magnetized.
4.   The sample was allowed to dwell between the head stocks for 1 minute before being transferred to the imaging cart.
5.   The GigE Vision camera was used to capture an image of the sample, and the corresponding current was recorded from the bench readout.
6.   The sample was then returned to the bench, demagnetized, rinsed, and the process repeated.

5.4.5 Image Analysis for the Quality Indicator Study

The analysis of the images for the Castrol Strip and pie gauge was done using the CNDE custom-made MATLAB script, as seen in appendix I, and the procedure for the QQI image analysis is found in appendix L. The general process outlined in this script is as follows:

1.   Once the script is started, the user is prompted to locate and open an image.
2.   The script opens the image with a zoombox that can be adjusted by the user.
3.   Once the box has been adjusted and zoomed in, the user may draw a vertical line and then a horizontal line.
4.   The vertical line is drawn directly on the magnetic indication and encompasses the length of the indication being examined.
5.   The horizontal line is drawn to encompass the indication and includes a minor area to the left and right of the indication.
6.   The script then calculates and outputs a value being referred to as the mean contrast ratio, the mean pixel level brightness level in the noise region, and the length of the vertical line drawn by the operator on the indication.

These outputs and the corresponding amperage of each image were recorded in a Microsoft® Excel® spreadsheet. Then the mean contrast ratio was plotted against the amperage in several comparison graphs; a graph was made for each bath comparing the repeatability of each quality indicator on that bath, and a graph was also made for each quality indicator comparing the repeatability of each bath used with that quality indicator. The dimensions and position of the zoombox, as well as the length and position of the lines, differed according to each of the three methods (e.g., QQI, Castrol Strip, and pie gauge). For QQI, the zoombox dimensions were not changed and encompassed the entire QQI patch. The curved nature of the indications for QQI required that the vertical line be drawn from the height of the visible portion of the curve, which bisected the curve, and the horizontal line encompassed the visible ends to the outer rim. The curve analyzed for all QQI images was the right inner curve. For Castrol Strip, the width of the zoombox was adjusted to exclude the left and right stripes, leaving only the center stripe to be analyzed. The vertical line was drawn to match this center stripe's entire height. For pie gauge, the zoombox was not changed and placed such that the diagonal stripes made an X from corner to corner of the box.

The right vertical stripe was analyzed for all pie gauge images, and the vertical line was drawn to match the entire height of that stripe.

5.4.6 Results for the Quality Indicator Study

Results from this study were not as quantitative and repeatable as initially hoped, but were important nonetheless. Figures 37–39 show the three indicators and their results as recorded from the three different benches. Though the data points are more scattered than desired, the Castrol Strip did perform fairly well, with an increase in mean contrast ratio as the magnetizing current was increased (see figure 37).
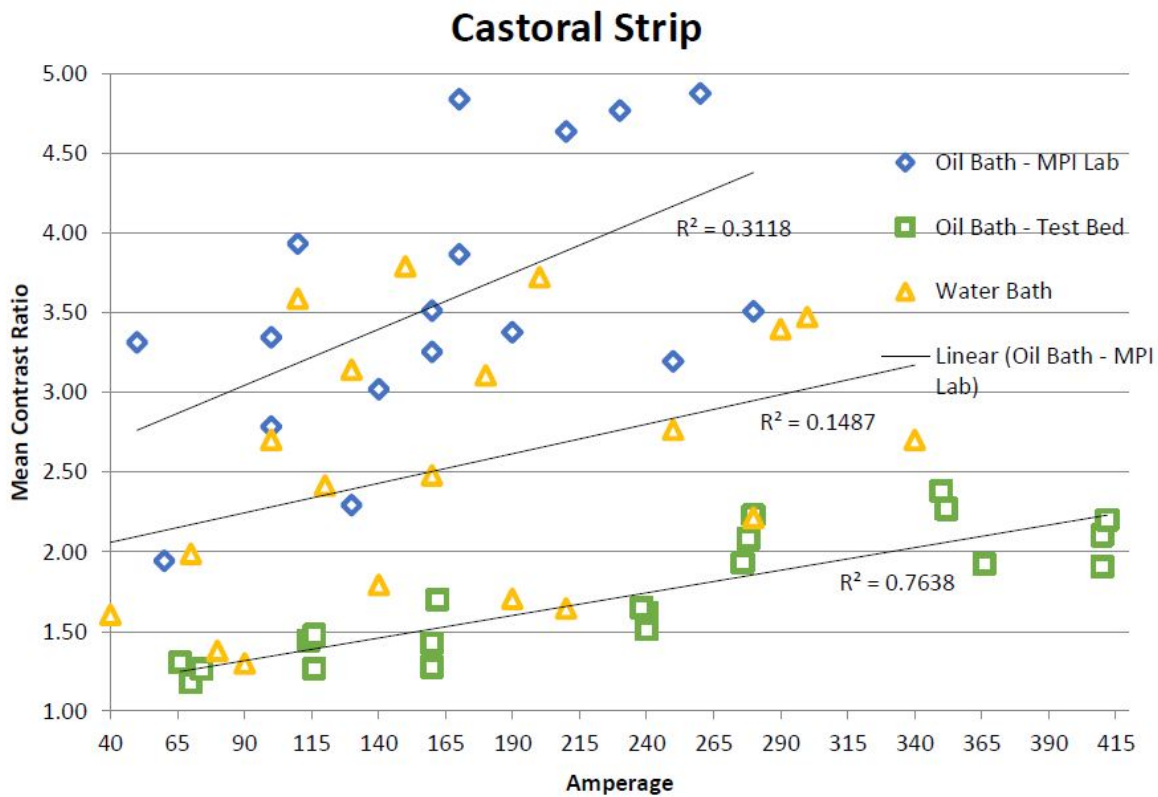

Figure 37. Results for the Castrol Strip sensitivity study

The QQI did not perform quite as well as the Castrol Strip, but the results were still encouraging, showing the general trend of increased mean contrast ratio with increased current (see figure 38).
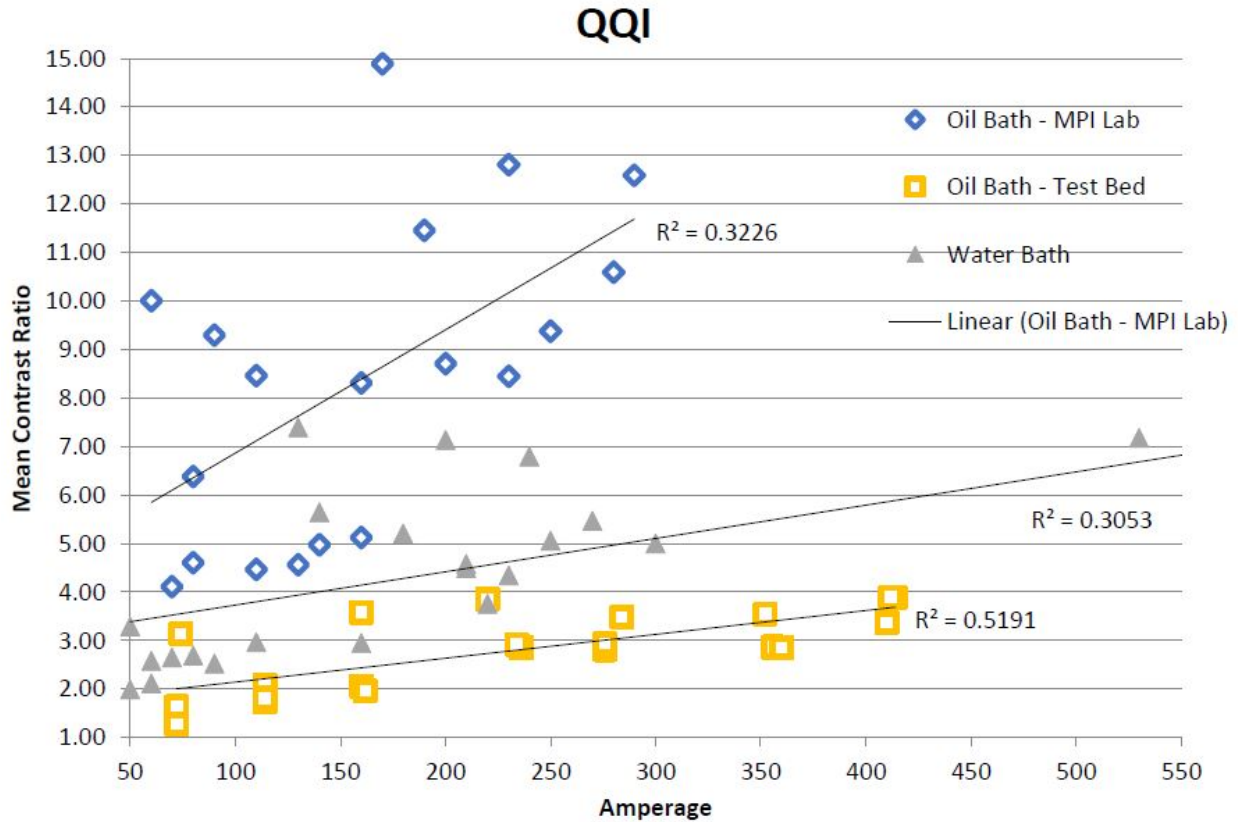
Figure 38. Results for the QQI sensitivity study

Pie gauge trended the poorest among all three indicators tested. This is primarily related to its use as a magnetic field direction indicator. Its use as a sensitivity indicator is also contrary to its intended purpose. On one particular bench, the pie indicator did perform in a similar fashion to the other two indicators, showing an increase in indication contrast with increased current. The results for the pie gauge study are shown in figure 39.
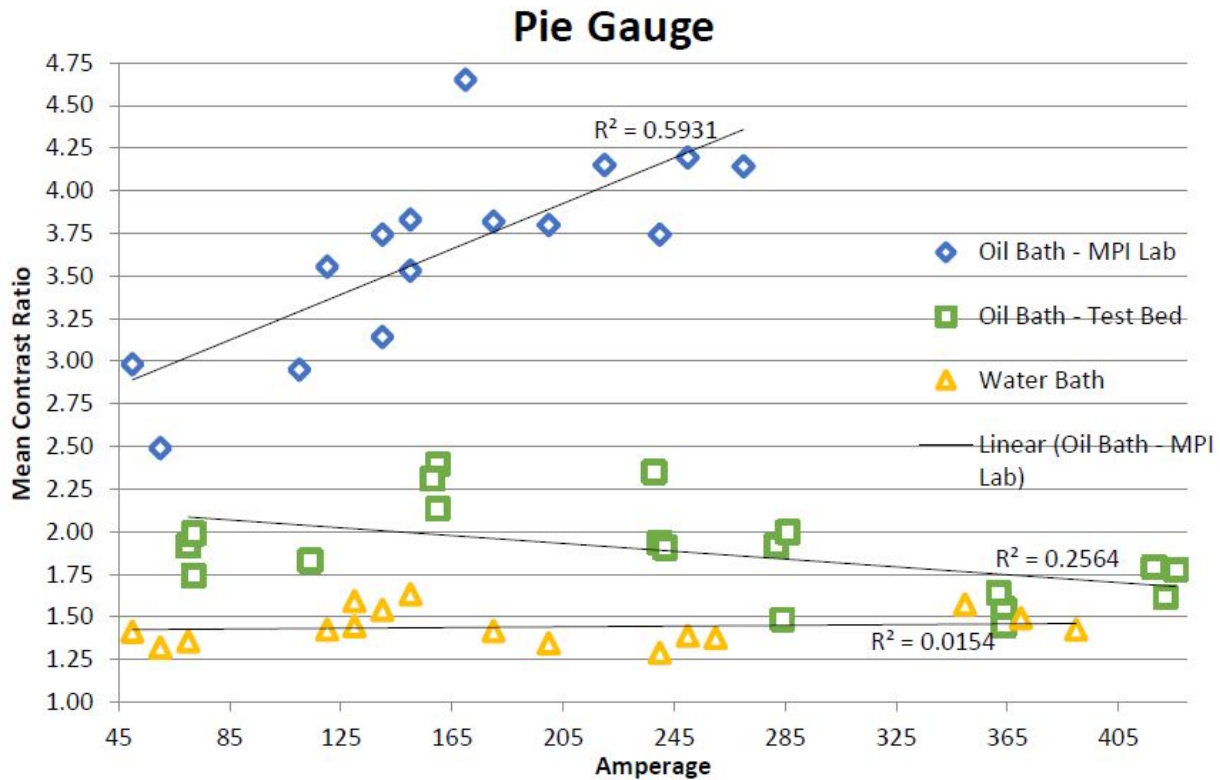
Figure 39. Results for the pie gauge sensitivity study

5.4.7 Conclusions for the Quality Indicator Study

Though in broad terms the study does illustrate an expected trend on increased sensitivity, it also brought to light the issue of increased refinement needed to the contrast ratio image routine. Given the nature of the shape of some of the indicators, the curvature needs to be accounted for. There is also a need for an increased filtering in the images taken with the imaging camera. Both the software and the filtration issues have been addressed at the end of this reporting period.

6. DISCUSSION

6.1 CHALLENGES

In a nondestructive method such as MPI, it would appear easy to identify those issues that need to be addressed by research. But that is not the case. Though the issues that need to be addressed have been identified, the task of taking them to a quantifiable level was not a simple one. Like other methods that are mostly subjective, taking a judgment call to a numerical determination proved difficult at times. One issue that made this research project a challenge was not simply the art of applying physics and science to a set of physical problems, but taking a method that is extremely forgiving and has been in existence for decades and making it quantifiable. This research team faced a most difficult issue when half of the initial research team, including the PI who authored the original proposal, left the university. With the support of CNDE, the program was able to carry out its objectives. Though a great deal of progress was made in the efforts to quantify the method,

and a great deal of knowledge was gained in how to overcome issues that were initial barriers to that progress, there are still recommendations for further work, which are discussed in section 6.3.

6.2 OVERVIEW OF KEY FINDINGS

6.2.1 Motion Cart

A motion cart system was developed to provide the capability to return to the same locations on samples to establish repeatable measurements of the indications as parameters are changed. To control the different devices on the motion cart, a LabVIEW program was written and tested. This program allows the user to control both the motion arm and the photometer from a single interface; to adjust features such as aperture, front filter, gain, and rear filter; and to move the motion tray to predetermined locations for brightness measurements.

6.2.2 Current Sensor

A current measurement system was developed that consists of a signal processing and acquisition unit interfaced to a laptop computer. The system uses four linear Hall sensor arrays, each of which consists of three Hall sensors separated by known distances to detect the circumferential fields at various distances from a current-carrying cable.

6.2.3 Training Modules

Development of five training modules was carried out according to the work plan defined during the early stages of the program. Each module presents different aspects of the research or issues commonly addressed in the discussion of MPI.

6.2.4 In Situ Measurements for Direct Current

The study of in situ measurements of leakage magnetic fields from EDM notches in the round bar stock was aimed to help identify, with the use of artificial defects with known dimensions, the optimum magnetizing conditions for MPI indications. Measurements were repeated at various additional sensor liftoffs up to 12.5 mil (0.32 mm) to study how the leakage field signal decays with distance. The RMS value of the detected leakage field decreases with increasing liftoff. The result can be used to estimate, by means of extrapolation, the radial component of the leakage field and field gradient at the bar surface.

6.2.5 Current Waveform Measurements

Characterization of the magnetization current waveforms of both coil and head shots on the MD3 bench using a portable current sensor system was performed. The objectives were two-fold: 1) to examine relationships between the bench current readouts and the characteristics of the current waveform, including the RMS value and peak current; and 2) to identify correlations between the magnetization current and the resulting surface magnetic field of a given part. It was found that the peak value of the current waveform first increases exponentially with time, with a time constant estimated by least-square fitting to be approximately 0.047 second. Not only the peak current but also the duty cycle of the magnetization current increase with the amperage. It was also found that the current waveforms for HWDC and FWDC coil shots were similar to the waveforms of AC coil

shots, both the amplitude and duty cycle of the current increase with the amperage. The FWDC current has a duty cycle approximately twice as large but a smaller peak current level than the corresponding HWDC current measured at the same amperage. It is evident that both the RMS value and the peak level of the current waveforms are linearly proportional to the bench readout within the amperage range (1%–50% full scale) covered in this study. These linear relationships can be used as empirical calibrations for estimating the peak current from the bench readouts for all three types of coil shots.

6.2.6 Accuracy of Current Sensor

The accuracy of the current sensor outputs was evaluated by performing a comparison study with the current waveforms that were measured using the shunt resistor. Specifically, the RMS value and peak current level measured using the current sensor system and the shunt resistor were directly compared and were found to agree with each other to within 2% in all cases. In general, the RMS values show better agreement than the peak current level, probably due to the fact that any offset in the acquired potential drop signals across the shunt resistor would more strongly affect the peak values of both HWDC and FWDC waveforms than the RMS values.

6.2.7 Time Domain for DC

The time-domain current waveforms and the surface magnetic field on a steel bar were characterized by subjecting them to HWDC head shots, as part of a study aimed at comparing quantitatively the sensitivities of common field indicators. It was found that the linear dependence of both the magnetizing current and surface magnetic field on the bench reading offers empirical calibrations used to quantify the sensitivities of common field indicators.

6.2.8 In Situ Measurements for AC

The magnetization current waveforms and surface magnetic field on a steel bar subjected to AC head shots have been characterized to evaluate quantitatively the usefulness of field indicators in determining the adequate current level for MPI inspections. The surface magnetic fields along both the transverse and longitudinal directions were measured at the center of the steel bar (see figures 19(c) and 19(d)) using a bi-axial Hall Effect sensor. The longitudinal field was measured as a means to check the alignment of Hall sensor along the samples axes, because the field induced by the head shot along the sample axis should, in principle, be zero. It was found that both the peak height and the duty cycle of the current waveform increase with the amperage. The peak height and the RMS value of the current waveform were found to vary linearly with the bench reading, therefore offering a simple, empirical calibration for estimating the peak current from the bench reading. It is evident that the waveform of the surface field closely resembles that of the magnetizing current. Note that the peak value of the surface field varies linearly with the peak height of the current waveform and the bench readout.

6.2.9 Permeability Measurements

Permeability measurements were made to measure spatial variation in magnetic permeability in steel components, which is considered one of the component effects that could affect MPI inspection. If spatial variation in permeability exists in a part, the MPI indication does not necessarily develop in regions with lower permeability even if an optimal magnetization condition

is used for the average permeability. Two steel bars made of 4130 and 4340 steel were examined. The magnetic hysteresis loop was obtained by plotting the magnetic induction signal as a function of the surface field, from which the magnetic permeability can be extracted. Strictly speaking, permeability is not a constant. It varies over the hysteresis cycle, attaining a maximum near the coercivity and then gradually decreasing as the part approaches saturation.

6.2.10 Shot Duration

A shot duration study was performed to determine the effectiveness of different shot durations, intending to determine the duration that maximizes contrast ratio and minimizes noisiness. In most instances, it is expected that the longer the exposure of the part to the magnetic field, the greater the contrast ratio.

6.2.11 Bath Comparison

A comparative study of oil and water bath approaches was completed for both the oil- and water-based baths. Initial results indicate that the water MPI carrier seemed to do a better job with the contrast ratio for most of the low-cycle fatigue samples. Though attempts were made to keep the comparisons the same, the water-based samples were processed on a different bench with a smaller 12″-diameter five-turn coil, and the oil-based runs were processed on a larger 18″- diameter five-turn coil with newer electronics.

6.2.12 Quality Indicators

A study was performed to try and determine the response, sensitivity, and effective current ranges for three different magnetic flux indicators (i.e., Castrol Strip, QQI, and pie gauge). Image repeatability measurements were made and analyzed using the adapted MATLAB script procedure. Results from this study were not as quantitative and repeatable as initially hoped but were important nonetheless. Though the data points are more scattered than desired, the Castrol Strip did perform fairly well, with an increase in mean contrast ratio as the magnetizing current was increased. The QQI did not perform quite as well as the Castrol Strip, but the results were still encouraging. The pie gauge trended the poorest among all three indicators tested. This is primarily related to its use as a magnetic field direction indicator. Its use as a sensitivity indicator is also contrary to its intended purpose.

6.3 RECOMMENDATIONS FOR FUTURE RESEARCH

Below are topics in which industry input was given during the course of the project in which, if time allotted, further work might be of benefit to the industry and the method:

1. Issues with chrome plating and its thickness versus pin-on-disc arrangement–Much of the industry information are inconsistent.
2. High-velocity oxygen fuel (HVOF)–The industry is moving from chrome plating to HVOF.
3. Bushing inspections–Is it acceptable to inspect tens of bushings at once? Common practice is to inspect large batches of bushings simultaneously.
4. Intricate geometries and getting the appropriate field strength–This is the reason Level-III-approved technique sheets were used after proving them out with QQIs.

5. Required degree of cleanliness–Do all coatings have to be stripped?
6. Differences in methods used to calculate field strengths–This is typically a metric unit conversion issue between Europe and the United States, but there can be several variations for calculations. This has been a problem with Airbus, which required the authors to nearly burn the parts with such a high field strength because they refused to acknowledge these differences.
7. Use of air to remove excess fluid (max 5 psi).
8. Reason why ASTM removed the max 60 Gauss.

7. REFERENCES

1. Yi, J. B., Li, X. P., Ding, J., & Seet, H. L. (2007). Study of the grain size, particle size and roughness of substrate in relation to the magnetic properties of electroplated permalloy. *Journal of Alloys and Compounds, 428*(1), 230–236.

2. Vereda, F., de Vicente, J., Segovia- Gutiérrez, J. P., & Hidalgo-Alvarez, R. (2010). On the effect of particle porosity and roughness in magnetorheology. *Journal of Applied Physics*, 110(6), 063520–063520-9.

3. Kim, Y. H., Park, B. J., Choi, H. J., & Seo, Y. S. (2007). Coating of magnetic particle with polystyrene and its magnetorheological characterization. *physica status solidi (a), 204*(12), 4178–4181.

4. El Nimr, M. K., Moharram, B. M., Saafan, S. A., & Assar, S. T. (2010). Particle size distribution, magnetic permeability and dc conductivity of nano-structured and bulk LiNiZn–ferrite samples. *Journal of Magnetism and Magnetic Materials, 322*(15), 2108–2112.

5. Dougnac, V. N., Alamillo, R., Peoples, B. C., & Quijada, R. (2010). Effect of particle diameter on the permeability of polypropylene/SiO 2 nanocomposites. *Polymer, 51*(13), 2918–2926.

6. Li, X. Y., & Yuan, Y. Settling velocities and permeabilities of microbial aggregates.*Water Research, 36*(12), 3110–3120.

APPENDIX A—DEFINITIONS

- RMS–Root mean square; a measure of the magnitude of a varying quantity

- Thyristor–A solid-state semiconductor device that acts as bi-stable switch, conducting when the gate receives a current trigger and continuing to conduct while it is forward biased (i.e., while the voltage across the device is not reversed)

- AC–Alternating current; a type of electrical current where the current repeatedly changes direction

- HWDC–Half-wave direct current that has some characteristics of both alternating current and direct current waveforms; the voltage of a direct current wave is roughly constant

- FWDC–Full-wave direct current that has some characteristics of both alternating current and direct current waveforms; the voltage of a direct wave is roughly constant.

- Rise Time–The time taken by a signal to change from a specified low value to a specified high value

- Head Shot–Method of direct magnetization in which the part is placed between the copper pads on the headstock of the bench and current is passed through the part

- Coil Shot–Method of indirect magnetization in which a part is placed inside the coil on the bench and is magnetized by an induced magnetic field

APPENDIX B—OPERATIONAL PROCEDURE FOR MD3 BENCH

1.   Use a level to make sure the bar lies at 45°. If not, adjust the plastic holder.
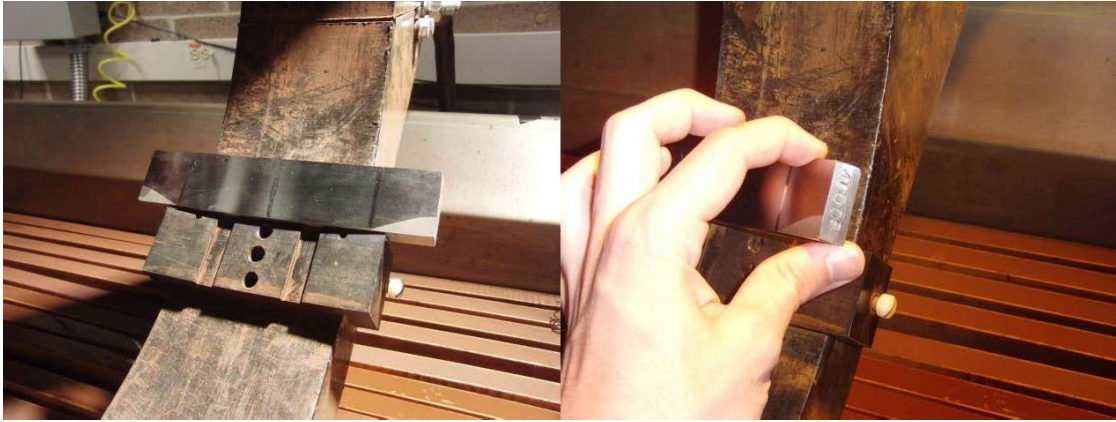
2.   Position the backmost auto bath nozzle 6″ directly above the sample and 0.5″ to the left of the sample. Make sure the blue hose going to the nozzle does not hit the coil when the auto bath extends and retracts.
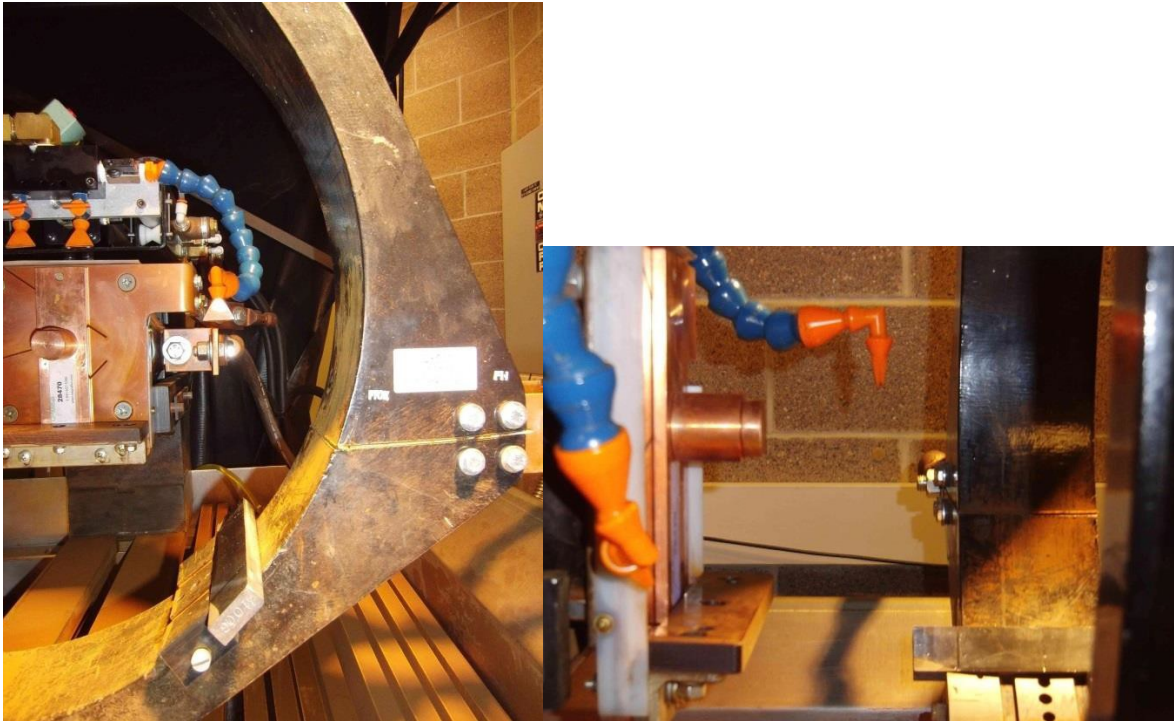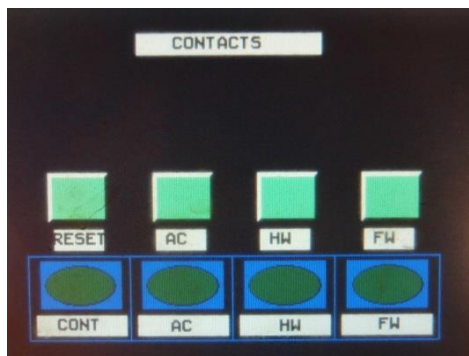
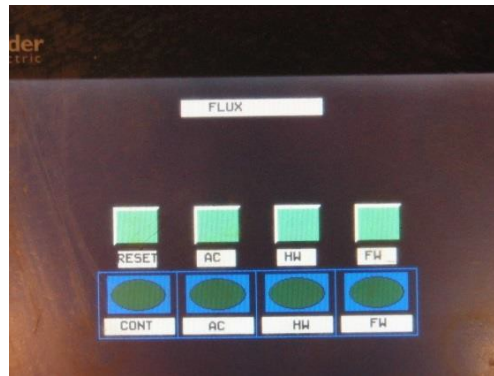3. On the process parameters screen, set the enter bath out time to 2.8 seconds, the mag shot time to 2 seconds, and the auto DMAG to off.
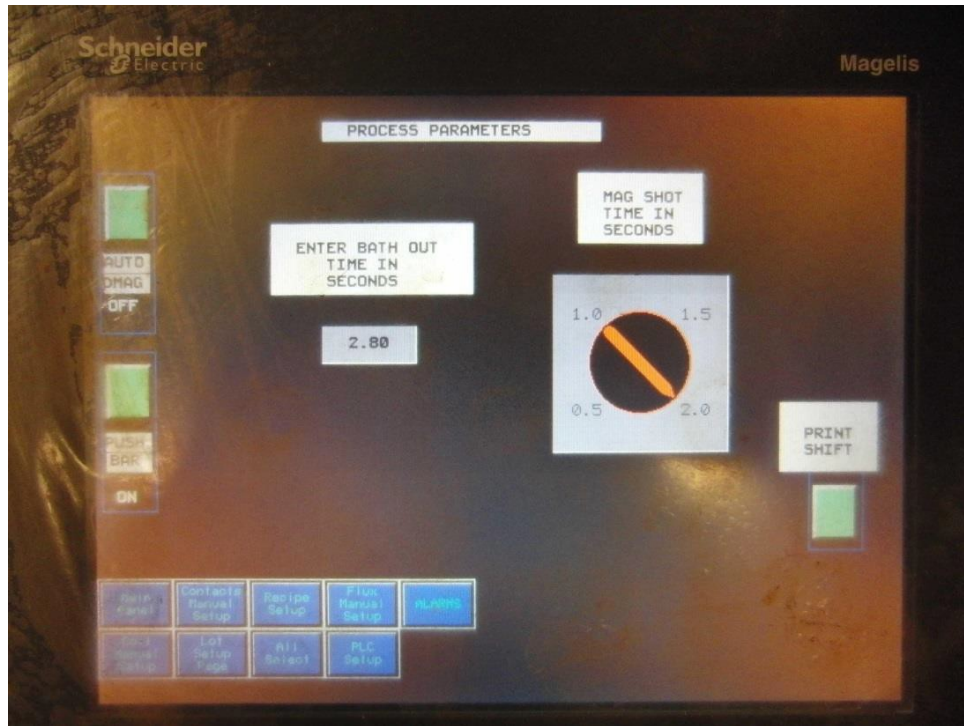
4. On the main control screen, turn the auto bath on.

5. On the contacts manual setup screen, push reset.

6.   On the flux manual setup screen, push reset.
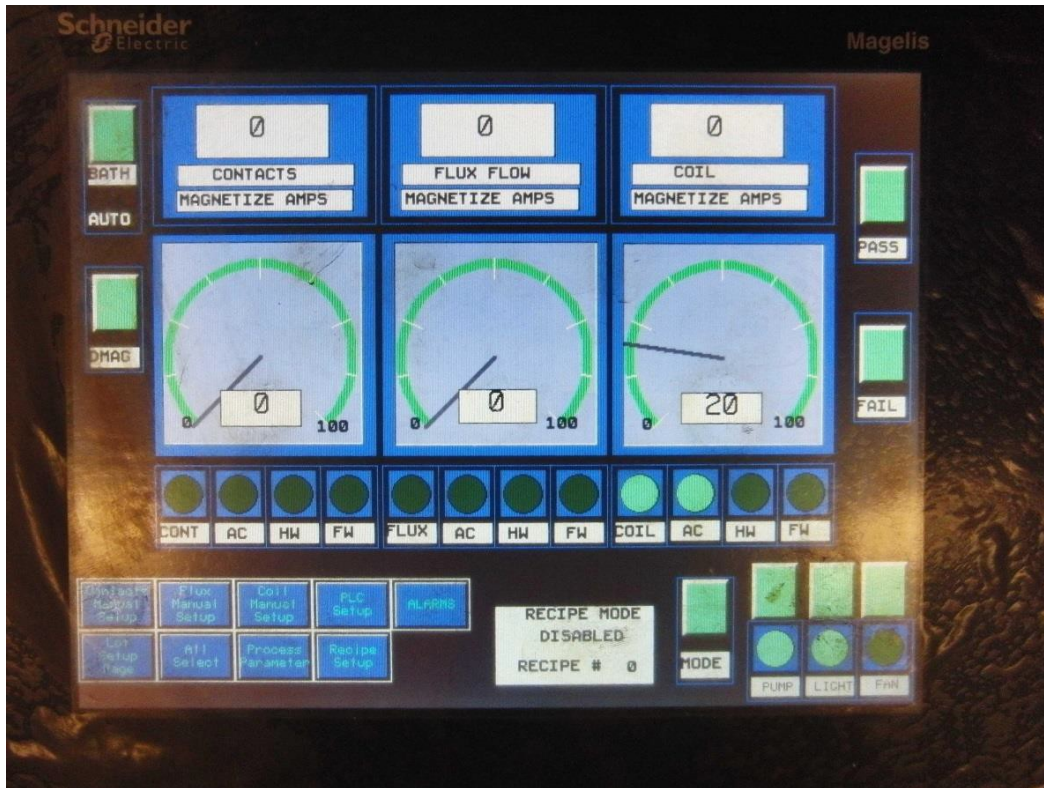

PROCEDURE

1.   Center the sample on the plastic holder with the crack up and the end number to the right.
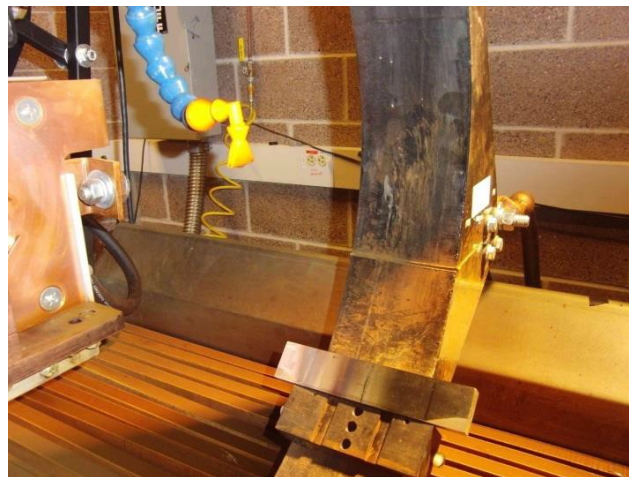
2.   On the coil manual setup screen, select AC, HW, or FW.
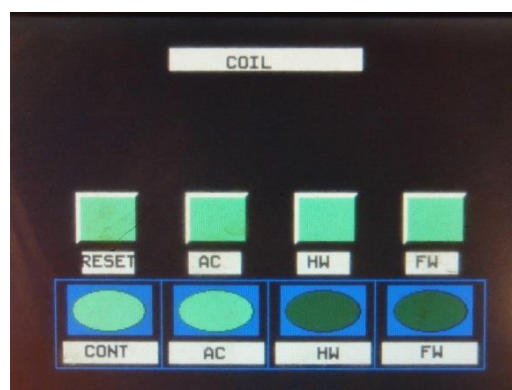
3.   On the main control screen, select a current percentage on the dial under coil.

4.   Press and release the foot pedal. The auto bath will spray the sample down and back. The coil will then magnetize the sample.

5.   Allow the sample to drip for 10–15 seconds.

6.   Move the sample to the MPI cart platform for testing.

7.   After testing, place the sample back on the plastic holder in the same orientation as before.

8.   Press the DMAG button on the main control screen to demagnetize the sample.

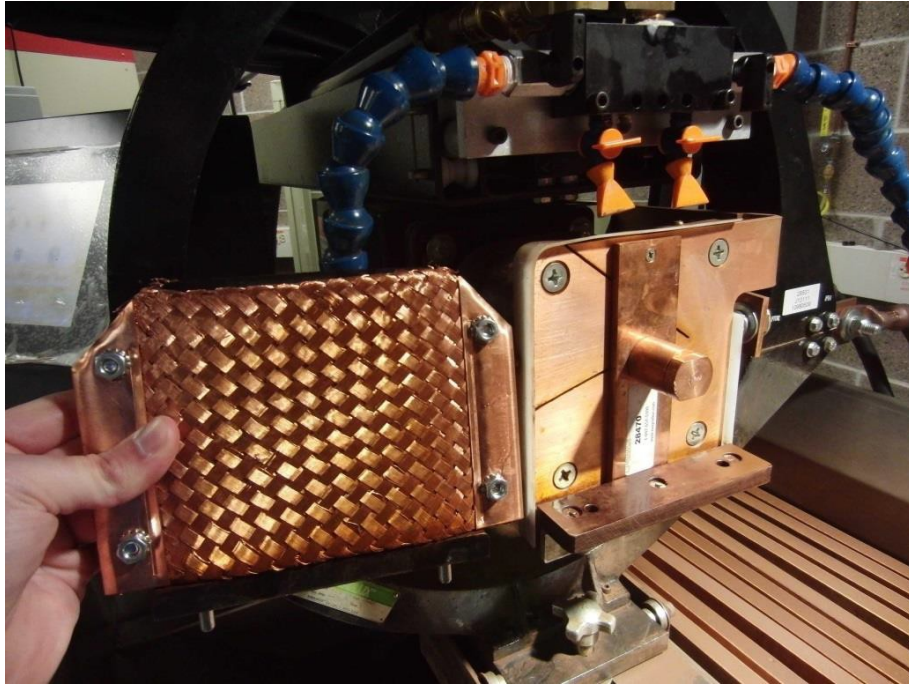9.   Repeat steps 2–8 for different variations of current type and percentage.

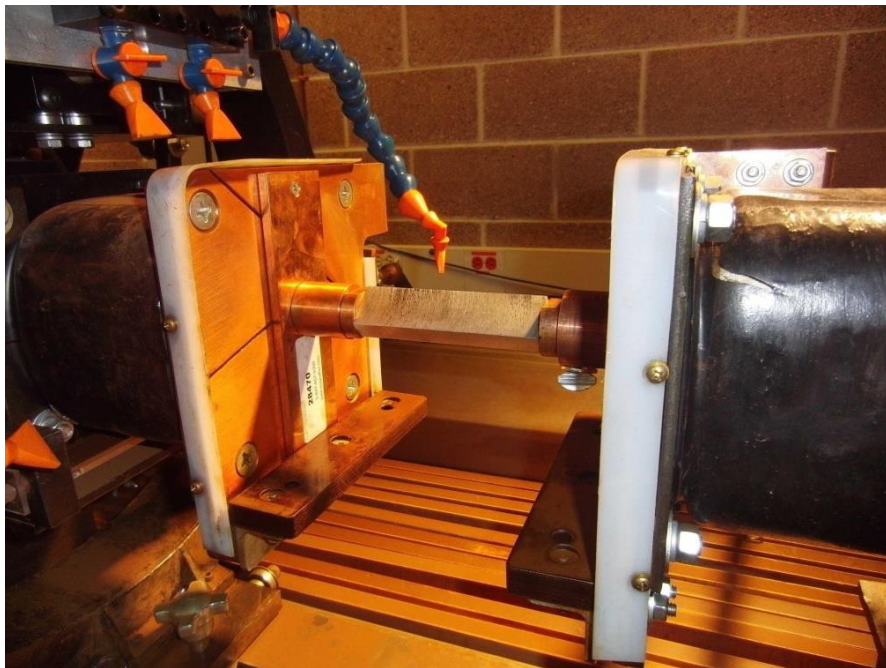VERTICAL CRACK SAMPLES (SHORT BARS)

SETUP

1.   Move the coil on the MPI bench out of the way.
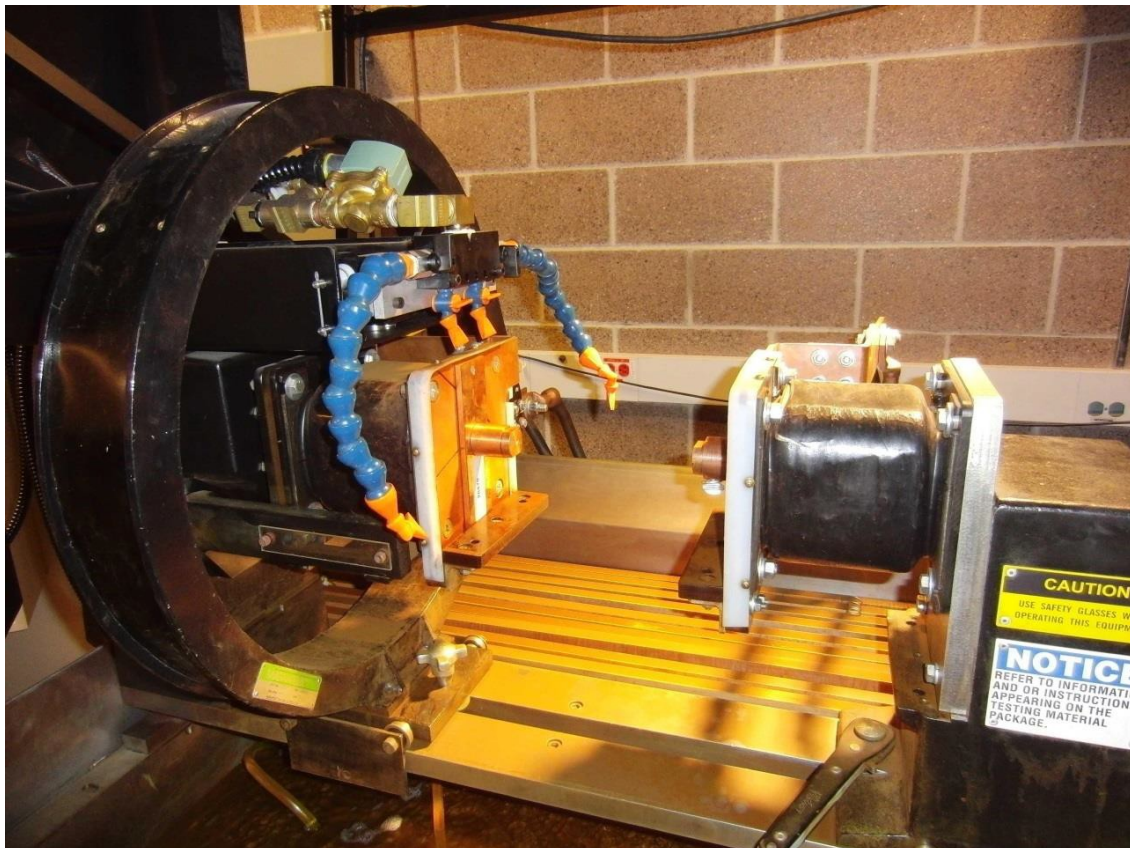
2.   Replace the copper mesh contact pads with copper contact studs.
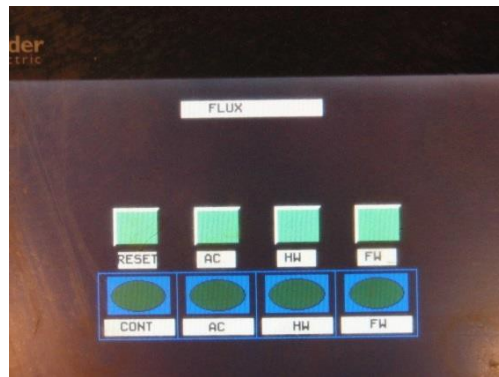

3.   Position the tail contact so that the bar is clamped when the head contact is extended.
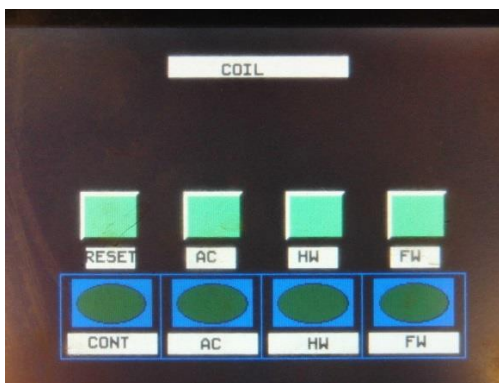
4.   On the main control screen, turn the bath to manual.

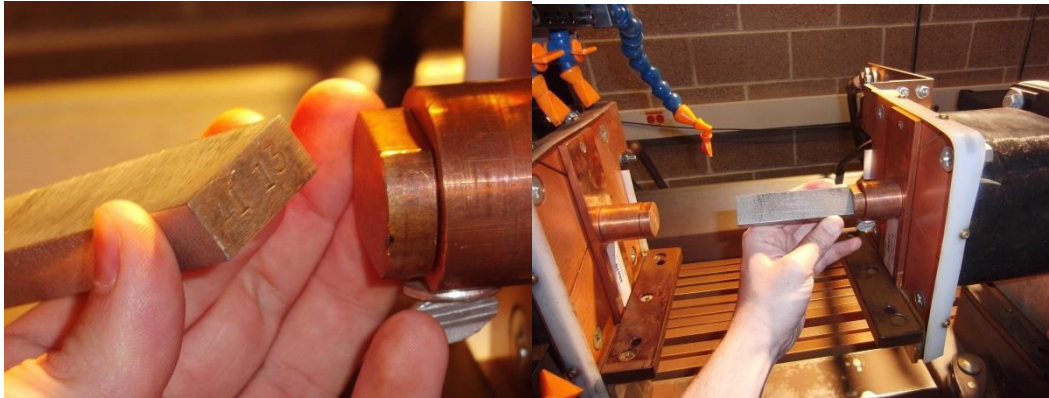5.   On the flux manual setup screen, push reset.

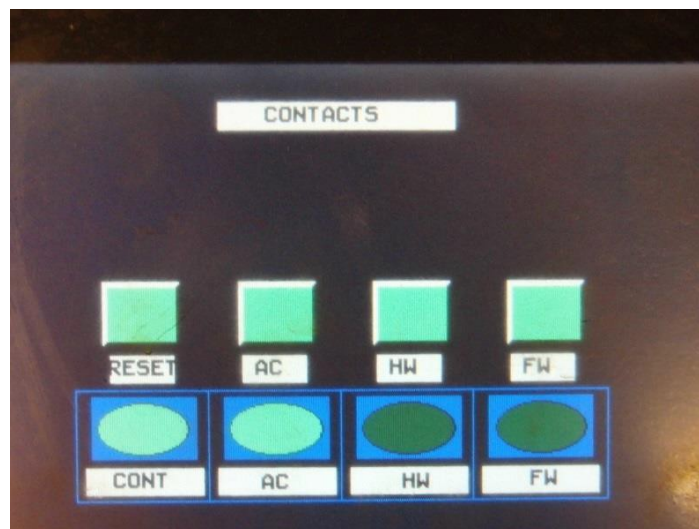6.   On the coil manual setup screen, push reset.

PROCEDURE

1. Hold the sample at a 45° angle with the numbered end against the tail contact stud and the crack up and facing towards the user.

2. Press and release the foot pedal to clamp the sample in place.
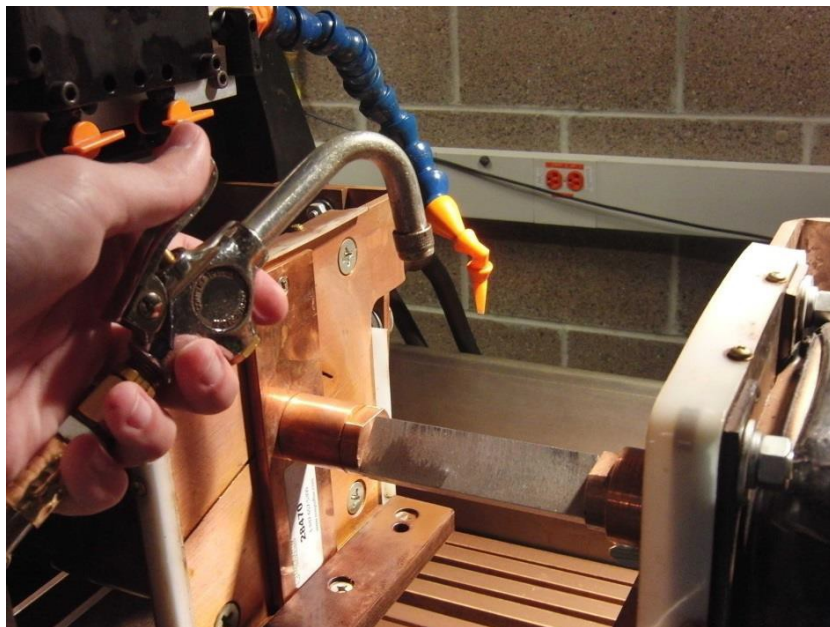

3. On the contacts manual setup screen, select AC, HW, or FW.

4.   On the main control screen, select a current percentage on the dial under contacts.


5.   Manually bathe the sample with the spray nozzle 6″ above the sample. Spray down and back once starting from the head contact side. The bath should take approximately 2 seconds.

6.   Immediately after the bath, magnetize the sample.

7.   Allow the sample the drip for 10–15 seconds.

8.   Hold onto the sample.

9.   Press and release the foot pedal to release the sample.

10. Place the sample on the MPI cart platform for testing.

11. When testing is done, hold the sample in the same orientation as before up against the tail contact stud.

12. Press and release the foot pedal to clamp the sample in place.

13. Press the DMAG button on the main control screen to demagnetize the sample.
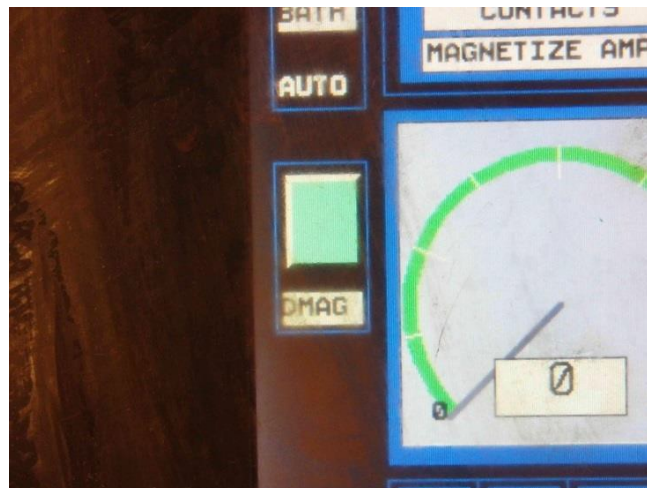
14. Repeat steps 3–13 for variations of current type and percentage.

APPENDIX C—PROCEDURE FOR OPERATING THE MOTION CONTROL CART
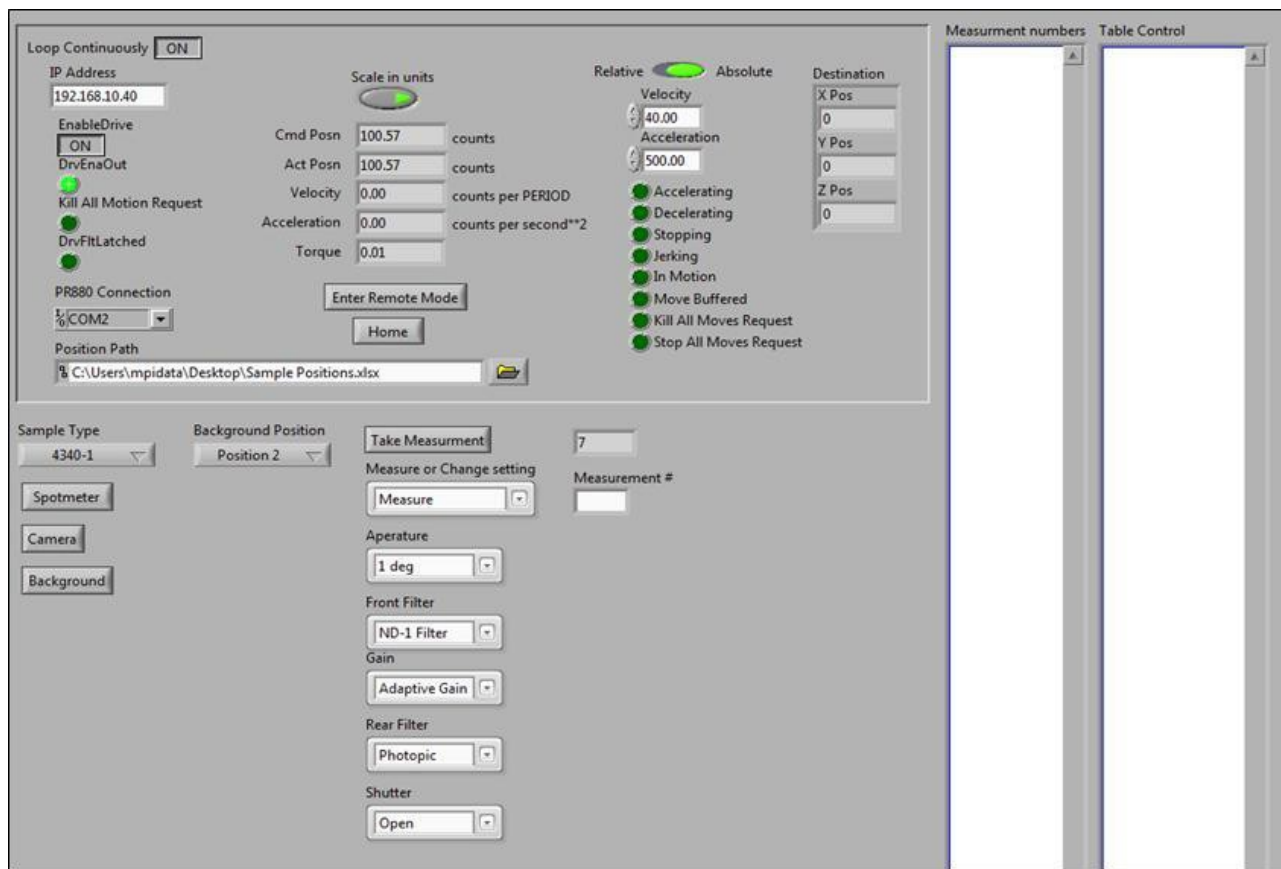
The LabVIEW™ program was created to collect data.

Figure C-1. User interface for LabVIEW program used to control the PR-880 spotmeter

STEPS FOR USING THE BASELINE MOTION CART

1. Turn on the three-axis motion arm, servers, UV light sources, and the PR-880 photometer.

2. Open the LabVIEW program, "Current Program.vi", and select "Loop Continuously." Press and hold the "Enter Remote Mode" button until the PR-880 photometer switches to remote mode.

3. Prepare a sample, and place it securely in the motion tray.

4. Change the settings for the PR-880 photometer according to experiment requirements.

5. Press "Spotmeter" to move the sample in position below the PR-880 photometer.

6.	Press "Take Measurement" and wait for a number to appear in the table (when starting, place the number that appears in the measurement numbers into the "Measurement #" box.)

7.	Press "Background," select the Background position, and then press "Take Measurement" and wait for numbers to appear in the table. Repeat for each Background Position.

8.	Press "Camera" and wait for the motion tray to move to beneath the camera. Then use the program EOS Utility to take the picture.

9.	Move the motion tray back to the Spotmeter position and repeat with each sample.

Magnetic Particle Inspection

Module #1 Variability of Equipment and Magnetizing Current

1

Purpose

- Magnetic particle inspection (MPI) equipment provides users with several options of waveforms and magnetizing methods.
- Users should make the optimum choice of a waveform and magnetizing method best suited for the inspection requirement.
- For guidance, this module shows characteristics of waveforms and magnetizing methods.

2

Module #1 Contents

Three sections discussing:

Characterization of current waveforms (AC, HWDC, FWDC)
- Types of waveforms and their differences
- Benefits and Detriments (uses, reasons for use)

Correlation of waveform to Bench Settings and Readout
- Measured RMS current versus bench setting and readout according to our interpretation
- Various calculation methods (different manufacturers have different methods)
- Changes in waveform with increased amperage

Correlation of waveform with magnetic field at part surface and with respect to amperage
- Benefits and Challenges (uses, reasons for use)

3

Experimental setup/Equipment used

Items	Details
Used bench	MD3-2060L
Maker	Magnaflux
Types of waveform	Alternating current (AC), Half Wave Direct Current (HWDC) and Full Wave Direct Current (FWDC)
Magnetizing method	Coil shots, Head shots and Flux flow
Specimens	Coil shots: N/A Head shots: Copper bar (Diameter 1 inch, Length 1 foot) Flux flow: Steel bar (2 inch × 2 inch × 18.125 inch)
Instruments	Shunt resister (2000 A, 100 mV) Differential amplifier (LeCroy DA1855A (Setting: Attenuator ÷10, Gain ×10)) Oscilloscope (LeCroy LT342)

4

- This table lists the details of the equipment used in this work.
- The bench is multidirectional and is capable of three different ways to create/induce a magnetic field.

Section 1: Characterization of Current Waveform

Overview of Current Waveform Characteristics

- There are three types of waveforms, with the primary frequency of 60 Hz
  - "AC" --- Nominally sinusoidal wave, with the option of reduced duty cycle
  - "HWDC" --- Positive half cycle of the AC waveform, with the negative portion of the wave removed
  - "FWDC" --- All positive waveform fully rectified from the AC waveform
- Bench readout amperage appears in RMS (root mean square)
- The drive current is the highest for AC, reduced for FWDC, and further reduced for HWDC
- Subsequent Pages 7 though 14 show that:
  - Magnetic flux density near part surface is the largest for AC among the three.
  - DC works better than AC for finding a crack below the surface.

- Root mean square (RMS) is a statistical measure of the magnitude of a varying quantity.
- Half-wave direct current (HWDC) is sometimes referred to as "Half Wave Rectified."
- Note: Not every bench in use is capable of providing all three types of waveforms. Some benches may only have alternating current (AC) or direct current (DC) selectors.
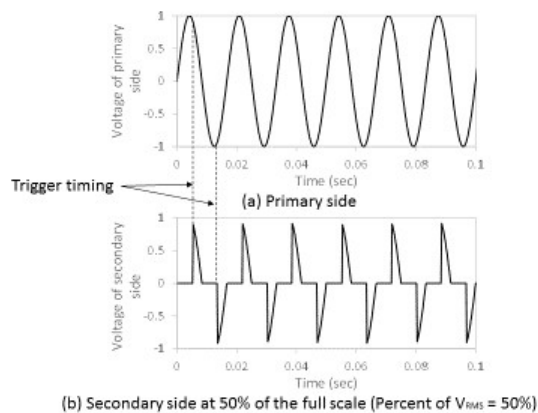
Characterization of AC Current Waveform

Types of Waveform and the difference between them
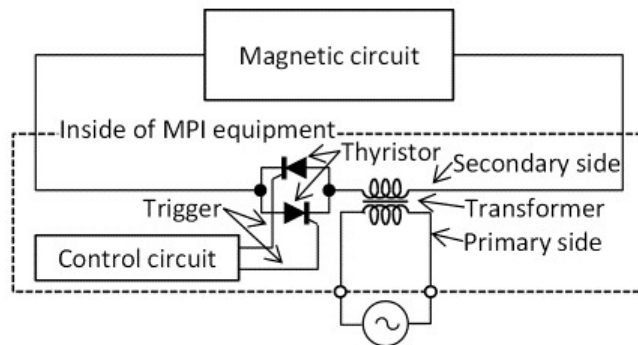
- Simplified schematic of the electrical circuitry for the AC excitation.
- A transformer turns a power source into a large current.
- A thyristor acts as a switch that can let large current flow in one direction when a gate of the thyristor receives a trigger signal.
- The thyristor can therefore control the duty cycle of the current waveform via the trigger voltage.

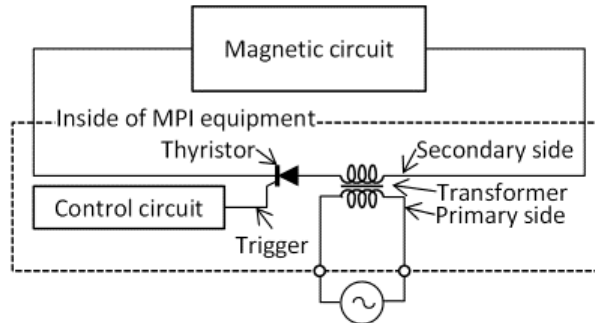Characterization of AC Current Waveform

Types of Waveform and the difference between them

- Magnetizing current has a harmonic component due to the switching of the thyristors.
- Excitation energy can be controlled by manipulating trigger timing or duty cycle.
- The lower plot, for instance, shows a limited duty cycle waveform, where RMS current is 50% of that of the full duty cycle AC.
- One consequence is that the bench can generate a switching noise.
- Note: The waveform amplitudes are normalized to unity.
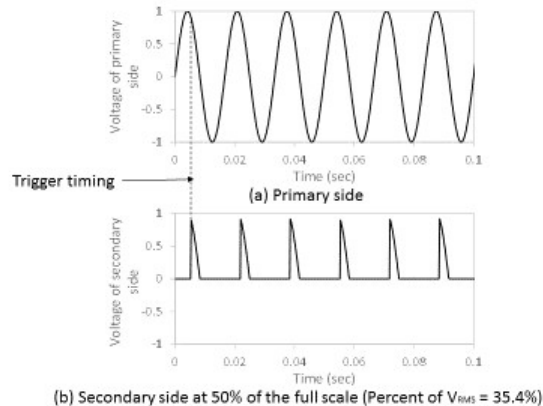
Characterization of HWDC Current Waveform

Types of Waveform and the difference between them

Magnetic circuit

Inside of MPI equipment
Thyristor
Secondary side
Control circuit
Transformer
Primary side
Trigger

9

- Simplified schematic of the electrical circuitry for the HWDC excitation.
- A thyristor acts as a switch that can let large current flow in one direction.
- The HWDC current waveform is obtained accordingly.
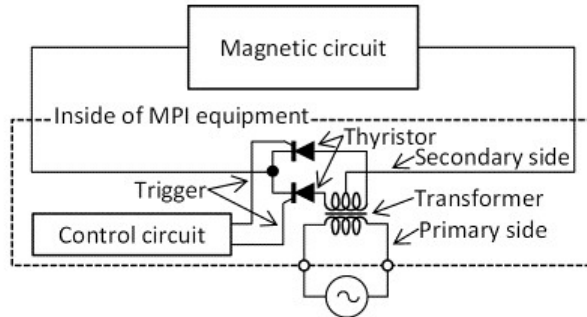
Characterization of HWDC Current Waveform

Types of Waveform and the difference between them

Voltage of primary side
Trigger timing
Time (sec)
(a) Primary side

Voltage of secondary side
Time (sec)
(b) Secondary side at 50% of the full scale (Percent of V_{RMS} = 35.4%)

10

- The HWDC waveform is derived from the AC waveform, with the negative part turned off.
- Therefore, the RMS current of HWDC is reduced from that of the AC waveform by the factor of $\sqrt{2}$ for the full duty cycle sinusoidal waveform.
- The reduction factor is larger for a lower duty cycle.
- For example, the lower plot shows a limited duty cycle HWDC, so that the RMS current is 50% of the full scale, which is $1/\sqrt{2}$ of AC (overall, $50/\sqrt{2}$ =35.4).
- Note: The waveform amplitudes are normalized to unity.

Characterization of FWDC Current Waveform

Types of Waveform and the difference between them

- Simplified schematic of the electrical circuitry for the full-wave direct current (FWDC) excitation
- Two thyrisotors convert the negative part of the AC waveform to positive.
- The duty cycle can be reduced by the thyristors.

Characterization of FWDC Current Waveform

Types of Waveform and the difference between them

(a) Primary side

(b) Secondary side at 50% of the full scale (Percent of V_{RMS} = 50%)
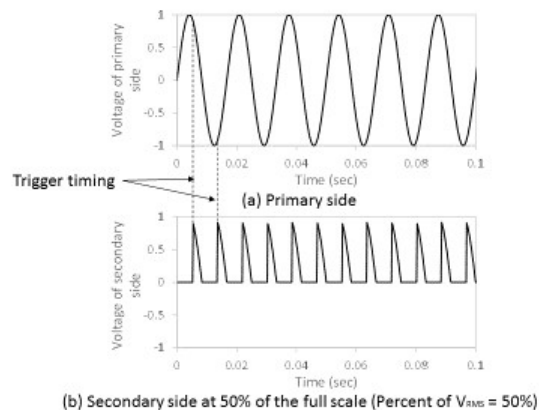
- The RMS current of the FWDC is equal to that of AC.
- The lower duty cycle reduces the RMS current.
- For example, the lower plot shows a limited duty cycle waveform, where the RMS current is 50% of that of the full duty cycle FWDC.
- FWDC may be found used as either single phase or as three phase.
- Note: The waveform amplitudes are normalized to unity.

Characterization of Current Waveform
Types of Waveforms and their differences
(Theoretical waveforms)
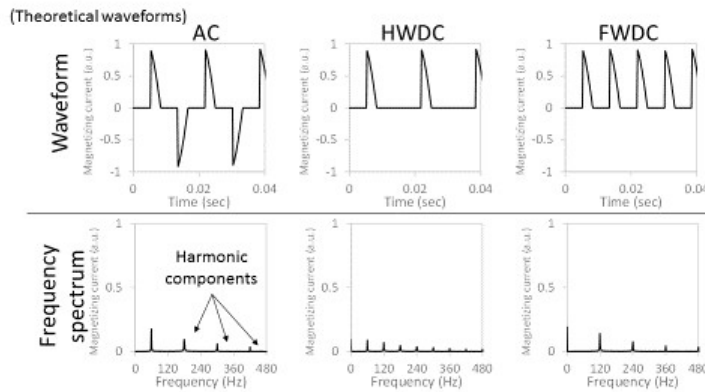
- Frequency components of the AC, HWDC, and FWDC waveforms of a common duty cycle.
- By looking at the waveforms of AC, HWDC, and FWDC, it is possible to illustrate the concept of HW-rectified and FW-rectified waves.
- The lower graphs emphasize the amount of available current within each wavetype.

Characterization of Current Waveform
Types of Waveforms and their differences
(Measured waveforms of Coil shots 50%FS)
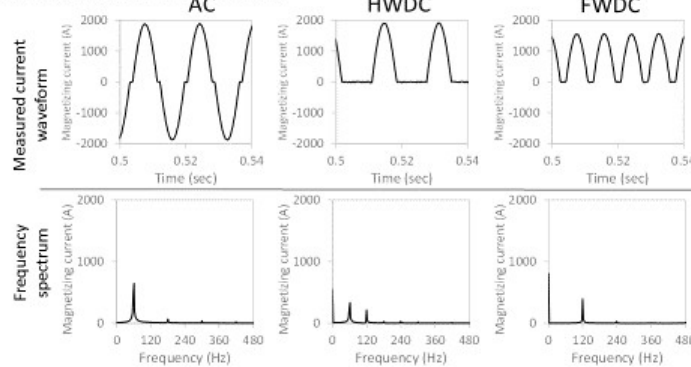
- These figures show measured current waveforms.
- Shapes of the waveform are changed by impedance.
- Frequency spectrum calculated from time period of 0.2–0.8 seconds of data collected from a 1-second shot.
- This slide shows a more realistic representation of what occurs when a part is placed on the bench.

Characterization of Current Waveform

Benefits of AC (uses, reasons for use)

- Can provide better surface inspection of complex shapes
- Easy to demagnetize a part after inspection
- Good particle mobility

15

- AC current travels better on the surface, and is therefore more often used for locating surface defects.

Characterization of Current Waveform

Challenges of AC (what can be missed)

- Reduced current strength leading to lower maximum magnetic field when using (coil, coil pack and cable wrap) due to the inductance effect

16

- When using magnetizing options other than direct magnetization, there is a reduction of current due to inductance effects from the inspected part.

Characterization of Current Waveform

Benefits of HWDC (uses, reasons for use)

- Better subsurface detection than AC
- Better mobility of the particles as a result of the pulsating field versus FWDC
- Higher maximum field generation in coils, coil packs and coil wraps than AC

17

- HWDC and FWDC are more often used to locate near-surface defects.

Characterization of Current Waveform

Challenges of HWDC (what can be missed)

- Not available on all benches
- Not as optimal for locating surface defects

18

Characterization of Current Waveform

Challenges of FWDC (what can be missed)

- Least particle mobility of the three wave forms (epically with a high duty cycle)
- Parts can be difficult to demagnetize if very thick or have complex geometries
- Not available on all benches

20

Characterization of Current Waveform
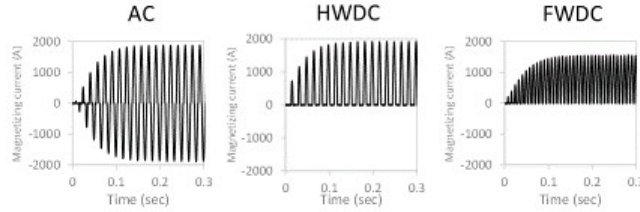
Benefits of FWDC (uses, reasons for use)

- Better for finding subsurface defects than AC or even HWDC
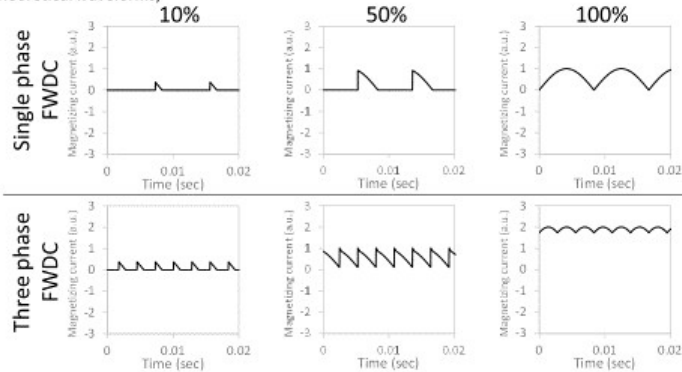- Highest current strength leading to maximum field generation when using coil, coil packs or cable wrap (lowest inductance)

19

- This slide shows the concept of rise time and the fact that reaching full current value is not instantaneous.
- Rise time–The time taken by a signal to change from a specified low value to a specified high value.

- Three-phase FWDC can obtain smoother waveform than single phase.
- This shows the difference in current waveform between the two phases.
- Operators should be familiar with the phase they are using.

Section 2: Correlation of Waveform to Current Setting and Bench Readout

23

Correlation of Waveform to Current Setting and Bench Readout

Table. Details of bench readout and experimentally measured current

Parameters	Details
Bench readout	AC : I_{RMS}. HWDC: Average × 2. FWDC : Average.

24

- This table shows the relationship details between bench readout and current measured experimentally.
- "Bench readout" for AC is RMS, and the HWDC and FWDC are based on the average X2 and average current, respectively.
- The current measurement experimental results are shown in the next three slides.

Correlation of Waveform to Current Setting and Bench Readout
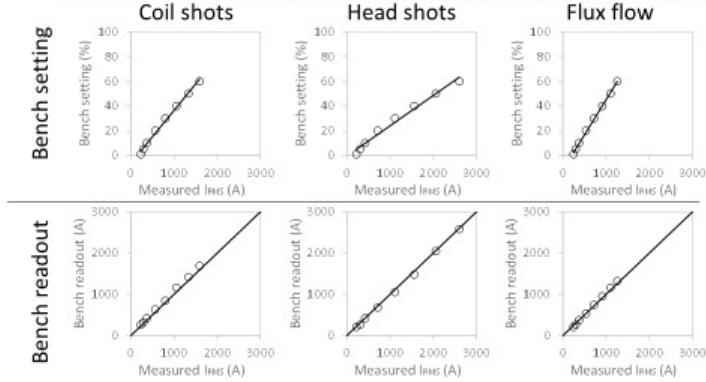
- In the wet-horizontal bench used for this research, the bench readout for AC is the RMS value of the current (similar to the peak current divided by $\sqrt{2}$). Bench Readout: I_{RMS}
- This bench readout agrees with the experimentally measured RMS values for all three modes of applying the current; coil shots, head shots, and flux-flow shots.
- Note that the relative distribution of current versus bench setting is not evenly distributed. There are more points near the bottom of the scale to allow for better fine-tuning of the current value to aid in complying with inspection protocols.

Correlation of Waveform to Current Setting and Bench Readout
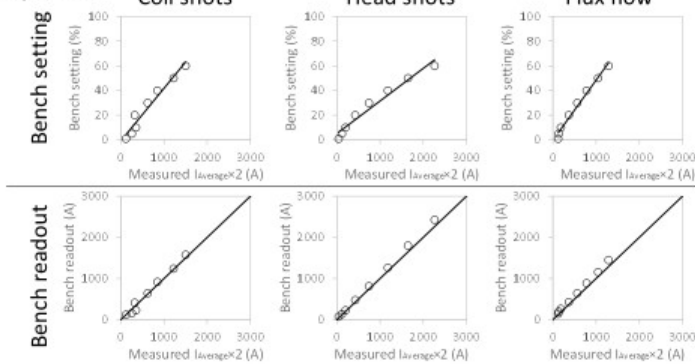
- Bench readout for HWDC is the average current multiplied by two. This readout matches experimental results for all three types of shots: coil, head, and flux flow.
- Bench Readout: Average x 2
- The goal of multiplying the average times by two for HWDC is to achieve the same peak current and, therefore, same peak field strength for both HWDC or FWDC. Because there

are twice as many pulses per unit time for FWDC, it would have twice the average current if the peak value of the waveform were held constant. Another way to put this is multiplying the value of the HWDC times by two allows the bench readout for HWDC to give very similar measured field strength to FWDC at the same readout.
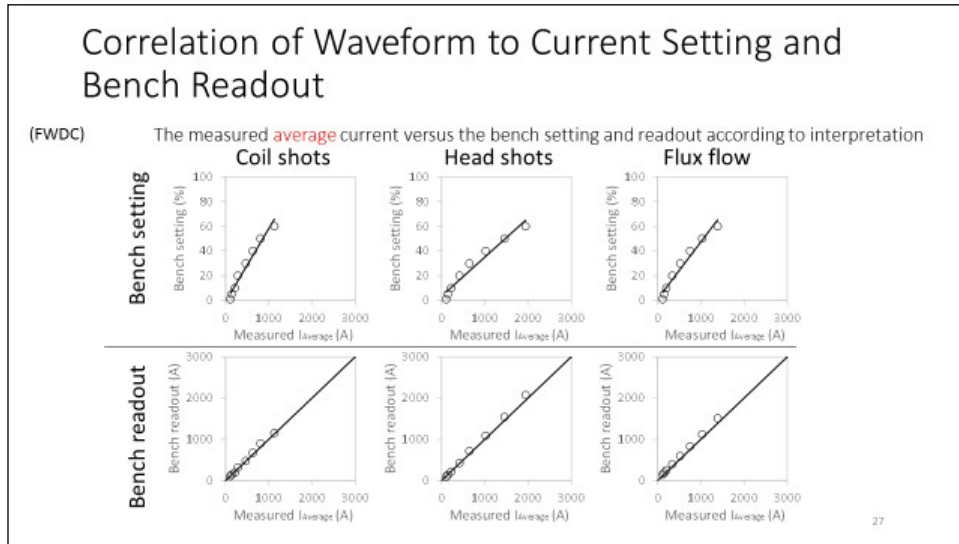
- Bench readout for FWDC is the average current of the measured waveform. This readout matches experimental results for all three types of shots: coil, head, and flux flow.
- Bench Readout: Average
- Because there are twice as many pulses per unit time for FWDC, it would have twice the average current of HWDC if the peak value of the waveform were held constant, so unlike HWDC, do not multiply the average value times by two for FWDC. Using the average for FWDC allows direct comparison between HWDC and FWDC in regards to peak current and peak field strength.

Section 3: Correlation of Magnetic Field at Part surface with respect to Amperage

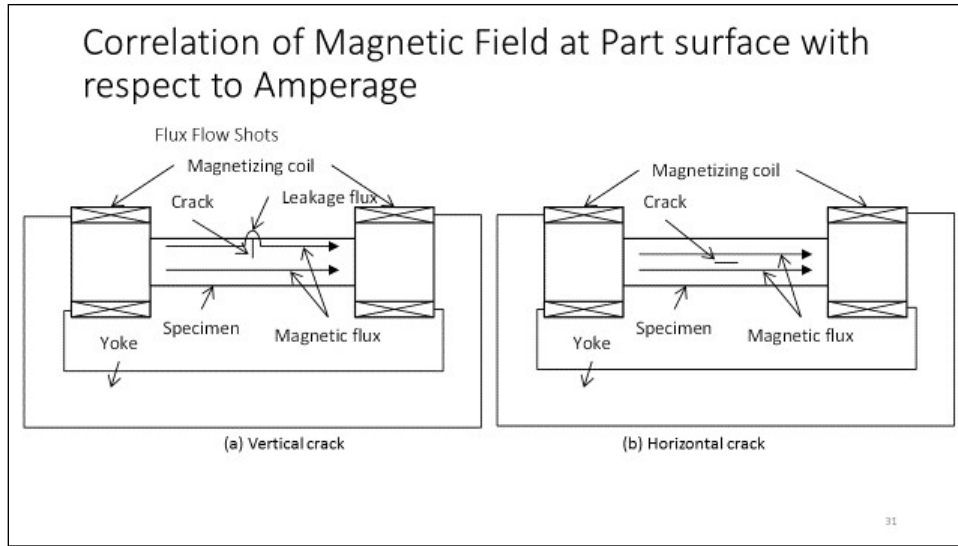Correlation of Magnetic Field at Part surface with respect to Amperage
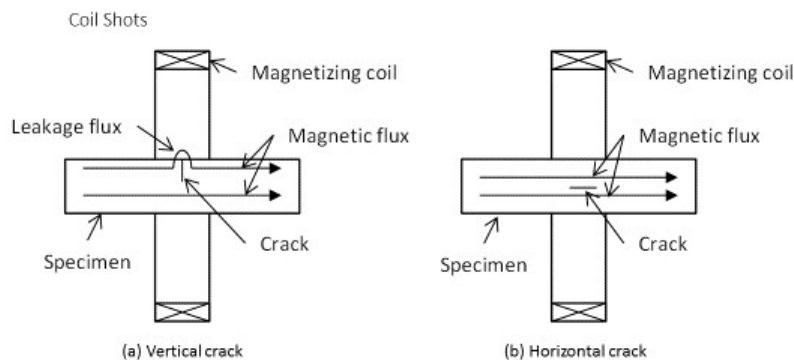
- As current is passed through the coil, an induced magnetic field is created in the part.
- The figure on the left shows the flux leakage that occurs with a defect that is perpendicular to the induced magnetic field.
- The figure on the right shows that there is no flux leakage present when the defect is parallel to the induced field.
- Presenter needs to refresh the audience with the concept of the "right hand rule."

Correlation of Magnetic Field at Part surface with respect to Amperage
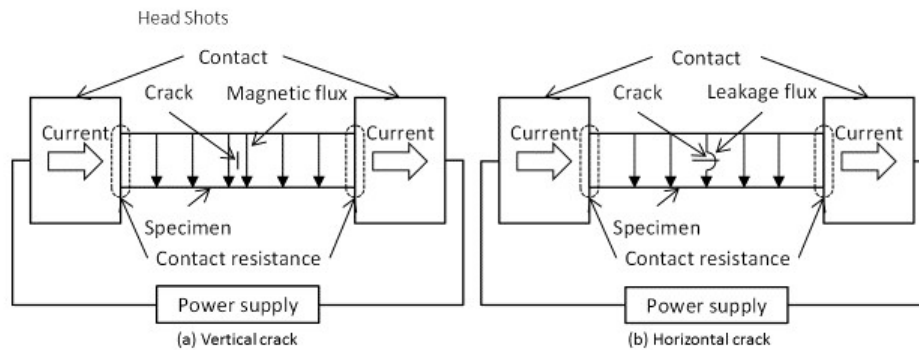
- As current is passed through a part, a magnetic field is created perpendicular to the direction of the current direction.
- The figure on the left shows that there is no flux leakage detected when the defect is parallel to the magnetic field and perpendicular to the current direction.
- The figure on the right shows that there is detectable flux leakage when the defect is perpendicular to the magnetic field and parallel to the current direction.

Correlation of Magnetic Field at Part surface with respect to Amperage

Flux Flow Shots

(a) Vertical crack   (b) Horizontal crack

- The flux flow option may not be available on all benches.
- The figure on the left shows that flux leakage occurs when the defect is perpendicular to the induced magnetic field.
- The figure on the right shows that no flux leakage may be detected when the defect is parallel to the induced magnetic field.

Correlation of Magnetic Field at Part surface with respect to Amperage

Table. Characterization of magnetizing methods (When same bench setting is used.)

Magnetizing method	Flux direction	Found crack direction	Primary factor of current repeatability
Coil shots	Horizontal	Vertical	Magnetic resistance of specimen
Head shots	Vertical	Horizontal	Resistance of specimen and contact
Flux flow	Horizontal	Vertical	Magnetic resistance of specimen

Magnetizing method	Magnetizing current	Magnetic flux	Primary heat factor
Coil shots	Small	Small	Eddy current
Head shots	Large	Middle	Magnetizing current
Flux flow	Middle	Large	Eddy current

- Correlation between the waveform of magnetic field on the part's surface and with respect to amperage.
- Relative directions between the flux flow and crack to be found is the most important, namely they should be perpendicular to each other for optimum detection.
- The direction of the magnetic flux flow and its relationship to defects is very important.
- The defect should be perpendicular to magnetic field to be detected.
- The reason is explained on pages 33–42 of the main report.

Correlation of Magnetic Field at Part surface with respect to Amperage

Coil Shots – Benefits

- Non-contact with part
- Longitudinal magnetization to locate transverse defects
- Can be easier to inspect some complex geometric parts
- Can be quick

33

Correlation of Magnetic Field at Part surface with respect to Amperage

Coil Shots – Challenges

- Longer parts may require multiple shots to inspect entire length
- Length to Diameter L/D ratio is important in determining current settings
- Sensitivity decreases towards the ends of the part due to general leakage field patterns
- Quick break is needed to reduce end effect on short parts with a low L/D ratio

34

- Remember that the range of the coil's effective field is limited to 6″–9″ on either side of the coil.
- Length to diameter or "Fill Factor" will be discussed in a later module.

Correlation of Magnetic Field at Part surface with respect to Amperage

Head Shots – Benefits

- Can be fast and easy
- Circular magnetic field surrounds entire part due to current flowing through the part itself
- Good sensitivity to surface and near surface defects

35

Correlation of Magnetic Field at Part surface with respect to Amperage

Head Shots – Challenges

- Connections with end pieces can play a role in the amount of magnetization
- Possible damage to part can occur if proper contact is not made
- Heat damage can occur at contact points
- Limited in ability to completely magnetize complex geometric parts

36

- It is important to ensure good contact between the copper pads and the part prior to current flow.

Correlation of Magnetic Field at Part surface with respect to Amperage

Flux Flow Shots – Benefits

- No electrical contact
- Entire length of part is subjected to magnetic field
- More uniform magnetic field than coil shot

37

- Not all benches have the option of flux flow.

Correlation of Magnetic Field at Part surface with respect to Amperage
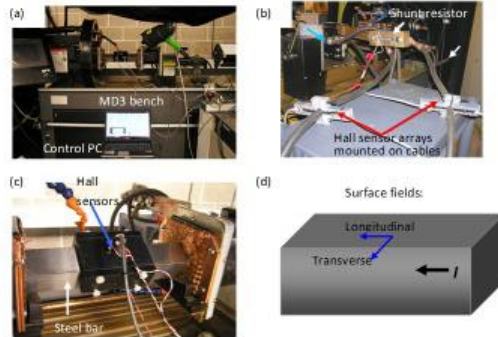
Flux Flow Shots – Challenges

- Not widely available on all benches, therefore familiarity may be an issue
- No standard guidelines to determine proper equipment settings

38

- There may not be formulas available to determine the settings, such as with head and coil shots.
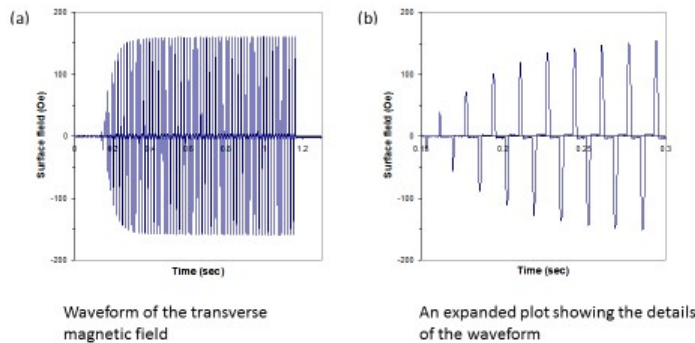
Correlation of Magnetic Field at Part surface with respect to Amperage

- The experimental setup used to measure magnetization current waveform and surface magnetic field under AC head shots on the MD3 bench
- Four linear arrays of Hall effect sensors were attached to two cables connected to the headstock. A shunt resistor was connected to one of the cables and used to measure the current directly.
- A bi-axial Hall sensor mounted onto a $2'' \times 2'' \times 12''$ steel bar to measure the surface field components. The steel bar was tilted 45°, in exactly the same orientation as it is used for the sensitivity study of QQI, Castrol Strip, and pie gauge.
- A schematic showing the surface fields measured using the Hall sensor integrated circuit.

Correlation of Magnetic Field at Part surface with respect to Amperage

- The waveform of the transverse magnetic field measured at the center of the steel bar for AC head shots at 18% full scale
- An expanded plot showing the details of the waveform.

Correlation of Magnetic Field at Part surface with respect to Amperage
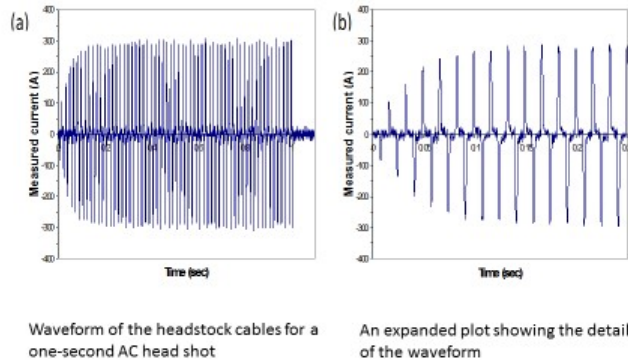
(a) Waveform of the headstock cables for a one-second AC head shot

(b) An expanded plot showing the details of the waveform

- The current waveform measured from one of the headstock cables for a 1-second AC head shot at 18% full scale.
- An expanded plot showing the details of the waveform, including the duty cycle.

Correlation of Magnetic Field at Part surface with respect to Amperage
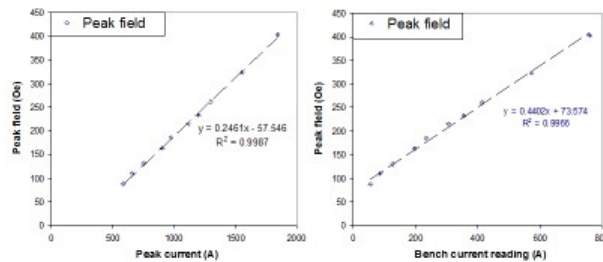
$y = 0.2461x - 57.546$
$R^2 = 0.9987$

$y = 0.4402x + 73.074$
$R^2 = 0.9966$

- The magnetization current waveforms and surface magnetic field on a steel bar subjected to AC head shots have been characterized.
- This is a plot of the peak value of the surface field (left) versus the peak current and bench readout (right) for AC head shots from amperages ranging from 1%–45% full scale.
- These plots show the relationship between current applied and magnetic field generated.

Definitions

- RMS - Root mean square, a measure of the magnitude of a varying quantity
- Thyristor - a solid-state semiconductor device which acts as bistable switch, conducting when the gate receives a current trigger, and continue to conduct while it is forward biased (that is, while the voltage across the device is not reversed).
- AC - Alternating Current, a type of electrical current where the current repeatedly changes direction
- HWDC – Half Wave Direct Current which has some characteristics of both alternating current (AC) and direct current (DC) waveforms. The voltage of a DC wave is roughly constant.
- FWDC - Full Wave Direct Current which has some characteristics of both alternating current (AC) and direct current (DC) waveforms. The voltage of a DC wave is roughly constant.
- Rise Time - the time taken by a signal to change from a specified low value to a specified high value

44

Conclusions

- Several options exist for users of MPI with a bench setup, including AC, HWDC, FWDC and Flux Flow
- Certain options work better for some inspections, such as AC for surface inspection
- Most bench readouts are within +/- 10 % of the bench setting
- There are benefits and challenges to each type of option selected for MPI
- Inductance from the inspected part can effect the amount of current required for a proper inspection

43

Magnetic Particle Inspection

Module #2

Purpose

- Magnetic material properties are important in MPI, when users decide the magnetizing method and current value. This module explains how material properties relate to the magnetic characteristics.

- Magnetic particles attach to a specimen by magnetic flux leakage. This module demonstrates magnetic flux leakage of a specimen.

2

Module #2 Contents

- Magnetization parameters of the part
- Measure in situ leakage field around fatigue cracks to identify optimal magnetizing parameters

3

Section 1: Magnetization parameters of the part

4

Types of steel used

Two alloys of steel were used in this program, 4340 and 4130

These alloys were selected after consultation with several industry partners, based on their suggestions for the steel alloys most often used in the aviation industry.

5

- Very few parts in aviation are made from steel, but steel or other ferromagnetic material is used in landing gear and engine components.

Magnetization parameters of the part
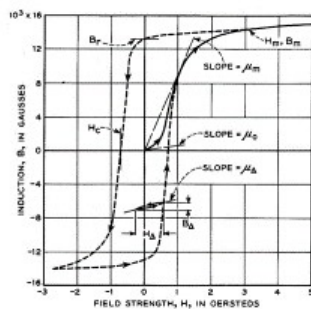Document B-H loop for permeability of the part

Fig. Prototypical B-H Loop*

- Flux density B [T]
  - The flux density is the flux per unit area.
  - B_r is called the residual flux density. Residual technique becomes easier to apply as the value is larger.
- Magnetic field H [A/m]
  - The magnetic field may be produced by a current as well as by a magnet, and the unit can be defined in terms of current.
  - H_c is called the coercive force. Demagnetization needs larger current as the value is larger.
- Permeability μ [H/m]
  - The permeability is the ratio B/H. $B = \mu H$ and $\mu = \mu_0 \mu_r$ are established. μ_0 is the permeability of a vacuum. μ_r is the relative permeability.
  - B-H of ferromagnetic materials loop has the hysteresis loop. Therefore μ_r of ferromagnetic materials is nonlinear to H or B. μ_r becomes a value close to one in too large magnetic field. The values of H and B at the tips of a loop are called H_m and B_m. The status of the specimen at that time is called the magnetic saturation.
  - A specimen is magnetized by using smaller current as the permeability of the specimen is larger. MPI can not apply to a specimen that has too small permeability.

*Richard M. Bozorth, "Ferromagnetism", IEEE Press, p. 4

6

- When determining the magnetization level, it is desirable to achieve saturation into the "knee" of the B-H loop.
- Magnetization beyond the "knee" of the B-H loop does not benefit the inspection process.
- The "knee" refers to the region of the curve where the slopes changes drastically, almost like a 90° curve.
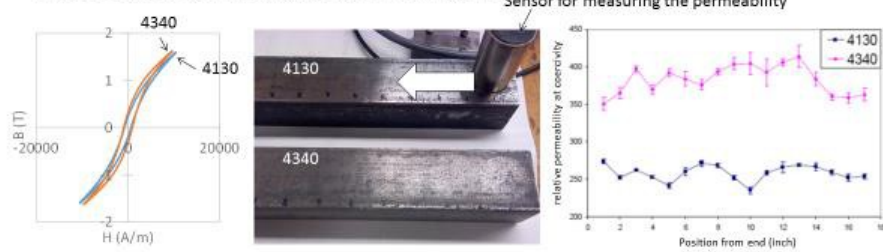
Fig. A. As measured B-H Loop by using Magnescope*
Fig. B. Picture of specimens
Fig. C. Magnetization parameters of the part by using Magnescope*

- As shown in Fig A, each of steels has different magnetization parameters.
- As shown in Fig C, steels have varying magnetization parameters.

(* A Magnescope is an instrument developed at ISU for measuring the hysteresis loop from one sided access to a part.)

- The B-H loops in Fig A show magnetization but not to saturation.
- Though changes in relative permeability do exist within a part, the limited studies conducted did not demonstrate any adverse effect on the magnetization.
- A Magnescope is an instrument developed at ISU for measuring the hysteresis loop from one-sided access to a part. It is a laboratory-based instrument.

Section 2: Measure in situ leakage field around fatigue cracks to identify optimal magnetizing parameters

Initial determination of current levels

- For situations where initial current levels need to be determined, engineers often use formulas in their initial calculations
- Often these calculations are verified and adjusted by actual measurements and aided by the use of field meters and other indicators such as QQI's
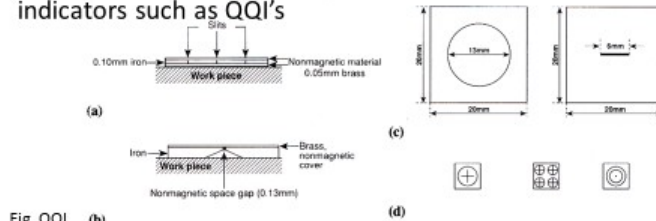
Fig. QQI (b)

(Louis Cartz, "Nondestructive Testing", ASM International, p. 157)

- These formulas can be found in ATM 1444.
- QQI stands for Quantitative Quality Indicators.
- Depth of the indication on a QQI can vary anywhere from 0.0004″–0.0008″.

Measure in situ leakage field around fatigue cracks to identify optimal magnetizing parameters

Initial determination of current levels

6.3 Magnetic Field Strength

- 6.3.1 The applied magnetic field shall have sufficient strength to produce satisfactory indications, but it must not be so strong that it causes the masking of relevant indications by nonrelevant accumulations of magnetic particles.
- Adequate magnetic field strength may be determined by one or a combination of the following methods:
  - In unidirectional, or multidirectional magnetizing applications,
    - by examining parts having known or artificial discontinuities of the type, size, and location specified in the acceptance requirements or by using the notched shims as defined in Annex A1;
    - by using a Hall Effect probe gaussmeter capable of measuring the peak values of the tangential field as with a minimum value of 30 Gauss (30×10^{-4} Tesla [T]) when measured at the part surface
  - Using the current levels specified by the formulas given in Appendix X3 and Appendix X4.

(ASTM E 1444-12, p. 6, 6.3 Magnetic Field Strength)

- These current levels and formulas provide only a rough guide and shall only be used in conjunction with either 6.3.1.1 or 6.3.1.2, or Cognizant Engineering Organization approval, or a combination thereof. In some cases, the formulas may lead to over magnetization of the work piece and care should be exercised when using them.
- ASTM 6.3.1.1 and 6.3.1.2 are paraphrased in the slide to reduce the amount of written words on the slide.
- This topic will be visited again in more detail in Module 3, found in appendix F.

Determination of proper current levels in a coil

- In the determination of the proper current levels in a coil one must first determine the fill factor level.

- Fill factor is the comparison of the free space of the coil to the size of the part when placed inside the coil
- There are four different situations that need to be considered when dealing with fill factor:
    - low fill when the part is next to the coil
    - Low fill when the part is in the center of the coil
    - High fill when the part fills most of the space inside the coil
    - Intermediate fill when the comparison is in between high and low fill

11

Low fill factor – Side
If $A_{coil} \geq 10 \times A_{part}$, use the following equation.
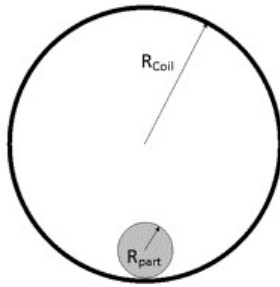
$A_{coil} = \pi R_{coil}^2$

$A_{part} = \pi R_{part}^2$

$$NI = \frac{K}{L/D}(\pm 10\%)$$

N = number of turns in coil

I = current in amps applied to the coil

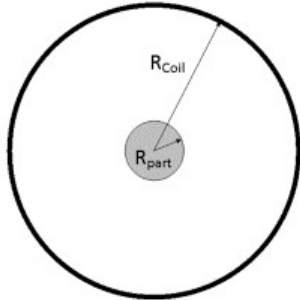K = 45000 permeability constant

L = length of part

D = diameter of part (same units as L)

12

- For small parts, a low fill factor is used with the coil

Low fill factor – Center
If $A_{coil} \geq 10 \times A_{part}$ and the part is centered in the coil, use the following equation.

$A_{coil} = \pi R_{coil}^2$
$A_{part} = \pi R_{part}^2$

$$NI = \frac{KR_{coil}}{\left(\dfrac{6L}{D}\right) - 5}(\pm 10\%)$$

N = number of turns in coil
I = current in amps applied to the coil
R_{coil} = radius of coil (mm or in)
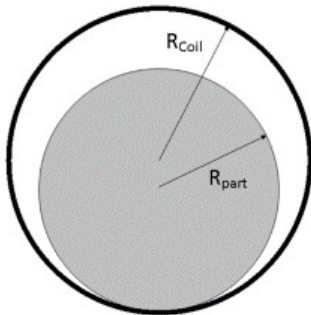K = 1690 if R is in mm or 43000 if R is in inches
L = length of part
D = diameter of part (same units as L)

13

- Small diameter parts can also be placed in the center of the coil for magnetization.
- This might occur with long parts where it is impractical to place the part on the coil.

High fill factor –
If $A_{coil} < 2 \times A_{part}$, use the following equation.

$A_{coil} = \pi R_{coil}^2$
$A_{part} = \pi R_{part}^2$

$$NI = \frac{K}{\left(\dfrac{L}{D} + 2\right)}(\pm 10\%)$$

N = number of turns in coil
I = current in amps applied to the coil
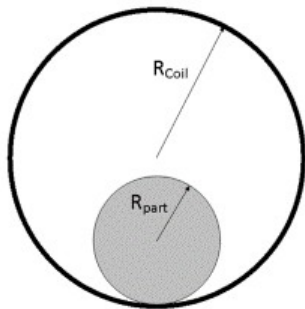K = 35000 A turns
L = length of part
D = diameter of part (same units as L)

14

- Example of a high fill factor part

Intermediate fill factor –
If $2 \times A_{part} \leq A_{coil} < 10 \times A_{part}$, use the following equation.

$$A_{coil} = \pi R_{coil}^2 \qquad NI = (NI)_h \left[\frac{10-\tau}{8}\right] + (NI)_l \left[\frac{\tau-2}{8}\right]$$
$$A_{part} = \pi R_{part}^2$$

N = number of turns in coil

I = current in amps applied to the coil
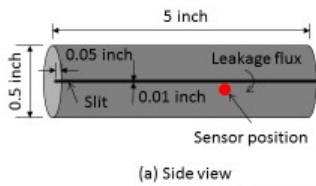
$(NI)_h = K/(L/D +2)(10\%)$ K=35000 A turns

$(NI)_l = K/(L/D)(10\%)$ K=45000 permeability constant
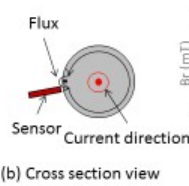
$\tau = A_{coil} / A_{part}$

- Example of an intermediate fill factor, where the part can be placed on the coil or on the headstocks.

Computed in situ leakage field around fatigue cracks to identify optimal magnetizing parameters

(a) Side view   (b) Cross section view
Fig. A. Notched steel specimen
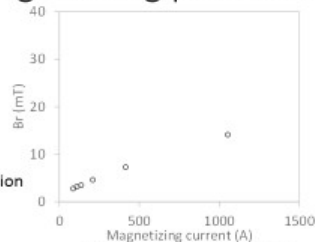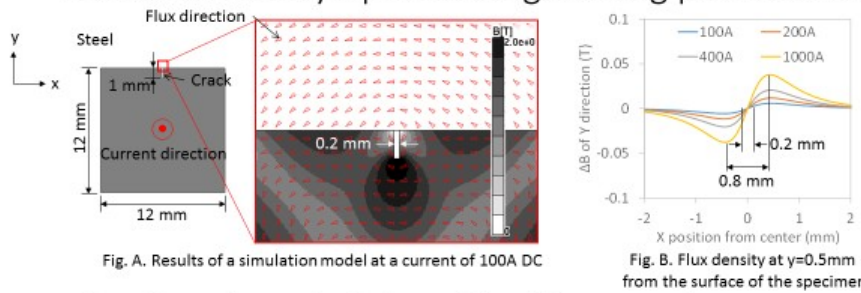
Fig. B. Measured leakage flux
(Head shot, Full wave)

- Figure B shows leakage flux of the radial direction when a specimen of Figure A was used.

- The current was injected into the part in Figure A (b).
- As the current is increased, the response will be as shown in Figure B.
- For circular magnetism, the amount of flux leakage is related to the amount of the current carried through the part.

Computed in situ leakage field around fatigue cracks to identify optimal magnetizing parameters
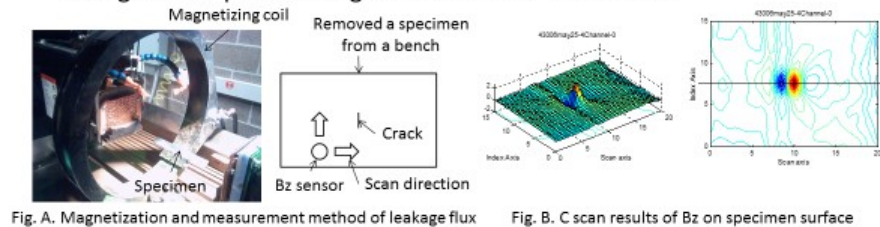
Fig. A. Results of a simulation model at a current of 100A DC

Fig. B. Flux density at y=0.5mm from the surface of the specimen

- These figures show a simulation model and the computations.
- Leakage flux is generated from a position of about ±0.4mm from center of a crack. The position is larger than the crack width. Therefore the magnetic particle pattern is larger than the crack width.

- This is a computed representation of magnetic field in and above a part being magnetized by passing current through the part.
- Graph B shows that the larger the current that is placed into a part, the larger the response from a defect, if one is present.
- Note that the leakage resulting from a defect drops off very quickly with distance from the surface of the part.

Measure in situ leakage field around fatigue cracks to identify optimal magnetizing parameters

- Transverse fatigue crack under coil shots
- Longitudinal parallel fatigue cracks under head shots

Fig. A. Magnetization and measurement method of leakage flux

Fig. B. C scan results of Bz on specimen surface

- This is how an actual field looks based on measurements made on a low-cycle fatigue sample.
- This measurement was not made in situ, but based on the residual field after the part was removed from the bench.

Summary

- Size of the part and fill factor should be a consideration when using a coil for inspection
- For any type of magnetization – either circular or longitudinal, current plays a direct role in the magnetic field created.
- For any magnetization level created, when checked with a Gauss meter, one needs to remember that the field in the Z direction drops off rapidly with increasing distance from the surface.

20

Summary

- There are very few parts in aviation made of steel, and very few alloys of steel used in aviation
- Parts need to be magnetized enough to create a magnetic field, but not to the point of saturation
- Although parts do not have varying degrees of permeability within the part itself, initial studies have not shown any adverse effects to this phenomenon
- Formulas are initially used to determine the level of current needed for magnetization, but they should always be checked with a QQI and Gauss meter in areas of interest

19

Magnetic Particle Inspection
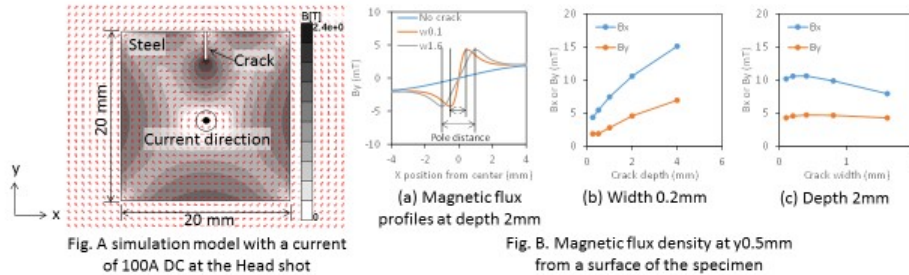
Module #3

Purpose

- The purpose of this module is to examine the strength of the excitation field or the flux leakage from a crack and how it compares to the detectability of a crack with MPI.

Module #3 Contents

- Detectability of cracks
    - Head shot
    - Coil shot

- Field strength or magnetic field and direction at critical locations of parts:
    - Head shot
    - Coil shot

Section 1: Detectability of cracks

Prototypical in situ leakage field around a fatigue cracks to understand the relationship between flux leakage and crack dimensions

Fig. A simulation model with a current of 100A DC at the Head shot

(a) Magnetic flux profiles at depth 2mm

(b) Width 0.2mm

(c) Depth 2mm

Fig. B. Magnetic flux density at y0.5mm from a surface of the specimen

- In Figure B(a), magnetic particles easily adhere more on a narrow crack than a wide crack because length between poles becomes smaller as crack width is smaller.
- In Figure B(b), flux leakage becomes larger as crack depth increases.
- In Figure B(c), flux leakage is not as influenced by crack width as much as depth when the cracks have enough depth. Therefore, MPI is more influenced by crack depth than width.

General Testing Process – Head Shot

Generation of Magnetic Fields: Circular

- Easiest to control due to the current passing directly through the object
- Creates circular magnetic field at right angles to the current path

Circular magnetization is used to detect lengthwise cracks
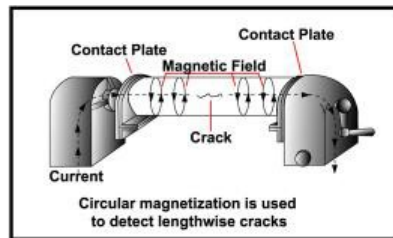
* Image obtained from FAA ASI NDT course

- In a head shot, the defect is affected by the magnetic field created as a result of the current traveling through the part.

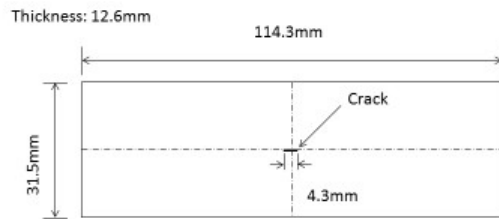Leakage flux on the bench – Head Shot

Thickness: 12.6mm

114.3mm

Crack

31.5mm

4.3mm

Fig. A. Sample shape

z
Flux direction
Hall probe
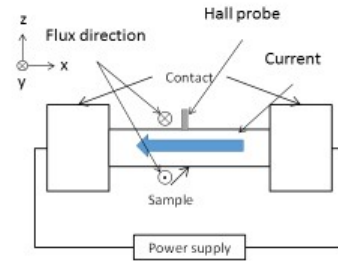Current
Contact
Sample
Power supply

Fig. B. Current and flux in the head shot

- Figure A shows a sample with a defect in the optimal position for detection.

- Figure B shows the magnetic field created when current is applied to the part. Note that the magnetic field goes into the slide at the top and comes out of the slide at the bottom of the part, reinforcing the right hand rule.

Leakage flux on the bench – Head Shot

12.3mT   12.5mT
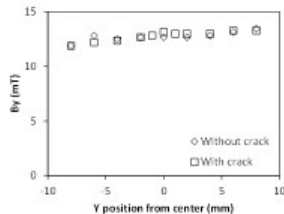σ=0.2mT   σ=0.1mT

Without crack
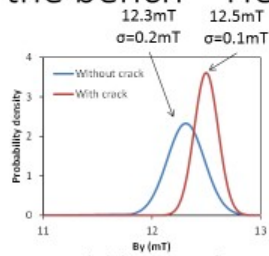With crack

Fig. A. Y direction profile at AC (260A)

Fig. B. Probability density of B on the crack
(A number of measuring times is Five times. It is assumed that the measured values follow a normal distribution.)
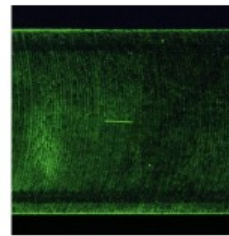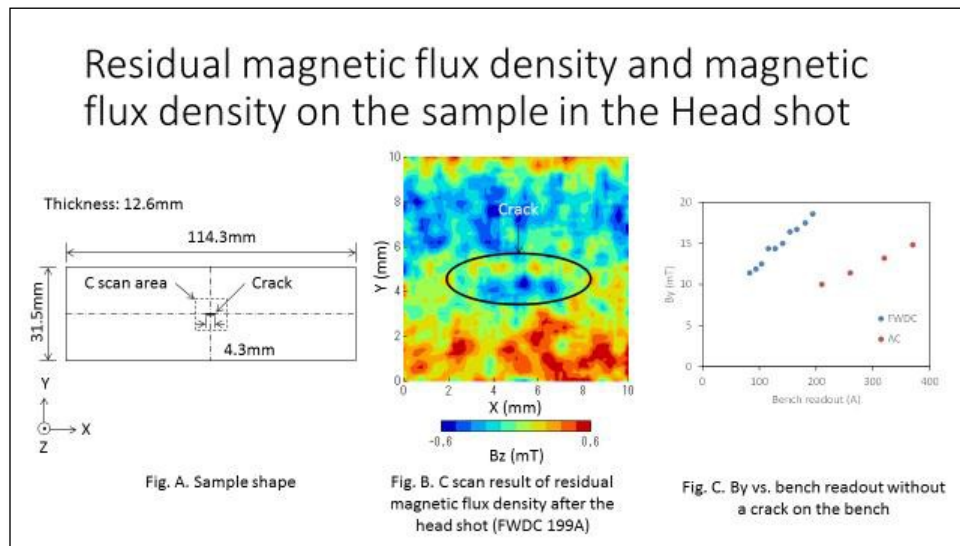
Fig. C. Photo of the magnetic particle pattern

- As shown Fig. A and B, Leakage flux is very small.
- However as shown Fig. C, the good magnetic particle pattern is made by the leakage flux.
- Because to obtain good magnetic particle pattern can't be determined by just strength of the leakage flux.

- In the measurement of flux leakage, there is only a very slight difference in the flux leakage due to cracks. This change, though noticeable by particle indication, is difficult to detect using standard probes.
- The crack of the sample used is relatively large. However, the leakage flux density is approximately 0.2mT, as shown figures A and B. It is assumed that the measured values follow a normal distribution.
- When smaller cracks than this sample were used, good magnetic particle patterns were still obtained.

- Therefore, minimum leakage flux that can obtain a magnetic particle pattern is smaller than the leakage flux measured on this sample.
- B_y is larger than B_z. However, B_y is not largely changing when the probe position is changing.
- The leakage flux becomes max on the crack.
- Therefore, probe positioning is easy.
- Results suggest that a magnetic particle pattern is affected by a differential of the leakage flux.
- Experiments were not able to quantitatively define the relationship between the magnetic particle pattern and the differential, but qualitatively one can say that larger differential fields will produce stronger attractive forces for particles.

Residual magnetic flux density and magnetic flux density on the sample in the Head shot

Fig. A. Sample shape

Fig. B. C scan result of residual magnetic flux density after the head shot (FWDC 199A)

Fig. C. By vs. bench readout without a crack on the bench

- Make sure to explain B_x, B_y, B_z fields.
- The fields exist in three directions; X, Y and Z, as shown on the left side of the slide in Figure A.
- Figure B is a pseudo color slide showing the intensity of the B_z field.
- Figure C shows the correlation between the bench readout in Amps (A) and the B field in the Y direction in milliTesla (mT).

Magnetic particle indication on the sample in the Head shot

- Flaw indication brightness is ~3.75 brighter than the average brightness in areas without any relevant indications
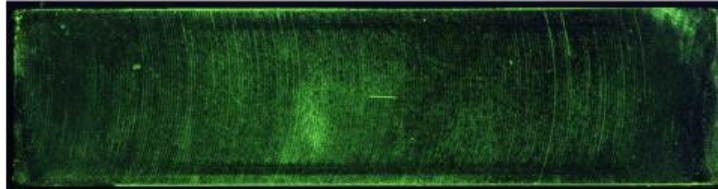
- This is an image of a sample with a crack after magnetization, representative of an indication that can be seen during a head shot (circular) inspection if a defect were present (the image has been enhanced to better show the defect and is brighter than can be expected).

General Testing Process – Coil Shot

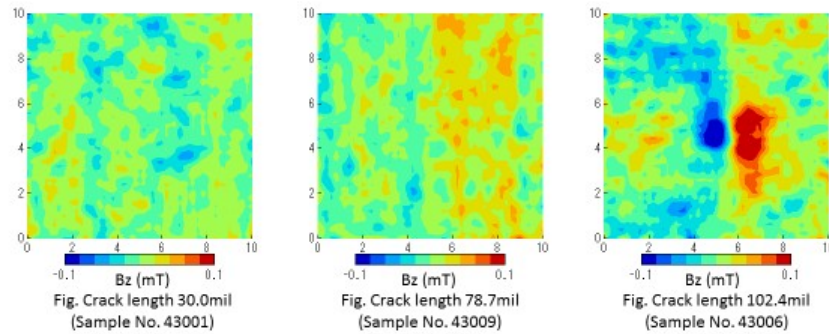Generation of Magnetic Field: Longitudinal.

- Magnetic field created by placing a test object inside a fixed current carrying coil
- The effective magnetic field created goes beyond the outer edge of the coil, approximately 6 to 9 inches on either side of the coil

Longitudinal magnetization is used to detect transverse (crosswise) cracks.
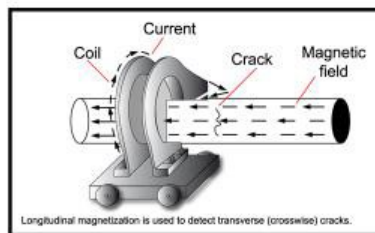
* Image obtained from FAA ASI NDT course

- In a coil, the part itself and any defects are affected by the magnetic field created in the air.
- Parts with greater permeability will draw more of the generated magnetic field into the part itself. This can result in changes in detectability for identically shaped parts of different magnetic permeability.

Residual magnetic flux density after coil shot

Fig. Crack length 30.0mil (Sample No. 43001)   Fig. Crack length 78.7mil (Sample No. 43009)   Fig. Crack length 102.4mil (Sample No. 43006)

- These results are produced from the magnetic field measured in the Z-direction above a magnetized sample. The measurements were taken with a standard, off-the-shelf FW Bell Gaussmeter using an axial probe (one that measures the field in the Z-direction). Note that the smaller cracks are not as detectable as the larger crack on the right side of the page.

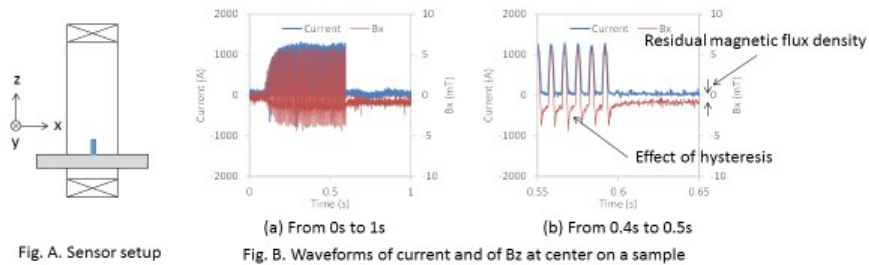Magnetic particle indication on the sample in the Coil shot

- Flaw indication brightness is ~5.75 brighter than the average brightness in areas without any relevant indications
  - Sample 43-006

- This is an image of a sample with a crack after magnetization, representative of an indication that can be seen during a coil shot (longitudinal) inspection if a defect were present (the image has been enhanced to better show the defect and is brighter than can be expected).
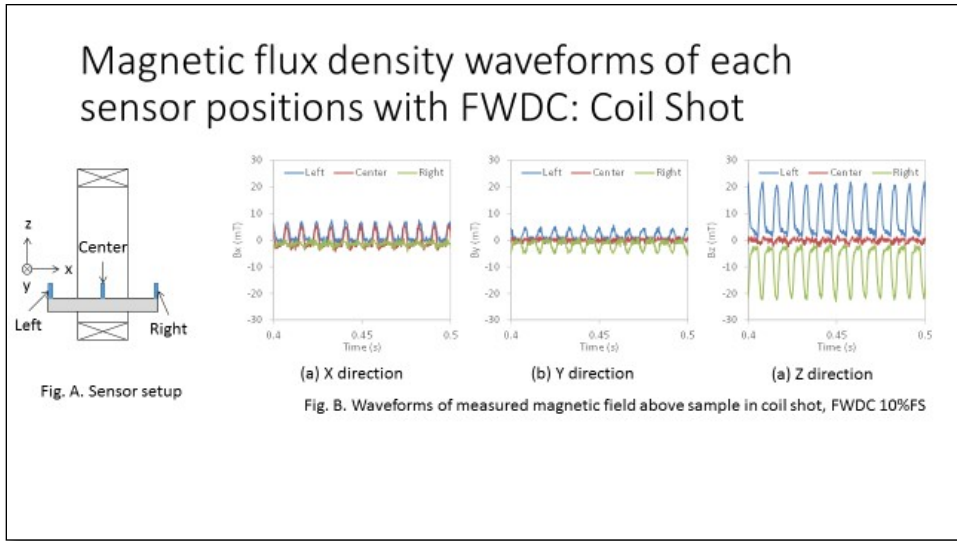
Section 2: Field strength

Transient and steady state of magnetic flux density by FWDC magnetization: coil shot

Fig. A. Sensor setup

Fig. B. Waveforms of current and of Bz at center on a sample

(a) From 0s to 1s

(b) From 0.4s to 0.5s

Residual magnetic flux density
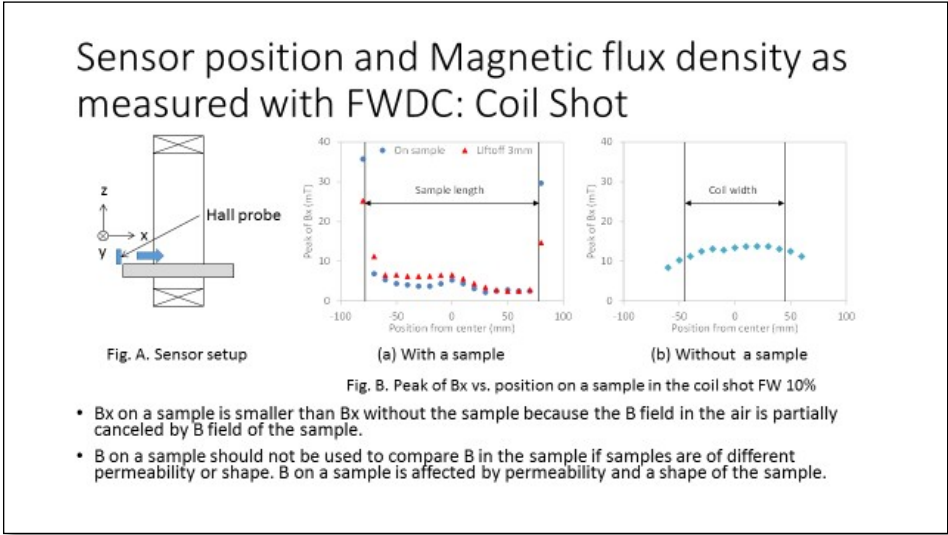
Effect of hysteresis

The waveform of magnetic flux density on the sample has effect of hysteresis and of residual magnetic flux density.

- A peak value of magnetic flux density on a sample is checked when MPI users need to know how strongly they have magnetized the sample. The users should be careful about the magnetic flux direction when DC is used because, as shown Figure B, there is magnetic flux of inverse direction with magnetic flux direction of magnetizing current by an effect of a hysteresis of the sample. Max peak of magnetic flux density should be measured because magnetic flux density of magnetizing current is larger than the effect of the hysteresis.
- Why are the magnetic flux directions of magnetizing current and of the hysteresis not the same? Because there is no magnetic flux of a magnetizing coil when the magnetizing current is OFF. Residual magnetic flux of the sample is dominant when magnetizing current is OFF. The magnetic flux direction of outer of the sample is reverse direction with inner of the sample.

Magnetic flux density waveforms of each sensor positions with FWDC: Coil Shot

Fig. A. Sensor setup

(a) X direction　(b) Y direction　(a) Z direction

Fig. B. Waveforms of measured magnetic field above sample in coil shot, FWDC 10%FS

- Figure A shows three different positions of a Hall sensor on a part that was placed into the coil, and then the coil was magnetized.
- Figure B shows the relative magnitude of each of the three fields (X, Y, Z) and each of the three positions on the part within the coil

Sensor position and Magnetic flux density as measured with FWDC: Coil Shot

Fig. A. Sensor setup

(a) With a sample　(b) Without a sample

Fig. B. Peak of Bx vs. position on a sample in the coil shot FW 10%

- Bx on a sample is smaller than Bx without the sample because the B field in the air is partially canceled by B field of the sample.
- B on a sample should not be used to compare B in the sample if samples are of different permeability or shape. B on a sample is affected by permeability and a shape of the sample.

- When permeability of a sample is low, the field from the coil that bends and flows through the sample is smaller than it would be if the permeability were higher. The field measured above the center of the sample can be larger than that measured over a high- permeability sample.
- Conversely, when permeability of a sample is higher, the field in a sample is larger, and the field measured above the center of a sample is smaller.
- Caution is needed when measuring the field above center of a sample in a coil shot because that measurement does not accurately show the field in the sample when different samples are used. Shape and permeability both affect the measurement.

Comparisons of permeability

• The next few slides will show the effect of magnetic permeability with respect to the field measured with a Gaussmeter when the sample is in a coil as well as the transient field in a head shot.
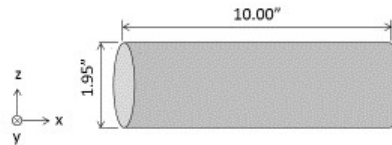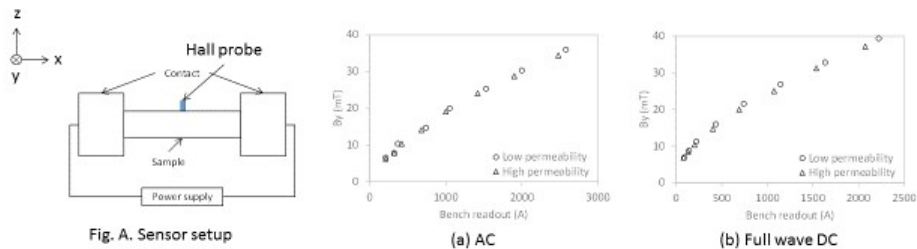
Fig. A. Shape of both low and high permeability samples

• Both samples were made from the same material, except one was heat-treated to soften the sample (annealed).

Comparison between low and high permeability: Head Shot

Fig. A. Sensor setup

(a) AC

(b) Full wave DC

Fig. B. Peak of By vs. Bench readout in the head shot

• In a head shot experiment or inspection, the ability to accurately measure the field strength with a Gaussmeter is not adversely affected by the permeability of the sample when the measurement is taken at the center of the sample with the probe touching the surface (minimum liftoff).

Cursory tale of the effects of placement of the Hall probe with respect to the round bar sample in the Head Shot
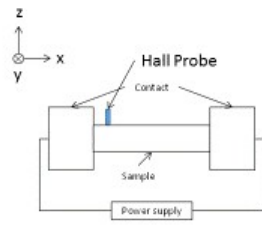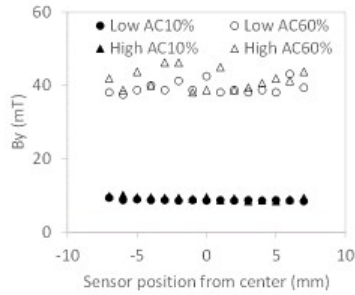
Fig. A. Sensor setup

Fig. B. Tangential magnetic flux density vs. sensor position

- At low current levels, the measured B_y field over the surface of the sample is uniform for samples of the same geometry. At higher current levels, the differences in the two samples may be attributed to local material variations in the samples themselves.

Comparison between low and high permeability: Coil Shot
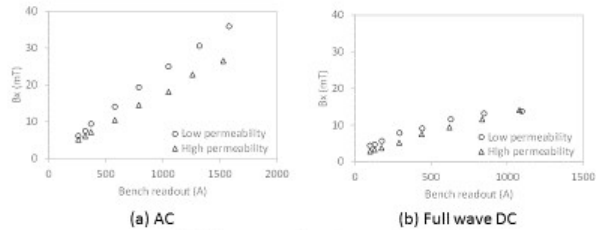
Fig. A. Sensor setup

(a) AC

(b) Full wave DC
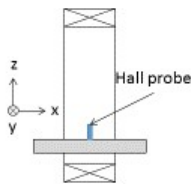
Fig. B. Peak of Bx vs. Bench readout in the coil shot

- When measured above the center of the sample, the B_x field strength for a low-permeability sample measures higher than it does for the same geometry of sample made of a higher-permeability material. This difference is most notable at higher AC current settings.

Cursory tale of the effects of placement of the Hall probe with respect to the round bar sample in the coil

Position of the Hall Probe to measure the strength of the field. Measurement is directly effected by both the placement of the probe and the permeability of the material
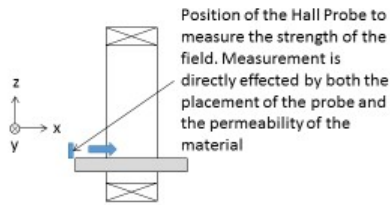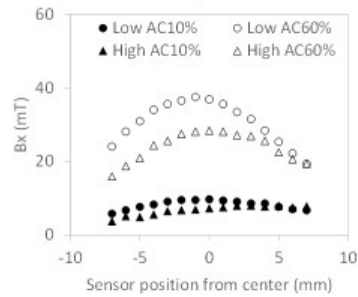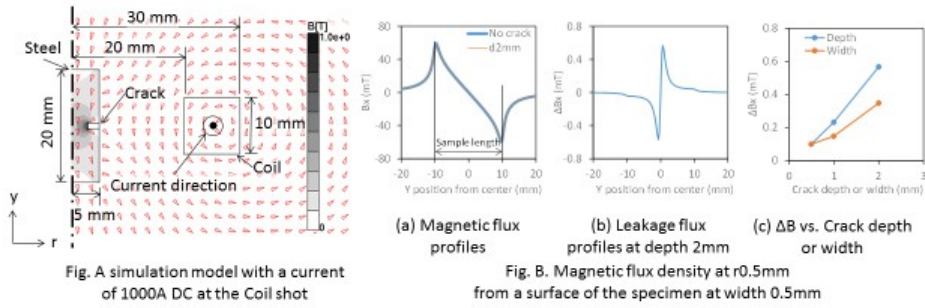
Fig. A. Sensor setup

Fig. B. Tangential magnetic flux density vs. sensor position

- At higher AC current levels, the differences between lower- and higher-permeability samples creates an inaccurate comparison of how magnetized each sample will be. The internal field strength of the higher-permeability material is expected to be higher than that for the lower-permeability sample, but the effect of the sample's own demagnetizing field and the concentrating of the flux through the higher-permeability path (the sample itself) causes the reading to be lower across almost the entire surface of the high-permeability material.

Summary

- Crack morphology (width, length and depth (depth being the most important)) can greatly effect detectability
- Small flux leakage differences are difficult to detect, therefore care should be taken when making measurements
- Magnetic permeability is of greater importance when doing a coil shot (SL 11)
- Residual magnetic flux direction is important when DC current is used (SL 15)
- Location of the flux sensor on a part is important for coil shots
- Permeability and position can effect sensor readings (SL 17)

Calculated in situ leakage field around a fatigue cracks to understand the relationship between flux leakage and crack dimensions
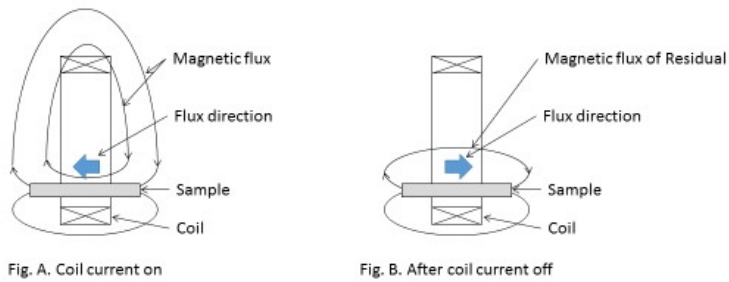
(a) Magnetic flux profiles

(b) Leakage flux profiles at depth 2mm

(c) ΔB vs. Crack depth or width

Fig. A simulation model with a current of 1000A DC at the Coil shot

Fig. B. Magnetic flux density at r0.5mm from a surface of the specimen at width 0.5mm

- In Figure B(a), a distance between "no crack" and "depth 2mm" cannot be found.
- Figure B(b) shows a distance between magnetic flux density with a crack and without cracks. The distance is flux leakage. The flux leakage is smaller than magnetic flux density of the filed at a surface of the sample.
- In Figure B(c), changing of flux leakage by crack depth is larger than crack width.


Comparison between low and high permeability

Fig. A. Sensor setup

(a) AC

(b) Full wave DC

Fig. B. Bench readout vs. a peak of Bx in the flux flow
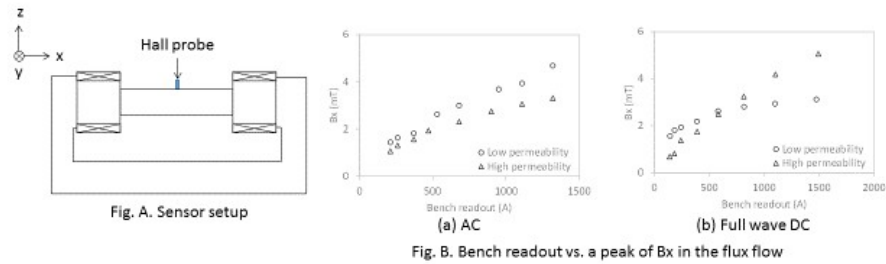
Magnetic flux direction after current off

Fig. A. Coil current on

Fig. B. After coil current off

- Q: Why was residual flux direction not the same with flux of magnetizing current?
- This slide shows the reason. However, many users may not need this slide.

Leakage flux on the bench

Fig. Shape of round bar Sample

(a) AC

(b) Full wave DC

Fig. Leakage flux in the head shot
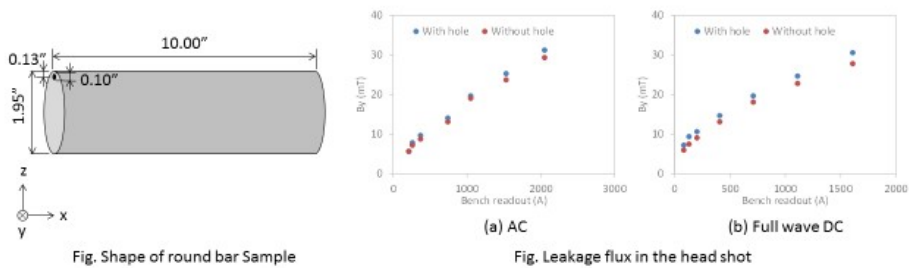
Magnetic Particle Inspection

Module #4

Purpose

- This module shows what effects sample status has on magnetic particle patterns, which is important as MPI users make decisions about magnetizing methods.

Module #4 Contents

• Descriptions of Component effects:
  • Surface roughness
  • Surface coatings
  • Cleanliness of the part (different types of contamination)
  • Geometry of the part (different shapes)
  • QQI vs. Gaussmeter vs. Formula: Which is better for determining the strength of the field in a complex shaped part ?
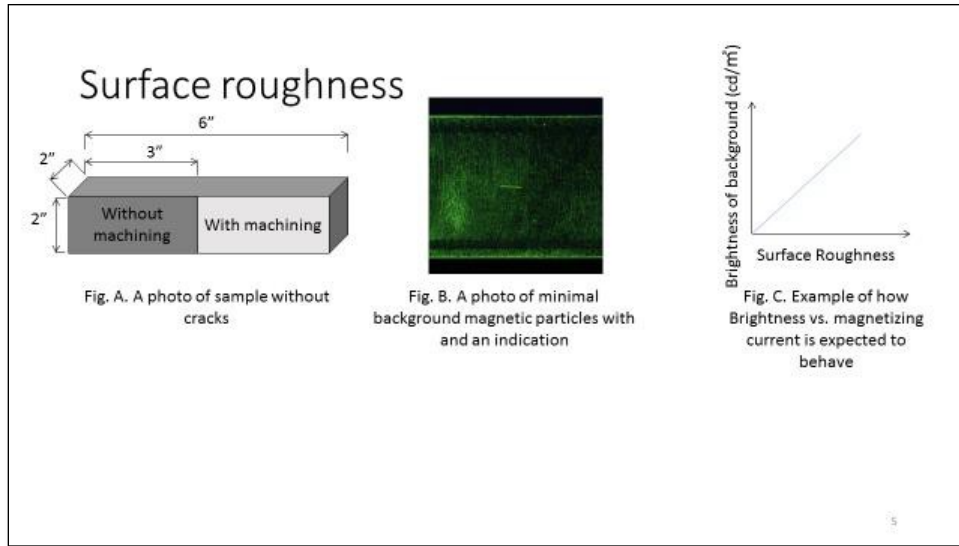
Surface roughness

• Surface roughness is a measure of the texture of the surface. It is typically measured in Ra, which is an "arithmetic average" of the vertical deviations measured from a mean line.
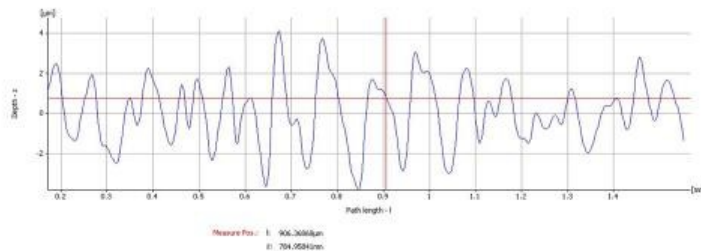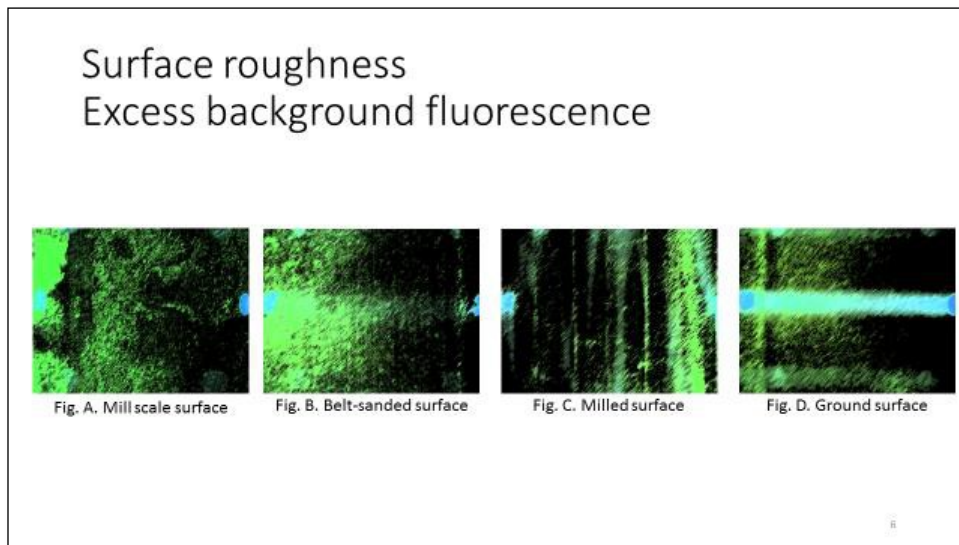

- This is an example of how a sample that appears smooth to the naked eye can appear rough upon close examination.

Surface roughness

Fig. A. A photo of sample without cracks

Fig. B. A photo of minimal background magnetic particles with and an indication

Fig. C. Example of how Brightness vs. magnetizing current is expected to behave

- As the roughness of a sample's surface increases, the chances of fluorescent particles becoming trapped by the surface increases.
- This effect in increased background brightness can also be noticed due to an increase in current.

Surface roughness
Excess background fluorescence

Fig. A. Mill scale surface   Fig. B. Belt-sanded surface   Fig. C. Milled surface   Fig. D. Ground surface

- Digitally enhanced images to show effects of surface finish on background fluorescence.

Surface coatings

- Coated samples that are inspected should be considered for the following points.
  - Liftoff by coating thickness
  - Magnetic characteristics of coating material

Surface coatings
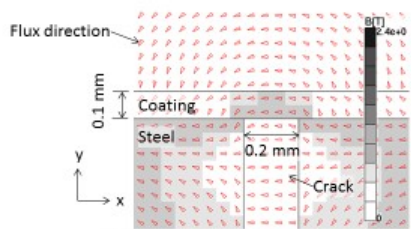Magnetic characters of a coating material

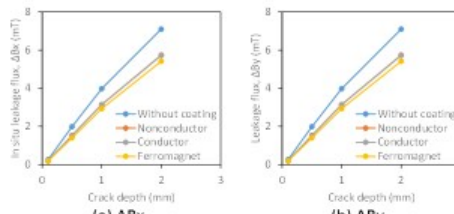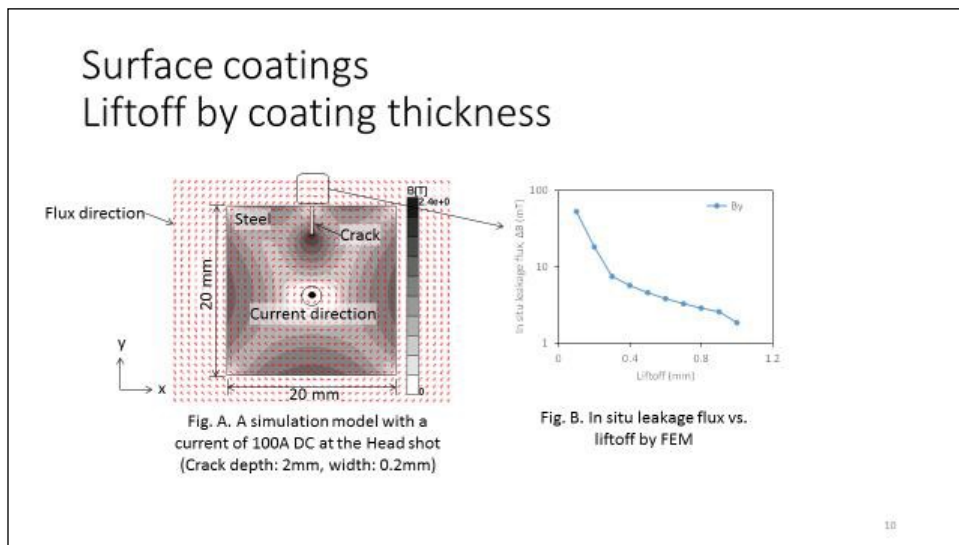Fig. A. A simulation result with a current of 100A DC and coating at the Head shot

(a) ΔBx   (b) ΔBy
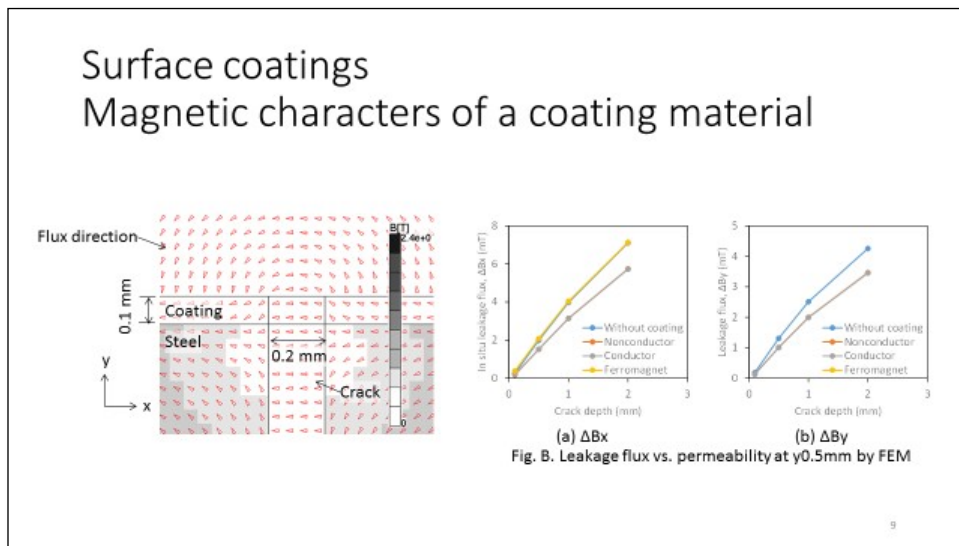Fig. B. Leakage flux vs. permeability at y0.5mm by FEM

- Steel elements were calculated by nonlinear BH modeling (more accurate). Ferromagnetic coating elements were calculated by linear Ni permeability values due to a lack of an accurate BH curve for Ni. As the maximum magnetic flux density of Ni is smaller than steel, the linear calculation is not ideal, but the results show the increased degradation in leakage flux from a ferromagnetic coating.
- Figure A shows a calculated result of magnetic flux density distribution of a ferromagnet coating sample. Used conductivity of coating is the same as a used sample. Used relative permeability of coating is equal to 100. In situ magnetic flux density of coating on a crack became larger than the around. It is expected that in situ leakage with coating flux was smaller than without coating.

- Figure B shows calculated leakage flux. Used conductivity of "Conductor" and "Ferromagnet" is the same as the sample. Leakage flux of "Nonconductor" and "Conductor" was almost the same, and leakage flux of "Ferromagnetic" coating was smaller than conductor. However, the distance between "Without coating" and other results was larger than other distances. This shows that an effect of coating thickness was larger than effects of conductivity and permeability of coating. Therefore, MPI users should be careful when thick coating samples are used.

Surface coatings
Magnetic characters of a coating material

(a) ΔBx   (b) ΔBy
Fig. B. Leakage flux vs. permeability at y0.5mm by FEM

Surface coatings
Liftoff by coating thickness

Fig. A. A simulation model with a current of 100A DC at the Head shot (Crack depth: 2mm, width: 0.2mm)

Fig. B. In situ leakage flux vs. liftoff by FEM

- Figure A shows a simulation model and result of "Head shot" that was calculated by 2D nonlinear finite element method.
- Figure B shows in situ leakage flux became exponentially smaller as liftoff is larger.
- In general, plating thickness is considered up for inspection up to 0.1mm.

Surface coatings
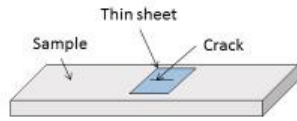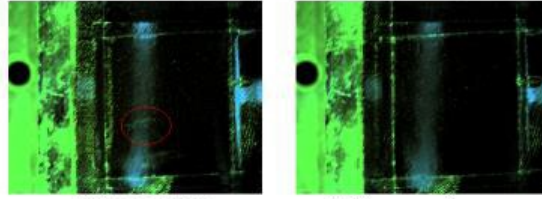Magnetic characteristics of coating material

Fig. A. Sample shape

(a) Nonconductive   (b) Ferromagnetic

Fig. B. Photos of magnetic particle pattern with thin sheets

- The sample is not the same as plating or coating samples.
- Figure A shows the sample used. The sample has an air gap between the sample material and the coating. Therefore, the sample is not the same as real plated or coated samples, and it is expected that in situ leakage flux of plated or coated samples is larger than these samples. If plating or coating thickness is the same as the metal sheet thickness, the magnetic particle pattern should show up better if there is no air gap between base material and the coating.
- Figure B. A ferromagnetic coating may have leakage flux, but the liftoff and thickness may be smaller than the thin sheet.
- A ferromagnetic coating can have the effect of shielding the flux.
- Therefore, the leakage flux of a ferromagnetic coating is smaller than a non-magnetic coating.

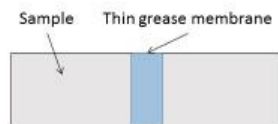Cleanliness of the part (different types of contamination)

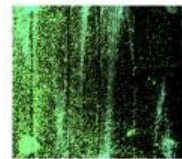Fig. A. A drawing of a sample with a grease smear

Fig. B. A photo of magnetic particle pattern

- Operators need to ensure that recommended cleaning practices are followed.
- Improper cleaning can result in missed indications and a contaminated bath.

Geometry of the part (different shapes)

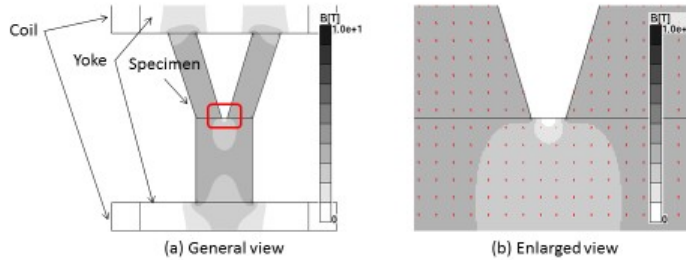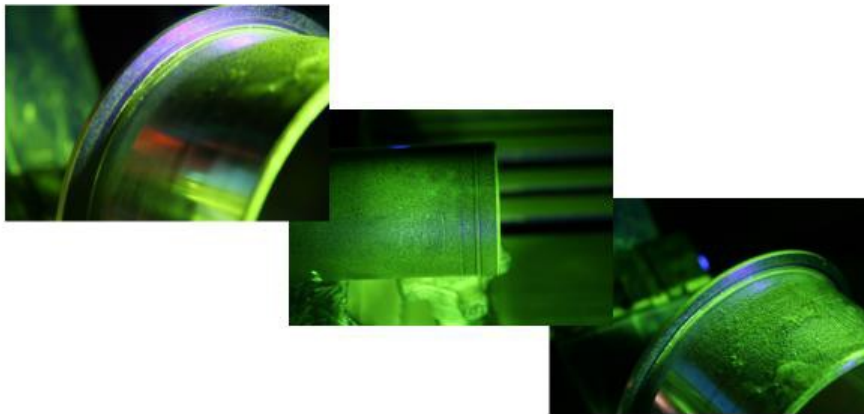(a) General view (b) Enlarged view

Fig. Calculated magnetic flux density distribution of Y type specimen at the Flux flow

- MPI users should be careful about complex specimens.
- Parts of complex specimens tend to low magnetic flux density.

Geometry of the part (different shapes)

Geometry of the part (different shapes)

15

For complex shapes which method is best to determine field strength: QQI, Formula, Gauss meter

- Formula does not give accurate field strength in a complex shape
- Either QQI or a field measurement device can be used for verifying surface field strength in critical areas of complex shapes
- QQI is closer to the surface than most sensors on metering devices so it could be better at determining critical field strength
- Gaussmeter is likely to be faster and easier to use on real parts that can't have QQI's permanently attached.
- QQI's can be difficult to attach in certain areas
- Gaussmeters more susceptible to reading field in air from coil shots

16

Summary

- The roughness of a sample can have an effect on the ability to find defects due to particle accumulation on the surface.
- Coatings on the surface may hinder defect detection by creating too great a distance in the Z direction, between the generated field and the part's base material.
- Contamination may reduce the flow of particles on the surface of the part, thereby reducing effectiveness of the process
- Geometry may be one of the biggest detractors in MPI – complex geometries may be mistaken for defects, or may cover the defect by the natural accumulation of particles at sharp angles

17

Magnetic Particle Inspection
Module #5

Purpose

- This module illustrates some of the effects that bath characteristics, such as concentration and contamination can have on the MPI process and results

Module #5 Contents

- Bath characteristics:
  - Magnetic properties of particles
  - Concentration of particles
  - Contamination of the bath
  - Effects of Heat Damage

Magnetic properties of particles

- Kinds of Magnetic particles
  - Pure iron powder
    - Residual magnetic flux density of pure iron is smaller than iron oxide. Therefore the pure iron powder is likely to be removed from samples when magnetization is off. On the other hand, pure iron is likely to be oxidized.
  - Iron oxide powder
    - FeO: The color is black. It isn't used. Because it isn't ferromagnetic.
   - Fe$_2$O$_3$: The color is red. It is commonly used oxide powder.

- Not all iron oxides are used as particles in MPI.

Magnetic properties of particles

- Particle size: 0.2μm～60μm
  - Magnetic particle can find smaller crack as particle size is smaller.
- Colors
  - Black, Grey, Red or White
    - These colors are selected by surface color of samples. Largest contrast between particle color and sample surface color should be used.
  - Fluorescent
    - Fluorescent particle can be used without regard for surface color of samples. In general, the fluorescent particle can get largest contrast. Therefore the fluorescent particle the most commonly used particle. However the fluorescent particle needs dark place because visible light without visible light from Fluorescent particles should be removed when the particle is used.

- Powders used in a bench inspection are typically coated with a fluorescent polymer coating. This is what enables the particles to glow under UV light.

Concentration of particles
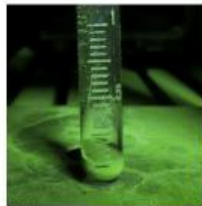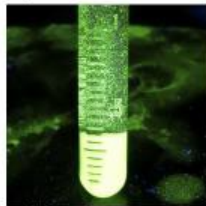
(a) Low concentration   (b) Good concentration   (c) high concentration

Fig 1. Photos of magnetic particle pattern

- **Problem:** low concentration – results in lack of material to illuminate indications when present causing them to be missed.

- **Problems:** high concentration – results in too bright of a background, where indications can blend into the background and be missed

- Figures 1(a–c) show various types of particle concentrations, from low to acceptable to high concentration.

Concentration of particles
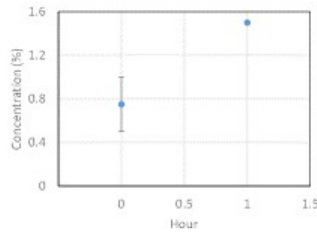Without warm-up of the bath

Fig 2. Concentration of particles in the bath

- The concentration is unstable at just after starting of the bench.
- The concentration is stable after particles are fully dispersed in the bath.
- It is important that the bath is stirred by a pump.

- Because this is a qualitative slide, data is approximated.
- Improper warm-up of a bench will result in the particles resting or "sticking" to the sides of the tank and failing to be in solution. At the beginning of the warm-up procedure, the side of the tank and anywhere that particles may fall to the bottom when the bench is turned off should be agitated or scrubbed down to put the particles back into solution.

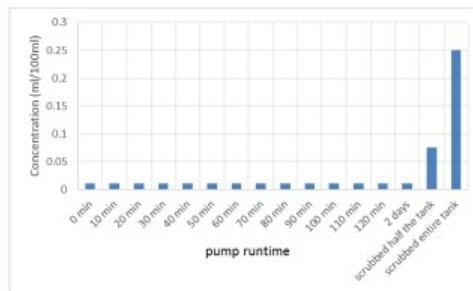Concentration of particles
Without warm-up of the bath

Fig 3. Concentration of particles in the bath

- Warm-up of the bath needs time. However time is not enough in some cases. Particles must often be scrubbed to loosen them from surfaces within tank.

- Figure 3 represents the results of concentration measurements made from running the bath for over 48 hours without scrubbing the sides of the tank down to put the settled particles back into suspension and agitated by the pump. The concentration of the bath can be seen after a proper scrubbing with the particles in suspension.

Concentration of particles

(a) Oil in bench after 2 days runtime   (b) Settling test after 2 days   (c) Brushes used to scrub tank
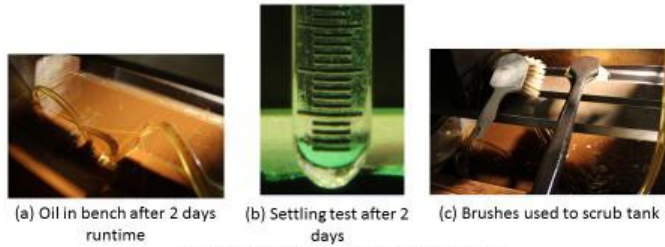
Fig 4. Concentration of particles in the bath

- Fig. 4 (a) shows particles still settled at bottom of tank after running for 2 days.
- Fig. 4 (b) shows settling test results after 2 days of running without any scrubbing of the tank. Reading is 0.01 ml/100ml
- Fig. 4 (c) shows the type of brushes used to scrub the tank. You can also see the bath has become opaque now that the particles are in suspension.

- This is an example of what will happen if the bench is not properly scrubbed, and the iron particles are not fully integrated into the bath.

Concentration of particles

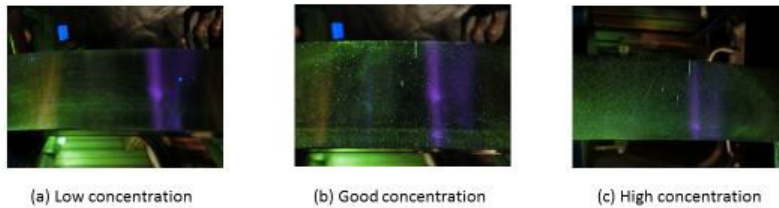(a) Low concentration   (b) Good concentration   (c) High concentration

Fig 5. Photos of magnetic particle pattern

- **Problem:** low concentration – results in lack of material to illuminate indications when present causing them to be missed.

- **Problems:** high concentration – results in too bright of a background, where indications can blend into the background and be missed

- By looking closely, you can see that the indication is not very visible in figure 5(a), and the background noise increases in figure 5(c).
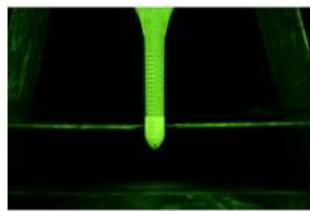
Contamination of the bath

- Items that can lead to contamination of the bath can include:
  - Damaged particles such as casings worn off the iron particle
  - Grease
  - Rust
  - Paint
  - Oil
 - Scale
  - Residual fluids from the cleaning process

- If the bath has contamination, results will be similar to a bad concentration of particles.
- For example, there are particle patterns without a crack by contaminations with magnet particles, but there are no a particle patterns on cracks by contaminations.
- Therefore the bath should be kept clean.

Contamination of the bath

- Need images of the centrifuge tube with low contamination (acceptable) and of high contamination
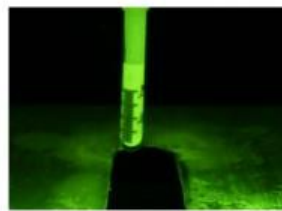
(a) Low contamination   (b) High contamination

Fig 6. Photos of magnetic particle pattern

- The bath is considered contaminated when the amount of foreign matter settling on top of the particles in a centrifuge exceeds 50% of the amount of particles present. An example would be having 0.4 ml of particles in the bottom of the centrifuge tube and 0.3 ml of contamination setting on top of the settled particles.

Results of Excessive Heat Damage
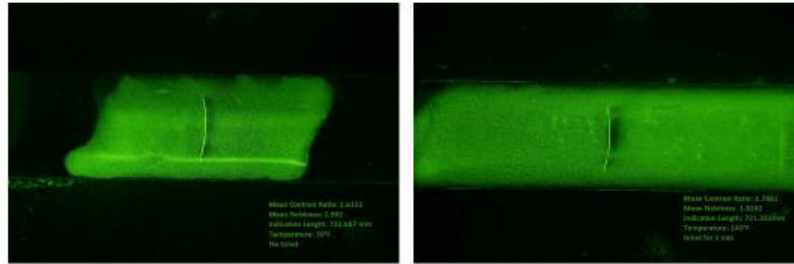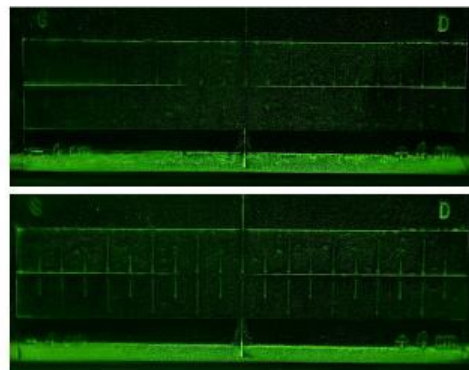
(a) 70°F no grind   (b) 140°F 1 minute grind

Fig 7. Photos of magnetic particle pattern from heat damage to the bath

- Figure 7 shows the effect of heat damage to the bath. The polymer fluorescent coating tends to clump with an increase in temperature for some of the particles in figure 7(b).

Results of Excessive Heat Damage

Bar: 80°F
(a)

Bar: 140°F
(b)

Fig 8. Photos of magnetic particle pattern from heat damage to the bath

- Another consequence of heat damage to the bath occurs when the heated bath passes through the pump, the polymer coating can be mechanically removed from the iron particles. This can result in several unwanted incidences, such as contamination of the bath, which can show up during the settling test. It may also result in missed indications due to lack of good particle concentration. Figure 8 shows the effect of heat damage to the bath on a test sample. Notice the lines do not go completely to the center in figure 8(b)due to heat damage.

Summary

- There are various types of iron powder, but few are used in MPI. The most often used is Fe_2O_3
- Pure iron powder is not used due to it's low flux density
- Particles are sized according to the use – smaller particles for smaller cracks
- In aviation most particles are florescent polymer coated
- Although there are recommended values for particle concentration, these values have been found to be conservative with respect to bath detriment

Summary

- Through scrubbing of the holding tank prior to any settling test is one of the most important aspects of bench startup
- There are many factors that can lead to contamination – not only to the bath itself but also to the surface of the inspected part
- Heat damage to the bath can result from long term operation. This can lead to a premature need for bath change out.
- Particle clumping and wearing off of the polymer coating from the particles are just a few negative effects of heat damage

APPENDIX I—IMAGE ANALYSIS PROCEDURE

The image analysis for the ring sample uses the following steps:

1. The folder containing the ring images is opened. These images are ordered from shallowest defect indication to deepest defect indication.
2. The shallowest image is selected first. The program opens the first image and all the images afterwards.
3. The program converts each image to gray scale and waits for the user to select the geometric center of the indication. Once the center has been located, the user then double clicks this position to enter the location into the script. The program will then continue to the next defect. This process is repeated until all images are processed.
4. Once all the images have successfully been processed, the program outputs the same number of plots as there were images, compiled in one window. Each plot includes the values for the Peak Pixel Value, the Width of the indication, and the Signal-to-Noise Contrast Ratio.
5. The Plots are then saved into the file containing the images that were initially selected.
6. The values obtained are entered into an Excel® spreadsheet for analyzing. Bar graphs are made that show Max Pixel Value versus Image Depth (1 being the shallowest and 10 being the deepest).

Typical results are shown in figure I-1. The term "lowess" is a filter type available in MATLAB® used for this analysis. The images shown provide a graphical depiction of the different effects of the filter being set high for maximum noise rejection or low for best maximum value measurement. The filter settings need to be chosen as to allow fitting to the peak from the AS5282 indication itself rather than the spurious high signal levels elsewhere in the image. For this reason, different filter types were tested, and two different filters were chosen as best depending on whether the focus is in the maximum height of the signal from the indication or in avoiding a false measurement from the spurious bright pixels in the image. The spurious bright pixels cannot be avoided due to the nature of the fluid settling on the surface of the ring.
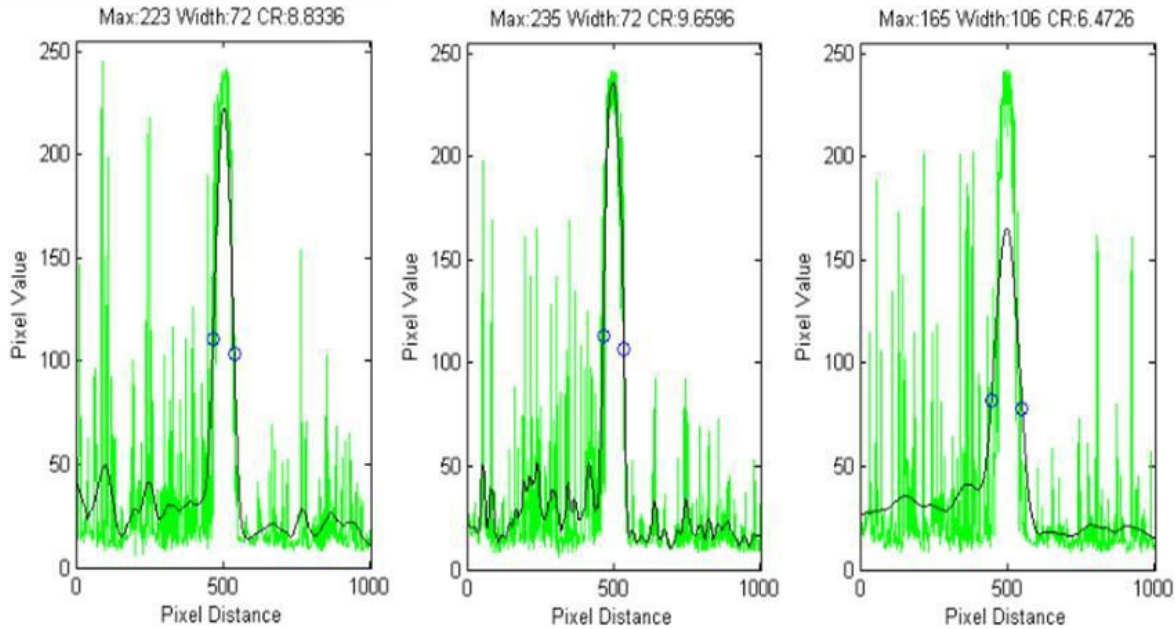
Figure I-1. Example results for script settings that produce the most accurate results possible by fitting the line profile closest to the signal

Procedures to analyze the longitudinal cracked steel samples are also being developed. The samples were inspected using MPI benches with either oil- or water-based carriers. A total of 12 bars were inspected three times for each steel type and imaged after each inspection. The imaging process consisted of imaging samples under ultraviolet radiation of 2,500 μW/cm^2 intensity while using a Canon EOS Digital Rebel Camera. The camera settings were set to a 20s exposure time, with an 85 mm focal length, ISO speed of 100, no flash. The images were shot 12″ away from the samples. Once the images were taken, they were then processed through a MATLAB script made to output a Mean-Contrast-Ratio, a Mean-Noise-Value, and, originally, Indication-Length in Pixels (pixel length was later converted to mils). In addition to the values, the script outputs a Signal-to-Max-Noise plot. To process the images with the script, the following steps are followed:

1.   Open 'fatiguecrack_Finalized.m' MATLAB Script.
2.   Run the script. The script will prompt the user to select an image; be sure to keep track of which steel type, MPI method, and bar number is selected. This information will be needed to save the output plot.
3.   Once an image is selected, the script opens the image as a gray scale image and then prompts the user to crop the image. This is useful for small indications. The user should double click on the frame to crop the image in its desired location.
4.   A zoomed in image will appear. The user must fit a line that is length wise on the indication, similar as it is shown in figure I-2. If it is difficult to tell where the indication starts or ends, zoom in using the zoom tool until the start and end positions are viewable. Double click on the line to proceed.
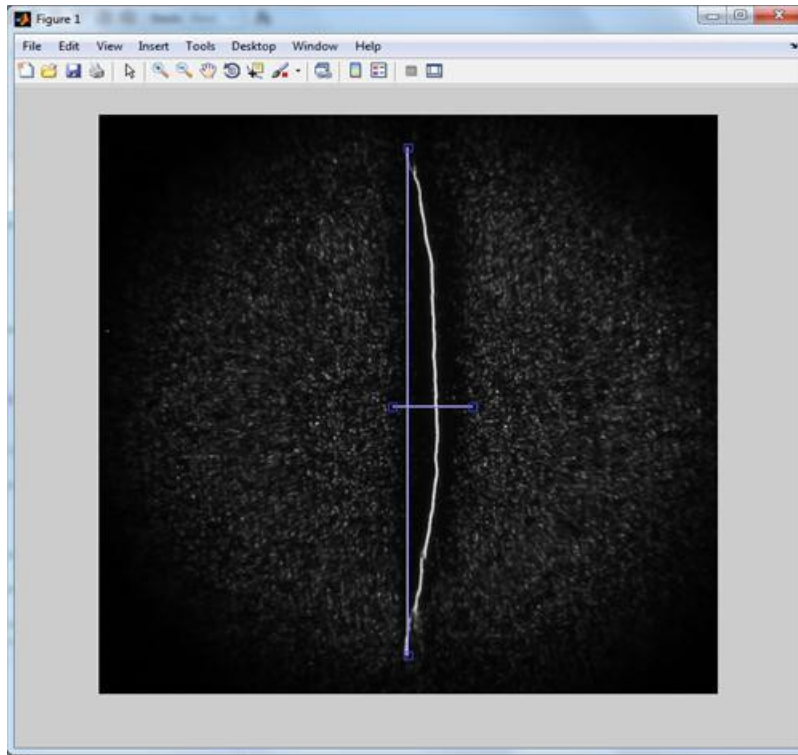
Figure I-2. Lines are fitted on the indication (shown in white). An enclosure is formed around the indication and its surroundings by the endpoint positions of the purple lines

5.   The script will then ask for a second line to be fitted. This line is perpendicular to the first line and should be long enough to cover the width of the indication. Once this line is in place, double click it to proceed.

6.   The script then takes the end points of all lines and forms an enclosure. If done correctly, the enclosure should only contain the indication and some of the area around it.

7.   After the Script is run, two windows should open. The first window is a plot showing the intensity of the indication versus the intensity of the noise. The second window outputs the values previously mentioned (see figure I-3). Save the plot as ['Steel type'-'bar number'-'MPI method'-'Amperage'-'image number'], example, '4130-04Oil_1500A_Image1244'. The plot should be saved in the same folder from which the image was selected.
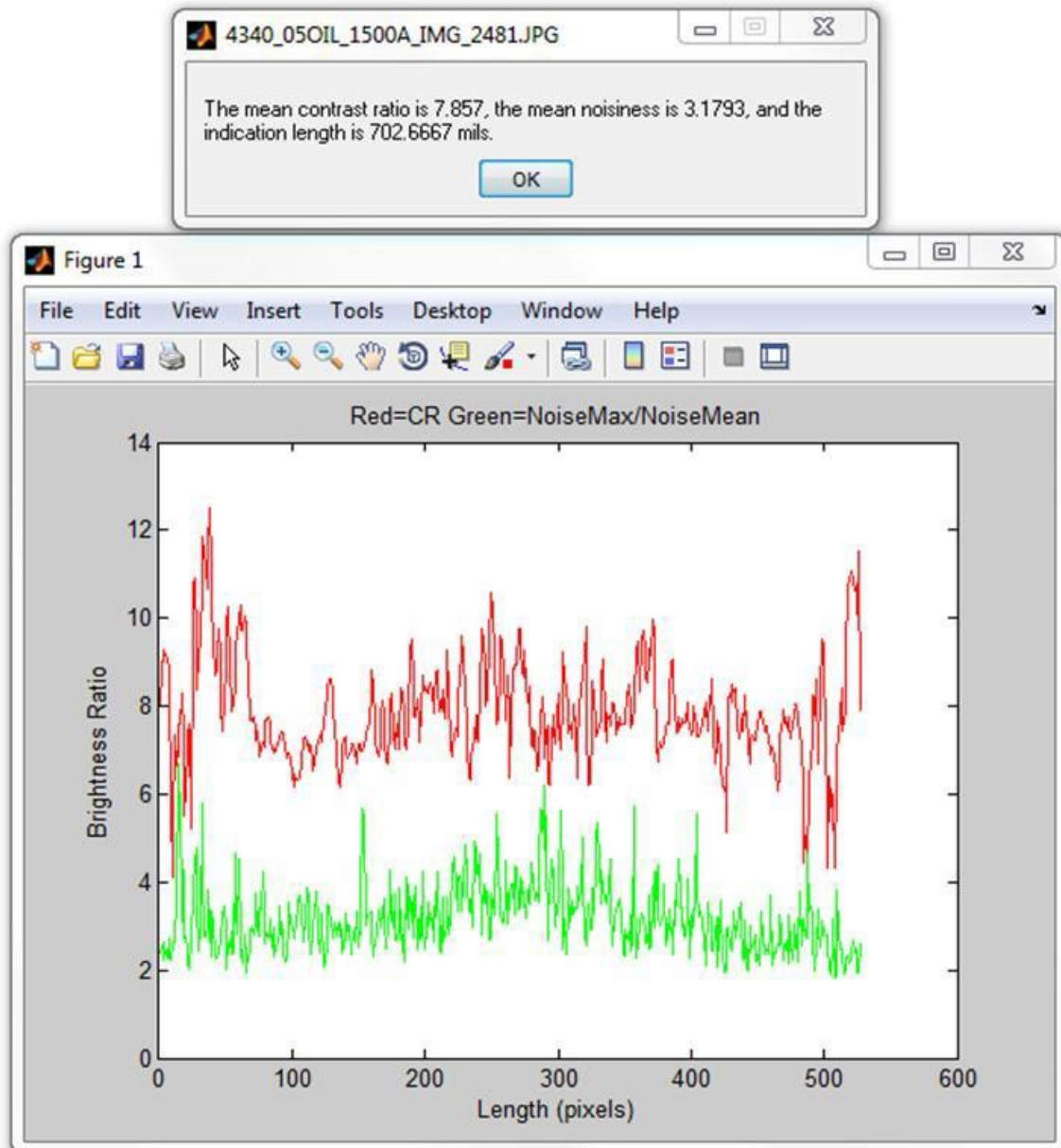
Figure I-3. Final output of the MATLAB script. Plot is saved and data logged for post analysis

This completes the summary of this quarter's focus on development and documentation of the image analysis process. Effort will continue in the next quarter in final installation of image recording and data acquisition approaches and use of this procedure in a number of experimental studies.

APPENDIX J—FATIGUE PARAMETERS

FATIGUE PARAMETERS

- Electric discharge machining (EDM) Notch: 30 mil long, 5 mil wide, 1–2 mil deep
- R ratio: 0.1
- All fatigue cracks will be grown at room temperature.
- Frequency used for fatigue growth was 6 Hz.
- Final surface finish will be less than 63 Ra, according to ISO 4287 and 4288.
- Load force used will be determined by the yield strength of the material and the individual sample dimensions. Example of the calculation is shown below:

$$I = \frac{width * thickness^3}{12}$$

$$Max\ Load = \frac{4 * I * 80\%Yield}{Span * \left(\frac{Thickness}{2}\right)} =$$

$$Min\ Load = Max\ Load * 0.1$$

When the starter fatigue crack has been grown to the prescribed length of 32–35 mil, the EDM notch is removed by wet grinding. The amount of material removed is based upon the depth of the EDM notch. Enough material is ground off the sample to remove the evidence of the notch without removing the existing crack from the sample. After the EDM notch is removed, the sample is fatigued and monitored until the desired final crack length has been achieved.

CRACK ASPECT RATIO

Several samples were broke open to examine the crack aspect ratio to ensure the proper crack aspect ratio is being achieved in the sample generation process. Target crack aspect ratios are between 2:1 and 2.5:1. Figures J-1 and J-2 show that target aspect ratios were achieved.
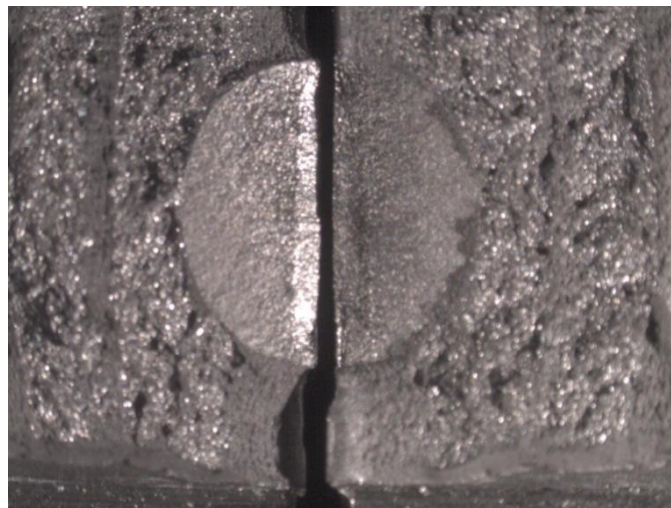

Figure J-1. Aspect ratio of 2.2:1

Figure J-2. Aspect ratio of 2.25:1

Prior to fracture, both samples were processed on the MPI bench to ensure that these two cracks responded in a similar fashion to magnetization as the remaining samples.

APPENDIX K—QUALITATIVE QUALITY INDICATOR PROCEDURE

QUALITATIVE QUALITY INDICATOR PROCEDURE

1.　　　Set up bench for auto bath, 1-second out and 1-second back.
2.　　　Set bench to 13% (~250–260 Amps) using half wave.
3.　　　Place a qualitative quality indicator shim in the center of the 2″ x 2″ x 12″ sample.
4.　　　For tests requiring 1 shot (0.5 sec, 1 sec, 1.5 sec, 2 sec), use the auto bath function.
5.　　　For tests requiring multiple shots (0.5 sec x 2, 0.5 sec x 3, 0.5 sec x 4, 1 sec x 2), use the handheld nozzle and attempt to replicate application of carrier solution similar to the auto bath function, 1-second down the sample and 1-second back, then magnetize with each of the shots fired in immediate succession.
6.　　　Allow a 1-minute dwell time.
7.　　　Transfer to the MPI cart, and take picture using GigE Vision® camera and LabVIEW™ code.
8.　　　Return sample to bench, demagnetize, and rinse.
9.　　　Repeat 10 times for each shot duration.

APPENDIX L—IMAGE ANALYSIS FOR QUALITATIVE QUALITY INDICATOR

IMAGE ANALYSIS FOR QUALITATIVE QUALITY INDICATOR

The images gathered were analyzed using a MATLAB® code developed at Iowa State. The images were opened individually, analyzed, and the contrast results recorded in an Excel® spreadsheet.

1.   The images were opened and rotated 90° counterclockwise. A more specific area of analysis was chosen (see figure L-1).
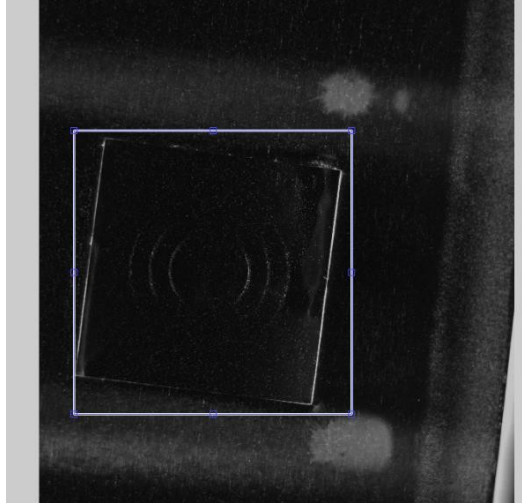

Figure L-1. Rotated and area chosen

2.   The contrast and brightness of the image were adjusted in the viewer window without numerically altering the actual image, so data analysis was not affected by the contrast changes needed to allow the following lines to be drawn correctly (see figure L-2).
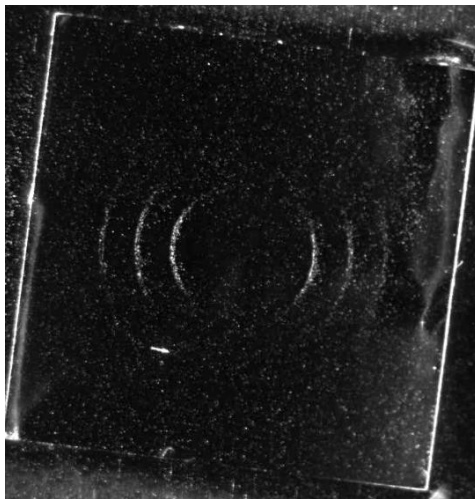

Figure L-2. Contrast and brightness adjusted

3.   A line was drawn between the top and bottom point of the third curve from the left. A second line was drawn from left to right to create a rectangle to be analyzed (see figures L-3 and L-4).
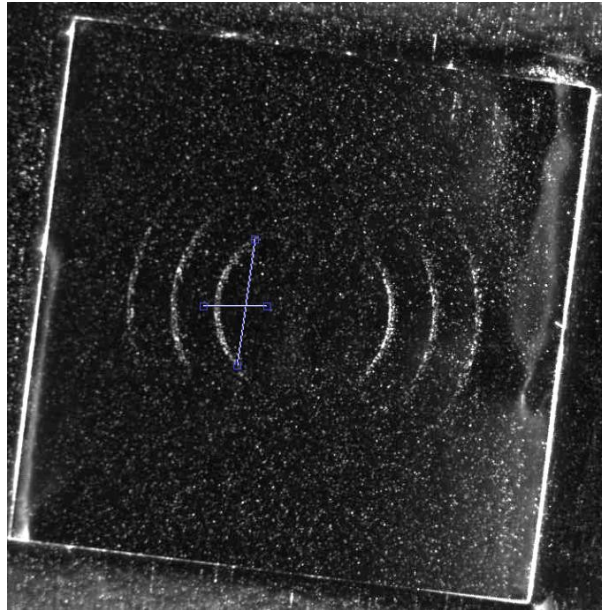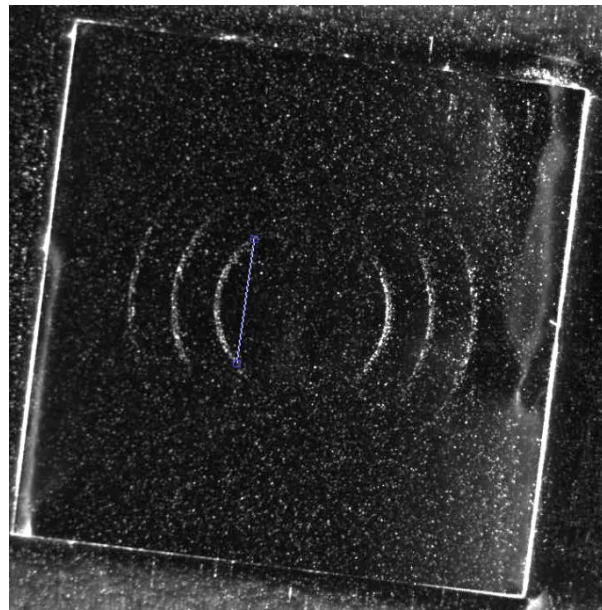

Figure L-3. Line from top to bottom

Figure L-4. Line from left to right

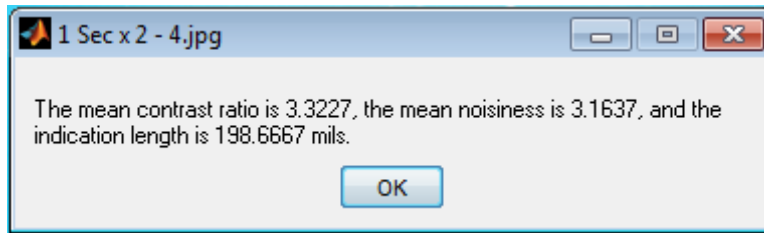4.   The values given by the MATLAB code (see figure L-5) were recorded in an Excel file.

Figure L-5. Example output